UCL Université catholique de Louvain

École polytechnique de Louvain (EPL)

# Multiple-year marine connectivity modeling in the Florida Coral Reef Tract to assess *Acropora Cervicornis* recovery

Dissertation presented by
**Victoria BECHET , Elise VERSTRAETEN**

for obtaining the Master's degree in
**Civil Engineering, Biosciences Engineering**

Supervisor(s)
**Emmanuel HANERT, Eric DELEERSNIJDER**

Reader(s)
**Pierre DEFOURNY, Sandra SOARES FRAZÃO**

Academic year 2017-2018

# Abstract

The massive decline in coral cover quantity and quality over the last decades reminds us the urgent necessity to assess coral reef resilience to threats affecting them. This study focuses on the resilience of *Acropora Cervicornis* in the Florida Coral Reef Tract. Despite being among the most productive corals world-wide, this species has faced a severe decline since the 1980s, so that it was listed as 'threatened' under the U.S. Endangered Species Act in 2006. This study intends to provide guidance on the selection of the most adequate locations for coral outplants as well as reef restoration and protection in the FCRT, by identifying connectivity patterns. A high-resolution ocean model of the FCRT's water circulation, constructed with the multiscale ocean model SLIM, is used to simulate the hydrodynamic over the studied area and periods. The hydrodynamic outputs, together with biological parameters (i.e. the rates of competence acquisition and loss and the mortality rate) are then used as inputs for a Lagrangian particle tracker which simulates larval dispersal. This allows to generate a connectivity matrix (CM) giving information about the number of connections between all reef pairs of the network. This methodology is applied here to four different years: 2007, 2008, 2009 and 2010. Graph theory tools and inter-annual variability study are used to highlight connection patterns and to point out most relevant reefs regarding coral reef management. The strongest candidate for protection measures is a spot to the south of the Marquesas Keys. More generally, protection is needed on reefs upstream of the Florida Current, seeding larvae to all reefs downstream. Reefs worth restoring are mainly located in the inner shelf of the Lower and Middle Keys. In parallel, a metapopulation model using the CM and biological parameters (e.g. clonal growth, egg production) is developed, allowing to compare the recovery times of the reefs and this for different years. For most of the reefs, the variability of the environmental conditions, inducing biological variability, is much greater than the inter-annual hydrodynamic variability. Finally this tool is used to asses the recovery of the FCRT after the major threat that was hurricane Irma.

# Acknowledgements

We would like to thank our supervisor Emmanual Hanert who guided us wisely all along our effort. He was always available, while he carefully followed our progress on a weekly basis. We would also like to thank our second supervisor, Eric Deleersnijder, for presenting us the different SLIM-related topics and showing us the possibility of contributing to such an inspiring research.

We are grateful to Antoine Saint-Amand, for his help, answering all our questions at any time and from anywhere and to Jonathan, Valentin and David, who spent a lot of time helping us understanding SLIM during -and even outside- the Friday sessions.

We would also like to thank Samantha King, studying coral biology in Florida. She shared and explained us the current results of her studies. Besides, the scientific exchange, we were glad to have her in Belgium for a month. We would like to thank her supervisor, Joana Figueiredo, leading the researches across the Atlantic. This present study is a result of their effort and willingness to improve the coral situation.

Furthermore, we would like to thank Aurélien and Thomas, for the mutual support.

Finally, we would like to show our gratefulness to our respective families for supporting us, not only during the realization of this master thesis but since the beginning of our educational path, keeping us in the best conditions for the achievement of our studies.

# Contents

# List of Figures

# List of Tables

# List of acronyms

| | |
|---|---|
| **ACER** | *Acropora Cervicornis* |
| **CFRS** | Climate Forecast System Reanalysis |
| **CM** | Connectivity Matrix |
| **CV** | Coefficient of Variation |
| **FC** | Florida Current |
| **FCRT** | Florida Coral Reef Tract |
| **GBR** | Great Barrier Reef |
| **GoM** | Gulf of Mexico |
| **HYCOM** | HYbrid Coordinate Ocean Model |
| **LC** | Loop Current |
| **LPT** | Lagrangian Particle Tracker |
| **NCEP** | National Center for Environmental Prediction |
| **NOAA** | National Oceanic and Atmospheric Administration |
| **OGCM** | Ocean General Circulation Model |
| **SLIM** | Second-generation Louvain-la-Neuve Ice-Ocean Model |
| **TAPPY** | Tidal Analysis Program in Python |
| **TLE** | Total Linear Extension |
| **UCL** | Université Catholique de Louvain |
| **WFS** | West Florida Shelf |

# 1 Introduction

## 1.1 Coral reefs : ocean's most vital but fragile ecosystem

Coral reef ecosystems are emblematic of tropical waters. Their biological diversity, their astonishing variety of colors and their undersea location are the sources of their somewhat mystical charm. One of the world's largest reef ecosystems is the Florida Coral Reef Tract, or FCRT. Extending over more than 500 km, it provides shelter to more than 6000 living organisms, plants or animals (NOAA, 2017). Next to offering a unique habitat to plentiful organisms, these coral reefs offer a broad range of other services, essential to nature balance and human activities. They contribute significantly to the coastal economic sectors. For instance, in Monroe County Florida, reef-based recreation and tourism alone generate over 33000 jobs and $2.3 billion annual sales (NOAA, 2018). For the fishing industry too, coral reefs are highly beneficial. One of the most valuable ecosystem services the reefs provide is coastal protection, by reducing wave energy of 97 percent on average (Ferrario et al., 2014). This avoids numerous flood damages every year, representing substantial economic savings.

These diverse benefits make coral reefs a habitat that needs to be preserved, especially knowing that they are extremely vulnerable. To grow in favorable conditions, corals need clean and clear water, as low turbidity and high light exposure allow the photosynthetic micro-algae living inside reef-building corals to thrive. These micro-algae, called zooxanthellae, live in symbiosis with the coral organisms, providing them up to 90% of their nutrients (Stanley, 2006) in exchange of a sunlight exposed shelter. As the zooxanthellae are extremely sensible to water temperature and acidity variations, the corals react to such changes by expelling the zooxanthellae living inside them. This leads to a color loss, leaving the corals' tissues translucent so that their white skeleton is visible. To date, this phenomenon, commonly referred to as **coral bleaching**, has known three major worldwide outbreaks in 1998, 2010 and 2015-2016 (Heron et al., 2016), in addition to multiple regional events. Bleaching events have threefolded between 1985-91 and 2006-12, causing the return time between successive severe events to diminish increasingly to only 6 years nowadays, a trend that will continue according to climate model projections (Heron et al., 2016; Hughes et al., 2018).

**Climate change** does not only causes ocean temperature and acidity levels to rise (the latter by an increase in CO2 concentrations), but also tends to increase the occurrence of tropical storms and hurricanes. Solely during the 2017 hurricane season, two category 5 hurricanes, Irma and Maria, touched the Caribbean coral reefs. Hurricanes and storms affect coral reefs by causing severe physical damages and by stirring up huge amounts of sediment, reducing light exposition (figure 1.2). Also extreme rainfall events are multiplied due to climate change. This will alter drainage and **run-off**, impacting coastal water turbidity and light availability. Run-off also brings nutrients and other pollutants along. Concentrations are highly increased by **coastal urban development**, a major threat to coral reefs. Other threats to the FCRT ecosystem are overfishing, ship grounding, tourism, aquatic invasive species and coral diseases (NOAA, 2008).

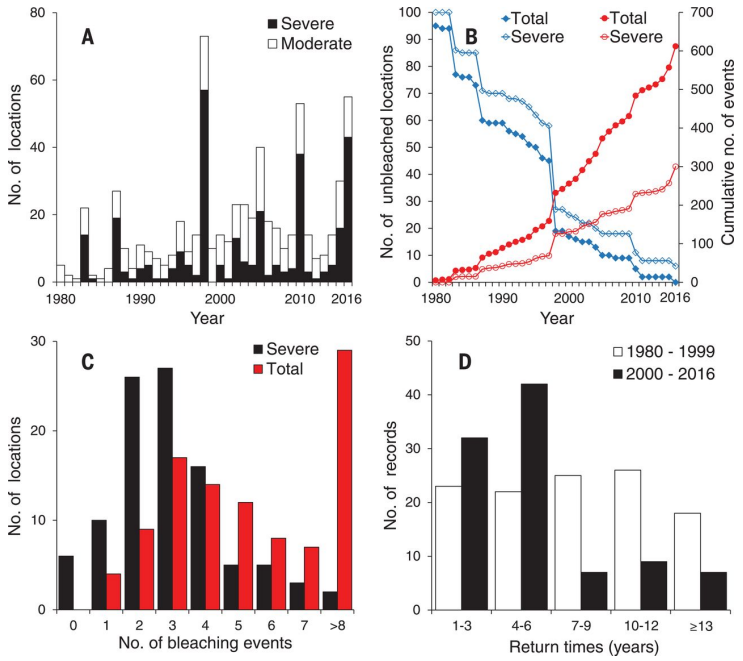


Figure 1.1: Temporal patterns of recurrent coral bleaching. (A) Number of pantropical locations (×100) that have bleached each year from 1980 to 2016. (B) Cumulative number of severe and total bleaching events since 1980 (red; right axis) and the depletion over time of unbleached locations (blue; left axis). (C) Frequency distribution of the number of severe (black) and total bleaching events (red) per location. (D) Frequency distribution of return times (number of years) between successive severe bleaching events from 1980 to 1999 (white bars) and 2000 to 2016 (black bars). (Hughes et al., 2018)

### 1.1.1 An endangered species : *Acropora Cervicornis*

The upsurge of all previously mentioned threats has caused an important decline in both live coral cover and species diversity worldwide. In 2008, only on a few reefs in all the U.S. Caribbean and Atlantic the living hard coral cover still exceeded 10%, although once they were structurally complex reefs (NOAA, 2008). These structures are the fruit of reef-builder corals (= stony corals). A major and highly productive reef-builder is the species *Acropora Cervicornis*. Whereas for most of the past 500,000 years these corals were dominant throughout the Carribean region, *A. Cervicornis*, alike *A. Palmata*, has known a vast decline over the last decades. For instance, at Looe Key in the Florida Keys, its population has declined by 98% between 1983 and 2000 (Miller et al., 2002). Henceforth it was listed as 'threatened' under the U.S. Endangered Species Act in 2006 (Hogarth, 2006).

*Acropora Cervicornis* has a structure in branches, reason why it is also called staghorn coral. Their cream white to brown color comes from the zooxanthellae living inside their tissues. As a scleractinian -or stony- coral, it produces a hard calcium-carbonate skeleton. It grows as a colony, made of a large number of small polyps, whose diameters generally do not exceed 2 mm (Porter, 1976). An individual colony can go up to 2 meters high. *A. Cervicornis* grows in wide range of depths, usually from -1 to -25 meters, and occasionally up to -60 meters (IUCN, 2008). With a branch growth rate of 10.9 to 15.9 cm/year in favorable conditions, *A. Cercivornis* is one the most productive corals world-wide, but it is extremely sensible to its environment. The major cause of its recent decline is disease, especially white-band disease which affects all Caribbean acroporid corals since the 1980s (IUCN, 2008). Other causes include thermal-induced bleaching, storms, predation by the Damselfish -*Stegastes planifrons*- and habitat competition

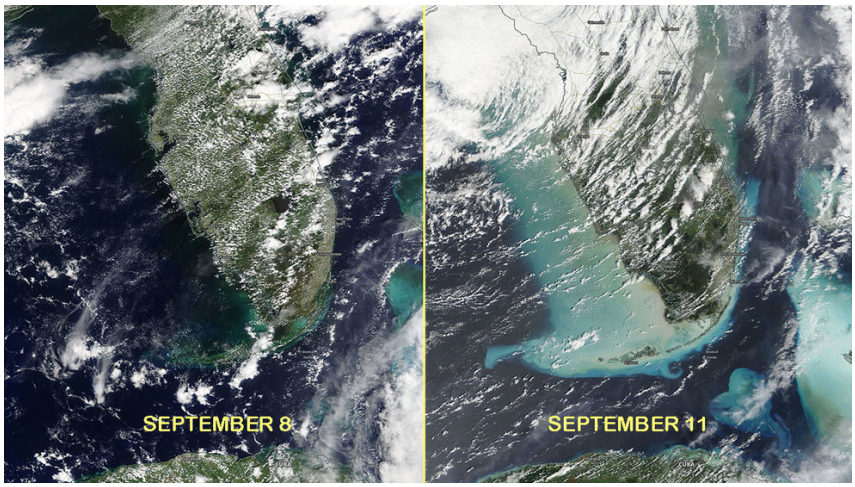


Figure 1.2: Satellite images showing the southern Florida coasts before and one day after the passage of hurricane Irma. The strong waves and currents have resuspended huge sediment amounts. Photo credits : NASA/MODIS.

Figure 1.3: *Acropora Cervicornis*, also called Staghorn Coral, is a hard, reef-building coral. A colony can grow up to 2m high. Photo credits: Albert Kok, *Coral.org*

with fast-growing macroalgae (Lirman et al., 2010).

*A. Cervicornis* can reproduce both asexually and sexually. The asexual reproduction includes budding and fragmentation. Budding is a clonal reproduction by cell division, where a young polyp is created as a bud on the existing coral. It shares the same skeleton and DNA as the parent individual. Fragmentation is the result of coral breaking. As branches are long and thin they are vulnerable to wave induced forces and thus break easily during storms. The broken fragments can reattach themselves further away if the soil is suitable, and create a new colony with the same genotype as the parent colony (Tunnicliffe, 1981).

Sexual reproduction of *A. Cervicronis* occurs once a year for all the corals in the Caribbean, through a mass spawning event occuring at the full moon of August. Since this species is hermaphroditic, the gametes released are of both genders. When two gametes from different individuals with different genotypes fecundate each other, they produce a larva. If the gametes are of the same genotype the larva will not be viable, even if they come from different individuals. The larvae, called planulae, are passive and not capable of swimming, so that their transport is dictated by the local water flows. In order to settle the larvae require natural consolidated hard substrate such as dead coral skeleton or hardbottom. Only a low percentage of the fertilized

larvae actually settle, as much of them never pass over a suitable settlement spot before dying. Sexual recruitment of a population, i.e. income of new larvae that will settle and produce a new colony, is limited compared to asexual reproduction. Once settled, a larva still has a high mortality rate of about 13% during the first six weeks (Ritson-Williams et al., 2010).

## 1.2 Marine connectivity of coral reefs

In response to the alarming decline of coral reefs conservation and restoration measures have been vastly boosted over the last decades. The most common approaches to support reef rehabilitation include coral transplantation, in situ and ex situ nurseries, implementation of artificial reefs, substrate stabilization and restoration of ship grounding sites (Rinkevich, 2005). To enhance the efficiency of these measures, the aim is to obtain high growth rates and attain highly successful recruitment. Both targets depend on a series of parameters and processes like light availability, nutrient concentrations, gamete production and larvae mortality rates, which are highly controlled by the environmental conditions. Recruitment, by resulting of larval dispersal, also depends on the hydrodynamics. Indeed, the local water flows define the track of the larvae and their possible destinations. They thus determine from which reefs and to which reefs larvae can be transported.

The whole process of gamete production and fertilization followed by larvae dispersal, settlement and post-settlement survival defines the possibility and the quantity of physical and genotypic exchanges between reefs and is known as connectivity in the marine biology domain. Physical exchanges help to maintain coral populations at a high level. Genotypic diversity is important to facilitate fertilization as for *Acropora Cervicornis* the gametes need to be of different genotypes. Data on connectivity patterns is actually scarce, yet understanding them would allow to target more efficiently where to increase conservation and restoration efforts. As these connectivity patterns depend on the biology of the species considered as well as on the local hydrodynamics, a first step in better assessing them can be made by reproducing realistically the governing water flows.

### 1.2.1 Water circulation in the Florida Coral Reef Tract

The Florida Coral Reef Tract (FCRT) extends from the Dry Tortugas in the Gulf of Mexico (GoM) along the Florida Keys, following an east-west orientation that curves into a north-south orientation, to reach St. Lucie Inlet, north of Palm Beach (figure 1.4). Following a seaward direction from the Key's coastlines, the first coral habitat type encountered are patch reefs, which are small, individual heterogeneous reefs that rarely reach the surface. A wide shallow lagoon, constituted of abundant seagrass, scattered coral heads and a few small patch reefs, separates these inshore communities from the offshore bank reefs. The bank reefs are characterized by a high species diversity, which is why they are the major touristic sites. Seaward of these, beginning at a depth of about 10 m, vast intermediate and deep reef habitats can be found (NOAA, 2017).

The bathymetry south of the Keys forms a narrow (7 to 10 km) continental shelf, consisting of an extremely shallow zone with depths less than 3m, that evolves in a deeper zone, the Hawk Channel (running from Biscayne National Park to Key West). Seawards of this Channel the bathymetry first rises again where a complex patchwork of reefs and coral structures are located, farther away it decreases rapidly and forms a shelf break where it plunges several hundred meters (Lee and Williams, 1999). North of the Keys a large continental plateau, the West Florida Shelf (WFS), extends all along the western coast of Florida.

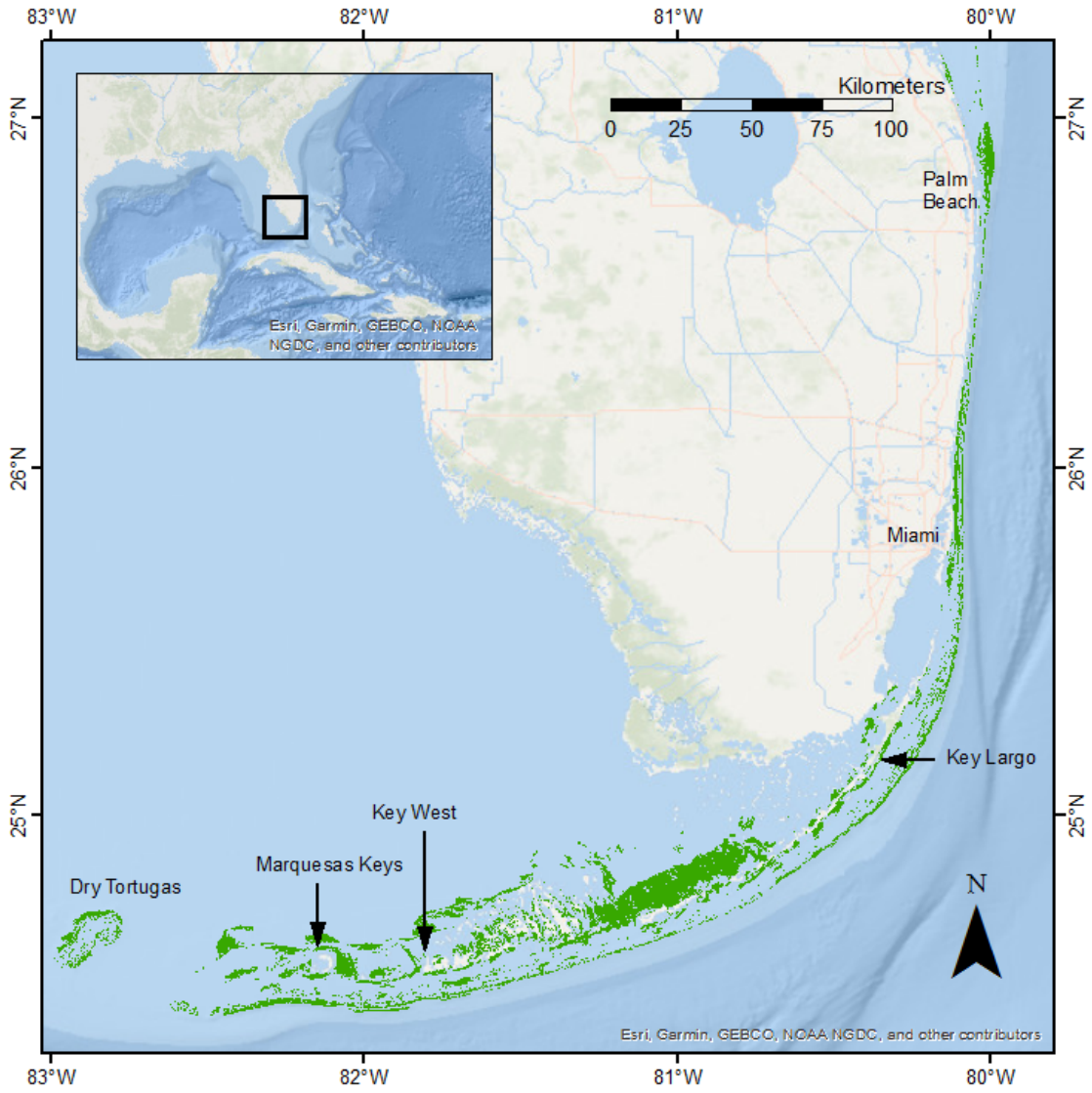


Figure 1.4: The Florida Coral Reef Tract (in green) extends over more than 500 km, from the Dry Tortugas in the Gulf of Mexico to north of Palm Beach, which makes it one of the largest barrier reef ecosystems in the world.

The hydrodynamics around South Florida are mainly dominated by the Florida Current (FC), which originates from the Loop Current in the Gulf of Mexico and flows through the Florida Straits to join the Gulf Stream in the Atlantic Ocean. The meandering of the FC all along the Keys is associated to the presence of cyclonic eddies and gyres that travel on its shoreward side (figure 1.5), affecting larval transport between the reef structures (Kourafalou and Kang, 2012). Various studies indicate that the FC is subject to seasonal variability.

The local water circulation in the FCRT results from three factors : the wind, the tides and the Florida Current. Two distinct flow regimes can be distinguished, depending on which factors are predominant (Lee and Williams, 1999). The first one consists of the inshore waters, including the Hawk Channel. There the influence of the Florida Current is very low, so tidal and local wind forcings govern the water flows, accounting respectively for 20 to 50 % and 50 to 80 % of the current variance (Lee and Williams, 1999). Seasonal wind direction shifts lead to coupled

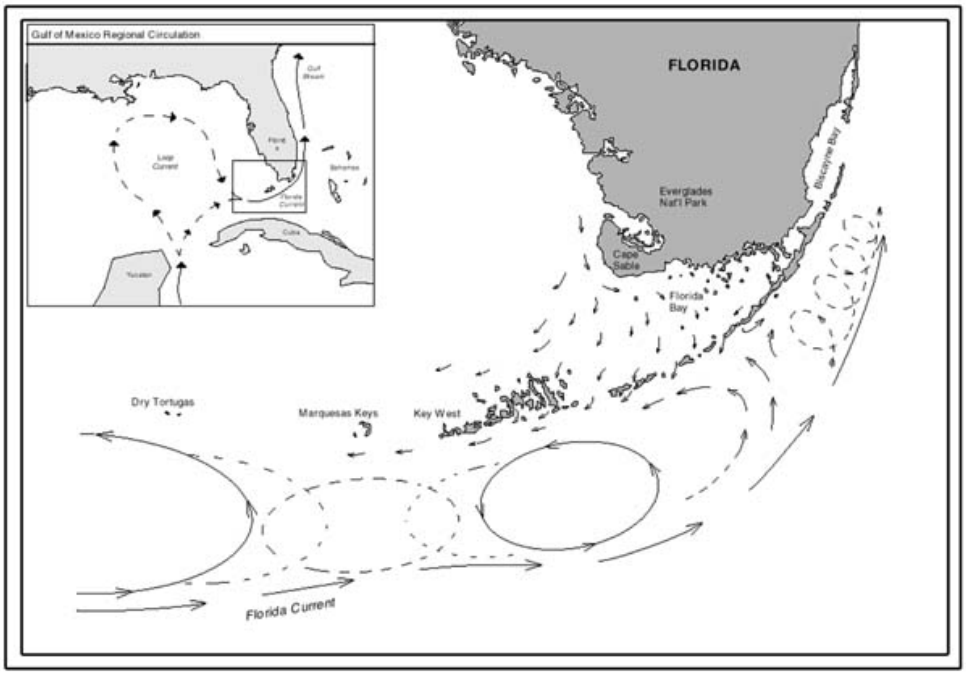


Figure 1.5: The Florida Current is a branch of the Loop Current that flows through the Florida Straits to the Atlantic Ocean, where it joins the Gulf Stream. Its meandering is associated with cyclonic eddies and gyres propagating eastward along the Florida Keys, at a monthly (lower Keys) and weekly (upper Keys) scale. Source figure : National Oceanic and Atmospheric Administration (NOAA, 2010).

current direction shifts in the upper Keys, this appears to be typical of extended shallow coastal waters (Lee and Mayer, 1977). In the lower Keys westward flowing currents persist all year long (Lee and Williams, 1999). The second flow regime consists of the waters seaward of the Hawk Channel along the northern Keys and the coastal zone from Miami to Palm Beach. In these regions bordering the shelf break, the influence of the FC is strong, resulting in a forceful mean northward flow. More locally the currents are impacted by the FC meanders and concomitant cyclonic eddies and gyres, appearing at a monthly time scale near Dry Tortugas and the southern Keys and at a shorter weekly time scale along the upper Keys and the southeast coast of Florida (Lee and Williams, 1999).

### 1.2.2 Modeling coastal hydrodynamics

To simulate this water circulation, several numerical hydrodynamic models are at one's disposal, among which the HYbrid Coordinate Ocean Model (HYCOM, `https://hycom.org/`). This open source ocean general circulation model (OGCM) is a widely used tool and is believed to be extremely reliable in open sea areas. Only, alike the most hydrodynamic models, it is constrained by its resolution. In Hycom's case the resolution does not exceed 1/25°, which is to coarse to account for the numerous small-scale flow features that affect the hydrodynamics in coastal waters and around reef structures, and hence influence larval dispersal by increasing local retention. This creates a need for high resolution ocean models, adapted to shallow waters and capable of simulating flow features down to a resolution of 100m. The Second-generation Louvain-la-Neuve Ice-Ocean Model (SLIM, `www.climate.be/slim`), developed at the Université Catholique de Louvain, uses an unstructured mesh, which allows to increase the elements' resolution only in specific areas. This is why this model is chosen to compute the FCRT's water circulation. The

main features of both models, Hycom and SLIM, are described hereafter.

The **HYbrid Coordinate Ocean Model (HYCOM)** is a data-assimilative hybrid isopycnal-sigma-pressure coordinate ocean model. Unlike traditional isopycnic coordinate circulation models, this hybrid model is applicable in shallow coastal seas and unstratified regions of the oceans. Hycom is used in eddy-resolving, real-time global and basin-scale ocean hindcast, nowcast, and prediction systems. The legacy experiments from Hycom's GOMl0.04 dataset provide 3 hourly outputs of a spatial resolution of 1/25°, for January 2003 till March 2012. Among other things, it provides ocean temperature, salinity, eastward and northward sea velocity, and sea surface elevation. The GOMl0.04 dataset covers the Gulf of Mexico (GoM), including the Florida Coral Reef Tract. The output data are available in netcdf format online (`http://ncss.hycom.org/thredds/catalog.html`).

The use of unstructured grids in ocean models has been a major revolution, giving birth to a second generation of ocean models. This revolution has strongly been promoted at the UCL with the development of the **Second-generation Louvain-la-Neuve Ice-Ocean Model (SLIM)**. This was encouraged thanks to a funding from the Communauté Française de Belgique (2004-2009). Since then the model has already been used to simulate the hydrodymanics of various areas, among which the Great Barrier Reef, the Scheldt river-to-sea continuum, the Indonesian Mahakam delta and the Florida Coral Reef Tract (Thomas et al., 2014; de Brye et al., 2010; Pham Van, 2014; Frys, 2017).

SLIM uses a finite element method, allowing the use of unstructured grids. This means the mesh elements are of varying size. The mesh can thus be computed to have a fine resolution in complex areas and have a coarser resolution in uniform areas, which means computational resources are used efficiently. The flexibility of SLIM makes it possible to apply the model to a variety of situations. It is therefore required to define the applicable equations, the initial and boundary conditions, the parameters as well as the post-processing data. Hence, it can be used in case of a 1D river model, a 2D depth-averaged model and a 3D barotropic or baroclinic model (Lambrechts, 2011).

The use of SLIM to model the FCRT's hydrodynamics in stead of a coarser resolution model like Hycom would allow to simulate the numerous small-scale features around the reefs and hence increase insight in the connectivity patterns determining reef resilience and recovery.

## 1.3 Objectives

Coral cover quantity and quality have massively declined over the last decades. A major asset to preserve them is to assess the resilience of the reefs to the threats affecting them. This study intends to provide guidance on the selection of the most adequate locations for coral outplants and of the most relevant reefs to protect and restore in the FCRT, by determining the reefs for which the connectivity is most optimum. Indeed, the resilience of a reef is strongly dependent on its connectivity, as a reef which receives many larvae from other reefs will have the capacity to recover quickly after a disturbance and will have a high genetic diversity. A reef which provides many larvae to other reefs will be helpful to the global network resilience. Frys (2017) used SLIM to compute a high-resolution hydrodynamic model of the FCRT water circulation and estimated connectivity through the simulation of larval dispersal. This study reproduces his work and, by considering the variability of the connectivity patterns and using them to evaluate reef recovery rates, it increases the robustness of his results and exploits the tools provided in order to gain new insights in reef resilience. Moreover we adapted the model to replicate *Acropora Cervicornis*

behavior, as the protection and restoration of this highly threatened species is urgent.

The methodology used in this study can be broken up in several steps :

- Estimate, for *Acropora Cervicornis*, the values of the biological parameters needed;
- Build a high-resolution ocean model of the FCRT's water circulation;
- Simulate larval dispersal using a Lagrangian particle tracker in order to evaluate connectivity;
- Determine interannual variability of the hydrodynamics and the larval dispersal;
- Use relevant indexes to interpret the connectivity patterns and the interannual variability;
- Develop a metapopulation model which estimates coral population recovery rates and their variability.

For the first step we used data provided by S. King and J. Figuieredo (Nova Southeastern University). The second and third steps are realized using the tools developed by Frys (2017) and A. Saint-Amand.

# 2 Methods and materials

## 2.1 Simulating the hydrodynamics

In order to simulate the movement of the coral larvae, it is essential to produce a hydrodynamic model of the region of interest, reproducing the currents and water flows. The three main drivers of the water circulation in the FCRT are the local wind, the tides and the water exchanges with the broader circulation from the GoM, mainly the Florida Current. These drivers correspond to the three external forcings which will have to be applied to the model. The wind influences the entire domain, whereas the tides and the currents define the open boundary conditions. Frys (2017) put a great effort in developing a hydrodynamic ocean model for the FCRT, adapting the tools previously used to simulate the hydrodynamics of the Great Barrier Reef (GBR) (Thomas, 2015). As this section is entirely built on his methodology, one should refer to his work for a better insight on the physical and numerical parameter selection.

The first step is to produce an **unstructured, two-dimensional mesh** (2.1) using SLIM. Its resolution varies depending on the distance to the coastlines, with a maximum 100 meter resolution near the coasts of the FCRT, a maximum 900 meter resolution near the other coasts and a 15 km resolution for the coarsest elements in the open sea. This gives a total of approximately $10^6$ elements. The computational domain is larger than the exact region of interest (i.e. the FCRT) so that the open boundaries are located in the open sea, there, the available tidal and global water circulation data, corresponding to the forcings imposed at the open boundaries, are more accurate than on the shelf break. The **bathymetry** is extracted from the GEBCO_2014 Grid provided by the British Oceanographic Data Centre (BODC, 2014) (figure 2.2). This land and ocean terrain model has a spatial resolution of 30 arc seconds. To ensure that the entire domain is submerged at all time, the water depth in shallow waters is set to minimum $h = 5m$. SLIM has the capacity to take into account wetting and drying, but this is not used in this study as it markedly complicates the model.

To calculate the surface elevation and the mean horizontal velocity vector for each mesh element, at each time step, the 2D depth-averaged barotropic version of SLIM is used. This implies resolving the non-linear **shallow water equations** of mass conservation and momentum conservation :

$$\frac{\partial \eta}{\partial t} + \boldsymbol{\nabla} \cdot (H\mathbf{u}) = 0 \tag{2.1}$$

$$\frac{\partial \mathbf{u}}{\partial t} + \mathbf{u} \cdot \boldsymbol{\nabla}\mathbf{u} = -f e_z \times \mathbf{u} - g\boldsymbol{\nabla}\eta - \frac{g\,||\mathbf{u}||\,\mathbf{u}}{C^2 H} + \frac{\boldsymbol{\tau}}{\rho H} + \frac{1}{H}\boldsymbol{\nabla} \cdot [H\nu\,(\boldsymbol{\nabla}\mathbf{u})] \tag{2.2}$$

where $\eta$ is the water level fluctuation relative to a reference level $h$, $H$ the sum of $h$ and $\eta$ (i.e. the total water column depth), $\mathbf{u}$ the depth-integrated velocity and $e_z$ a unit vector pointing vertically upwards. The time-stepping method applied is an implicit second order Runge-Kutta scheme and the spatial discretization is done using the discontinuous Galerkin finite element method.

In the right-hand expression of the equation 2.2, the first two terms represent respectively the **Coriolis force** and the **gravitational force**, $f$ being the Coriolis factor and $g$ the gravitational

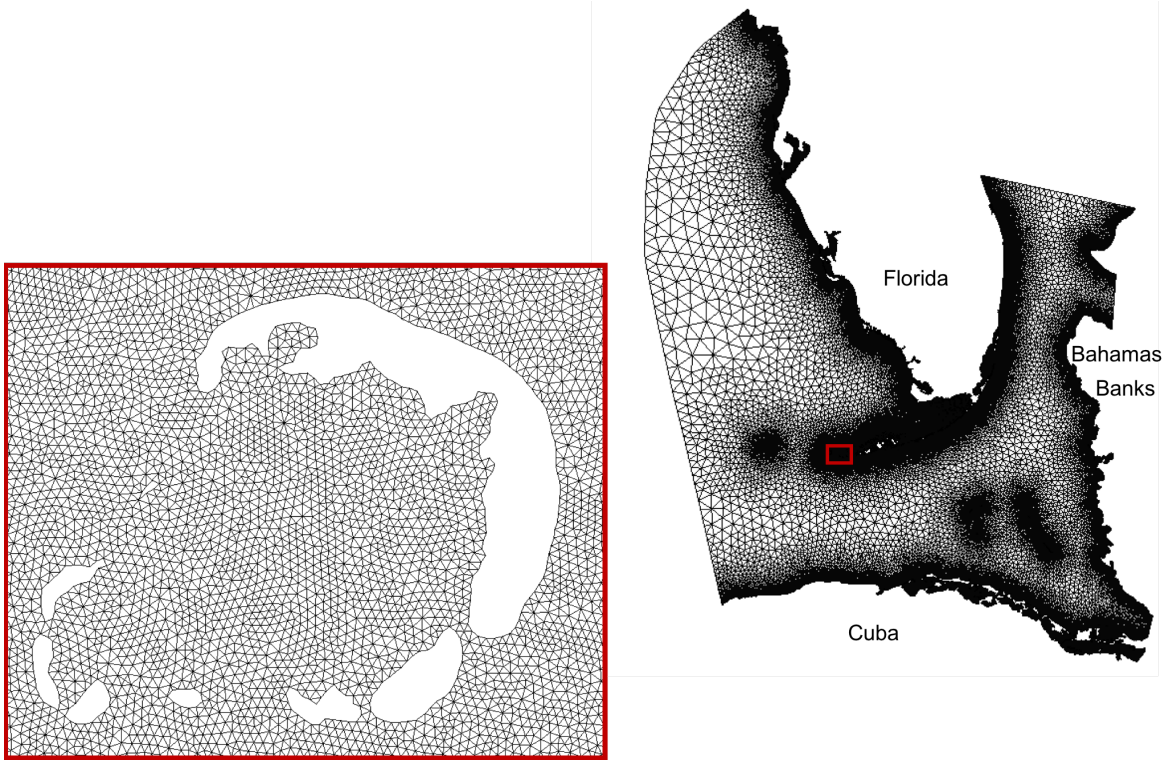


Figure 2.1: Unstructured two-dimensional mesh used for the modeling of the hydrodynamics around the FCRT. The difference in resolution can be observed. A close-up view on the Marquesas Keys allows visualizing the 100m high resolution mesh elements used in the zones of interest.

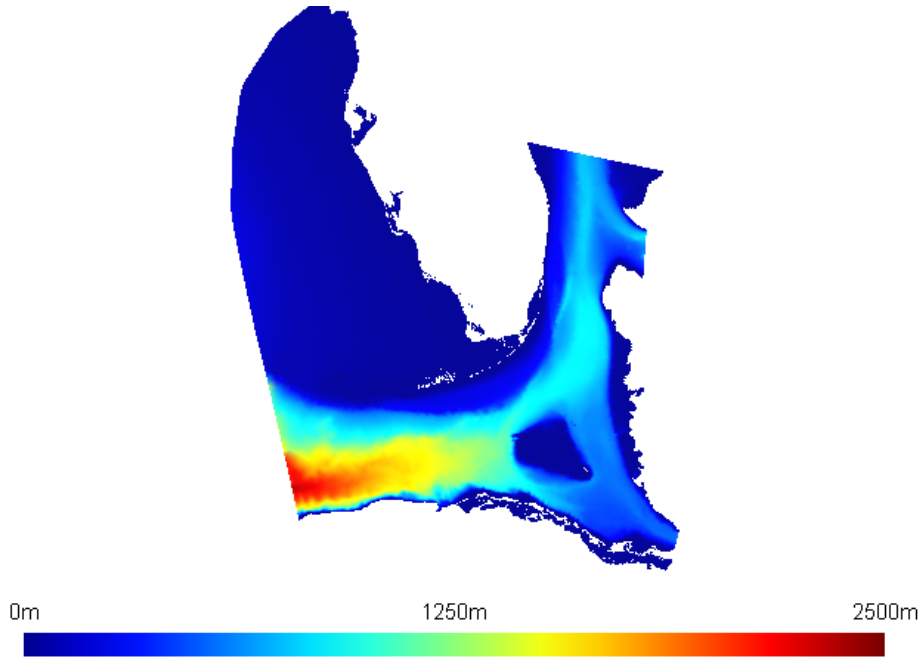


Figure 2.2: The bathymetry in the computational domain of the hydrodynamics model is characterized by strong slopes south and east of the FCRT and a shallow plateau northwest of the Florida Keys. The closed boundary around the Bahamas follows the 5m isobath.

acceleration. The third term corresponds to the **bottom stress**. The Chezy bottom-stress coefficient $C$ is equal to $\frac{H^{1/6}}{n}$ with $n$ the Manning coefficient, taken to be 0.25 on reefs and 0.025 elsewhere (de Brye et al., 2010; Andutta et al., 2011). The reefs are defined as being the polygons labelled as coral reefs and hardbottom in the shapefile layer of the Unified Florida Reef Tract Map (FWRI, 2016). Their surface vary from 170 $m^2$ to about 860 $km^2$ for the Vaca reef. As the median size of the reefs is 265 $m^2$, there are much more small reefs than big reefs. The fourth term of the equation, $\frac{\boldsymbol{\tau}}{\rho H}$, contains the **surface wind stress** $\tau$. This parameter is calculated as follow :

$$\tau = \rho_{air} C_D \, ||\mathbf{u}_{10}|| \, \mathbf{u}_{10} \tag{2.3}$$

where $\rho_{air}$ is the air density, $C_D$ the drag coefficient and $\mathbf{u}_{10}$ the wind speed at 10 meters above the sea surface level (Cushman-Roisin and Beckers, 2011). $C_D$ is defined using the Smith and Banke parametrisation (Smith and Banke, 1975). The wind velocities are taken from the National Centers for Environmental Prediction (NCEP) Climate Forescast System Reanalysis (CFRS) (`https://nomads.ncdc.noaa.gov/thredds/catalog.html`). This dataset has a temporal range from 1979 to March 2011. The last term accounts for **unresolved turbulent features**, which depends on the viscosity $\nu$. This parameter is calculated according to Smagorinsky's parametrisation (Smagorinsky, 1963) :

$$\nu = (C_s \Delta)^2 \sqrt{2\left(\frac{\partial u}{\partial x}\right)^2 + 2\left(\frac{\partial \upsilon}{\partial y}\right)^2 + \left(\frac{\partial u}{\partial y} + \frac{\partial \upsilon}{\partial x}\right)^2} \tag{2.4}$$

where $\Delta$ is the local element size, $(x, y)$ are the cartesian horizontal coordinates, $(u, \upsilon)$ the two components of the depth integrated velocity and $C_s$ is the slope friction coefficient, which for this study is set to $C_s = 5$, according to Frys (2017).

Frys (2017) also observed that better fitting results can be obtained by adding two terms to the conservation of linear momentum equation (eq. 2.2). The first term accounts for **slope-dependent dissipation** $F_{sd}$ (Döös et al., 2004) :

$$F_{sd} = -C_s \frac{|\mathbf{u} \cdot \boldsymbol{\nabla} H|}{H} \mathbf{u} \tag{2.5}$$

where $C_s$ is the slope friction coefficient, again taken to be equal to 5. The second additional term is a **global circulation forcing** $F_{gc}$, that adds a relaxation term to the model bringing the output currents closer to HYCOM's currents :

$$F_{gc} = \gamma \left(\mathbf{u}_* - \mathbf{u}\right) \tag{2.6}$$

where $\gamma$ is the inverse of the relaxation time $\tau$, and $\mathbf{u}_*$ the external depth averaged velocity, obtained by adding HYCOM's velocities to the velocities of the tides downloaded from the OSU TOPEX/Poseidon Global Inverse Solution dataset (Egbert et al., 2002). $\gamma$ is important near the open sea boundaries, in regions where a depth-integrated 2D model is not capable to simulate the hydrodynamics appropriately (so a 3D model like HYCOM would be necessary) and is equal to 0 for depths shallower than 50m, to assure that there is no forcing in the zone of interest, the FCRT.

The total equation consequently reads :

$$\frac{\partial \mathbf{u}}{\partial t} + \mathbf{u} \cdot \boldsymbol{\nabla} \mathbf{u} + f e_z \times \mathbf{u} = -g \boldsymbol{\nabla} \eta - \frac{g \, ||\mathbf{u}|| \, \mathbf{u}}{C^2 H} - \frac{C_s \, |\mathbf{u} \cdot \boldsymbol{\nabla} H| \, \mathbf{u}}{H} + \frac{\boldsymbol{\tau}}{\rho H} + \frac{1}{H} \boldsymbol{\nabla} \cdot [H \nu \left(\boldsymbol{\nabla} \mathbf{u}\right)] + \gamma (\mathbf{u}_* - \mathbf{u}) \tag{2.7}$$

To complete the hydrodynamic model, realistic **boundary conditions** have to be imposed. Along the coastlines, which are impermeable boundaries, the mass flux is set to zero and the tangential momentum flux is proportional to the mean tangential velocity (Lambrechts, 2011). At the open boundaries of the model, the water exchange and current velocities are imposed by adding the tides from the TOPEX/Poseidon dataset and the currents extracted from HYCOM.

### 2.1.1 Output validation

The outputs of this hydrodynamic model are the water velocity and water elevation at each time step, for each mesh element. The model is computed using the external forcings of four different years, 2007, 2008, 2009 and 2010. The water velocity results are graphically validated by comparing them with HYCOM's velocities at the points 1 to 8 shown in red in figure 2.3. The validation of the water elevation results is done by comparing them with observations from the buoys located at the points 9 to 11 shown in green in figure 2.3. This second validation is done with the Tidal Analyis Program in Python (TAPPY) which performs a harmonic analysis. This consists in calculating the amplitudes and phases of a set of sine waves generated from the water elevation values (Cera, 1991).

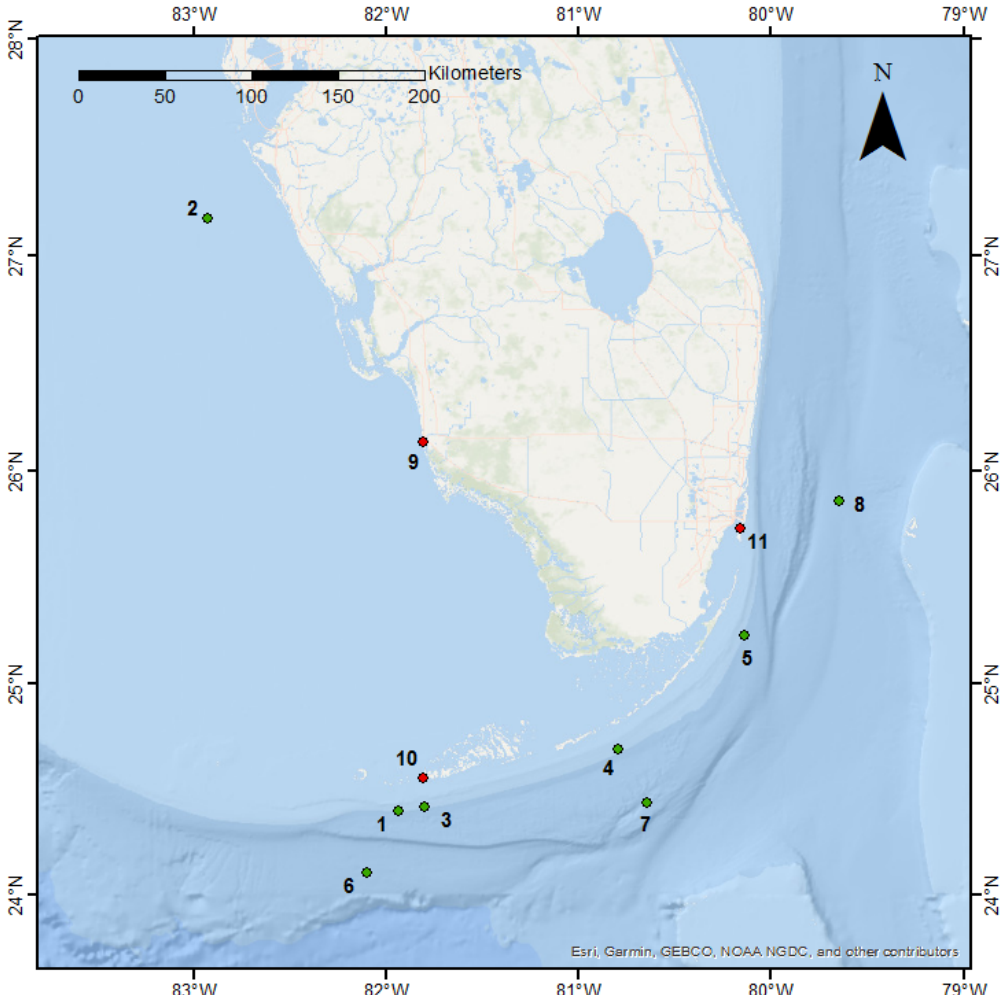


Figure 2.3: Locations of the validation points for the hydrodynamics model. Points 1 to 8, in green, are used to validate the velocities and points 9 to 11, in red, are used to validate the water elevations.

Indeed, the surface elevation versus the time is describing a curve that can be broken down into different sinusoidal functions, the tidal harmonic constituents. Each of these functions describes a wave, with a certain height (H), celerity (c), period (T) and phase ($\phi$). The celerity is calculated as 360 ° divided by the period. The phase is the phase lag of the time series constituents behind the theoretical equilibrium tide phase. Each harmonic constituent is due to the effect of the gravitational forces exerted by a heavenly body (the moon or the sun) or to the

rotation of the earth. Those harmonic constituents are then sorted and given a name according to their period and cause. The four main constituents in order of amplitude (Talley et al., 2011) are:

- $M_2$: Principal lunar semidiurnal constituent, with a period of 12,42 h.
- $K_1$ luni-solar declinational diurnal constituent, with a period of 23,93 h.
- $S_2$: Principal solar semidiurnal constituent, with a period of 12 h.
- $O_1$ Lunar diurnal constituent, with a period of 25,82 h.

The tidal analysis package, TAPPY , breaks down the time series into their harmonic constituents thanks to a Fourier data analysis. It is used here on both the surface elevation time series produced thanks to SLIM and the surface elevation time series recorded by real buoys at point 9 to 11. As the frequency of each component is determined astronomically whereas the relative amplitudes and phases of the components depend on location (Talley et al., 2011), the amplitudes and phase lags are here compared for each points.

## 2.2 Modeling larval dispersal

Once in possession of a hydrodynamic model, the next step is to generate a connectivity matrix representing the virtual larvae transport between each reef pair. Therefore it is necessary to simulate the release, the dispersal and the settlement of the larvae. The larvae are considered to be autonomous, buoyant, individual organisms, which are passively transported by the ocean currents, which signifies they have no control over their movements. Their behavior is defined by simple biological parameters, such as competence acquisition, mortality and buoyancy loss. The methodology adopted to generate the connectivity matrix is the same as that used by Thomas (2015) and Frys (2017) in their papers concerning marine connectivity modeling in the GBR and the FCRT respectively. This methodolgy is based on a Lagrangian particle tracker (LPT) model, described below.

### 2.2.1 Lagrangian particle tracker model

The Lagrangian algorithm used to simulate the larvae transport is a random walk formulation of the 2D advection-diffusion equation as outlined by Spagnol et al. (2002) and Hunter et al. (1993), in its discretised form :

$$\mathbf{x}_{n+1} = \mathbf{x}_n + \mathbf{v}_n \Delta t + \frac{\mathbf{R}_n}{\sqrt{r}} \sqrt{2K\Delta t} \tag{2.8}$$

with

$$\mathbf{v}_n = \left( \mathbf{u} + \frac{K}{H} \nabla H + \nabla K \right) |_{x_n} \tag{2.9}$$

where $\mathbf{x}_n$ and $\mathbf{x}_{n+1}$ are the particles positions at time iterations $n$ and $n+1$, $\Delta t$ is the time step between the iterations, which in this study is set to $\Delta t = 900\,s$, $K$ is the horizontal diffusivity coefficient, $u = u(x,t)$ is the instantaneous depth-averaged horizontal water velocity, $H$ is the water column depth and $\mathbf{R}_n$ is a two-dimensional vector of random numbers with a mean of zero and a variance of r, so $\frac{\mathbf{R}_n}{\sqrt{r}}$ is a vector of random numbers with unit variance.

For defining the horizontal diffusivity coefficient K, the formula used by de Brye et al. (2011) and inspired of Okubo (1971) is used :

$$K = \alpha \, \Delta^{1.15} \, m^2 \, s^{-1} \tag{2.10}$$

This simple formula depends on the local element size $\Delta$ of the mesh which is essential to account for the greater presence of unresolved water flows in large mesh elements than in smaller ones. The coefficient $\alpha$ is taken to be $0.041\, m^{0.85} s^{-1}$, as calibrated by Andutta et al. (2011) for coastal waters in the Great Barrier Reef.

Equation 2.8 defines a particle position at time step $n+1$ as being that particle position at time step $n$ plus two additional terms, $v_n \Delta t$ and $\frac{R_n}{\sqrt{r}}\sqrt{2K\Delta t}$. Those two terms represent the particles' movements respectively due to deterministic and stochastic forces. As shown in equation 2.9, the deterministic term takes into account the depth-averaged velocity at time step $n$ and a correction velocity $u'$ :

$$\mathbf{u}' = \mathbf{v} - \mathbf{u} = \frac{K}{H}\nabla H + \nabla K \tag{2.11}$$

This correction velocity tends to increase the transport of particles to deep regions with high diffusivity, and so avoid spurious accumulation in shallow waters and regions with less diffusivity (Spagnol et al., 2002). The stochastic term contains a two-dimensional vector of random numbers, $R_n$, that takes into account the effect of random sub-grid scale turbulence. This effect is increased for a high diffusivity coefficient, which stands for a coarse mesh resolution. To fully express the haphazardness of this term, the same LPT model is run several times for a same event, so that the random vector $R_n$ changes each time. The final result is a sum of the intermediate outputs.

The Lagrangian particle tracker is incorporated in SLIM as an offline module, meaning it takes the outputs of the hydrodynamic model, which are the water elevation and velocity, as the input parameters $H$ and $u$ of equations 2.8 and 2.9. The outputs of the LPT are the connectivity matrices and the coordinates of the particles' positions at the set time steps along with the number of particles seeded on each reef.

### 2.2.2 Biological parameters

The LPT model can be adjusted by incorporating the biological parameters of the larvae. These are implemented in the model as additional options that can be turned on or off depending on the applications. The main life history traits of *Acropora Cervicornis*, the species chosen for this study, are described in section 1.1.1.

A first set of parameters is the **spawning location**, **abundance** and **period**. The reefs' locations are taken from the Unified Florida Reef Tract Map (FWRI, 2016), which provides the areas on the continental shelf corresponding to coral reefs and hardbottom. In total 990 reefs are determined. The assumption is made that *Acropora Cervicornis* grows equally on the entirety of these areas, however, in reality, (subparts of) some reefs are not populated with this coral and other reefs are dead and contain almost no corals at all. To remove this assumption, the proportion of each reef covered with *A. Cervicornis* should be known, nut data on this is still very scarce. The spawning abundance is taken to be 100 larvae/km$^2$ of reef. This is not biological realistic, consequently, the output connectivity matrix, representing the strength of the connection between each reef pair, does not reflect the absolute larvae exchange, but is relative to the amount of particles seeded. As mentioned in section 1.1.1, for *A. Cervicornis*, the spawning occurs at the full moon of August. The model supposes that each year, all larvae are released at

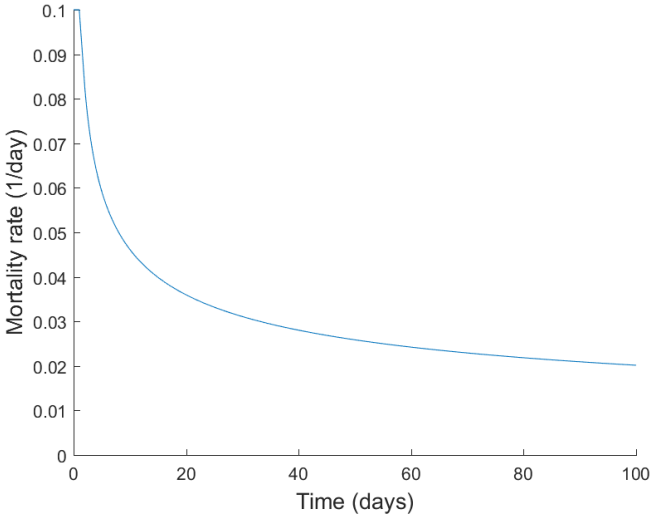


Figure 2.4: The mortality rate of *Acropora Cervicornis* larvae follows a 2-parameter Weibull distribution, involving a high initial mortality rate that decreases over time.

once, at 00:00 of the date of the full moon. This date is August 28 for 2007, August 16 for 2008, August 6 for 2009 and August 24 for 2010.

Another parameter is the **competence acquisition** and then **loss**. After a latency period, a larva has a certain probability to acquire competency, this means having the ability to settle on a reef. Once competent, the larvae will gradually lose their competency. For *Acropora Cervicornis*, the latency period is 5.13 days, and both acquisition and loss rates are constant over time, being respectively 0.065 $\text{day}^{-1}$ and 0.016 $\text{day}^{-1}$. All larvae lose their competency after 100 days (S. King and J. Figuieredo, personal communication).

**Settlement** is yet another parameter that is added to the LPT. This is the process during which a larva loses its buoyancy, sinks down and attaches to the reef surface. A simplification is made, supposing that a larva settles onto the first reef it passes over once it has become competent. The model allows to select reefs on which larvae can not settle, depending on their depth. In this model we suppose the larvae are able to settle on all the reefs. When a particle settles, it is taken out of the particle tracker and the event is recorded in the connectivity matrix by increasing the value of the cell corresponding to the right source and sink reefs of one unit.

The next implemented biological parameter is the **mortality** rate of the larvae. Depending on the species biology, this rate can be calculated either by supposing a constant mortality rate, either by supposing a two parameter Weibull distribution (Connolly and Baird, 2010; Figueiredo et al., 2013; Figueiredo et al., 2014). This second distribution assumes a high initial mortality rate which decreases with time. For *Acropora Cervicornis*, the Weibull distribution is the most accurate (S. King and J. Figuieredo, personal communication). Accordingly, the mortality probability $\mu$ for each larva takes the following form (figure 2.4):

$$\mu = \nu\lambda\,(\lambda\,t)^{\,\nu-1} \tag{2.12}$$

where $\nu$ and $\lambda$ are independent parameters. These are respectively set to 0.64 and 0.06, as found by Figuieredo and King (personal communication). Predation mortality is not taken into account considering the complexity to measure it. When a larva dies, its corresponding particle is taken out of the running model.

The mortality rate as well as the competency acquisition and loss rates define the state of

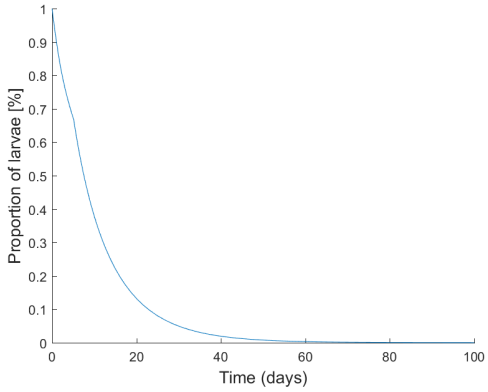


(a) Larvae alive and pre-competent

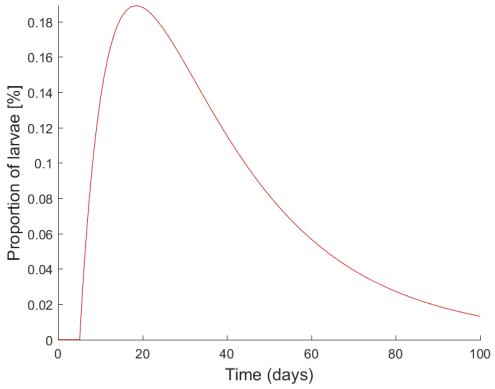


(b) Larvae alive and competent

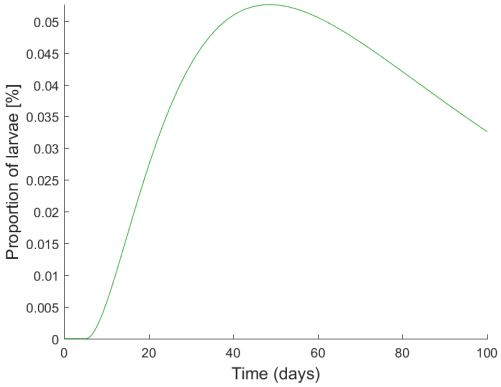


(c) Larvae alive and post-competent

Figure 2.5: The biological parameters fixed for Acropora Cervicornis define the mortality, competence acquisition and competence loss rates, and thus the state of the larvae at each time step after spawning.

the larvae, once they have been spawned (figure 2.5). The model is run between 30 and 50 days after the full moon, depending on the year considered. After that time, only between 2.8 and 4.8 percent of the total amount of larvae released were still alive and competent. This is summarized in table 2.1.

| | **2007** | **2008** | **2009** | **2010** |
|---|---|---|---|---|
| **Period [days]** | 44 | 38 | 50 | 30 |
| **Competent larvae remaining [%]** | 2.8 | 4.8 | 2.9 | 4.0 |

Table 2.1: Duration of the LPT runs

## 2.3 Analysing the connectivity matrices

The objective of this section is to extract useful information from the connectivity matrices in order to identify reefs with quantitative and qualitative connections in terms of coral restoration potential.

The connectivity between reefs can be studied from the outputs of the LPT. The main output

is a connectivity matrix (CM) in which each element $C_{ij}$ is defined as the number of particles released by a source reef $i$ and settled on the sink reef $j$ ($i$ and $j$ being the row and column index of the CM respectively). The index j that identifies the columns is covering the receiving reefs. The number of non-zero entries in row $i$ is equal to the number of reefs that receive larvae from reef $i$. The index i that identifies the rows is covering the seeding reefs. The number of non-zero entries in column $j$ is equal to the number of reefs that send larvae to reef $j$. In this study the CM has a dimension of $990 \times 990$ as there are a total of 990 reefs considered.

An other output is the seeding vector $S_i$, which contains the number of larvae released by each source reef $i$. The sum over the seeding vector elements is equal to the total number of particles seeded over the FCRT, including the ones that are not settling, whereas the CM contains only the amount of particles that are modeled as effectively settling.

The third output returns the coordinates of each reef. It is given as a 3-column matrix where each column has a length corresponding to the number of reefs. The first one is simply referring to the index of the reef and the two others are giving respectively the latitude and longitude of each reef. It corresponds actually to the coordinates of the center of each modeled polygonal reef and are used only for visualization purposes.

As described in the previous section, the CM and the seeding vector vary for each run of the model according to the stochastic part of the LPT. Therefore, the model is run several times for each year and the results are added together reducing the influence of any outlier and giving then a more probable connectivity matrix. Furthermore, some of the connectivity indices can also use a normalized CM. Each element of the normalized CM is noted as $\widetilde{C}_{ij}$. Two different normalizations of the CM are possible: either dividing the CM by the number of particles seeded (2.13), or dividing the CM by the number of particles effectively settled (2.14). However, only the first definition (2.13) is used in the present analysis.

$$\widetilde{C}_{ij} = \frac{C_{ij}}{S_i} \tag{2.13}$$

$$\widetilde{C}_{ij} = \frac{C_{ij}}{\sum_j C_{ij}} \tag{2.14}$$

This section presents the tools to analyze the large size LPT outputs. First some connectivity measures, allowing to highlight important reefs (with a lot of particles exchange), are presented. Then specific indicators to determine the need of protection and the suitability for restoration projects are defined. Finally, two different methods to bring out reef clusters and communities are presented.

### 2.3.1 Connectivity indices

Some connectivity indices have been selected below in order to determine important reefs and connectivity patterns. The indices have to be calculated for each reef and then compared among the reefs in order to describe the whole network.

### Local retention

The local retention of a reef $i$, $\lambda_i$, is the proportion of particles released by a source reef $i$ that settle on the same reef.

$$\lambda_i = \frac{C_{ii}}{S_i} \tag{2.15}$$

Precisely, the amount of particles $C_{ii}$ released over a reef $i$ and settling over the same reef is divided by the total amount of particles $S_i$ that are seeded by this reef $i$. The higher the value of the local retention of a specific reef is, the greater the reef capacity of self replenishment is. This means that from each reef's point of view, it is better to have a high value of the local retention. Of course, it is a selfish consideration as bigger local retention leads to a lesser amount of particles sent to the other reefs.

### Self Recruitment

The self recruitment of a reef $j$, $s_j$, is the proportion of particles settling on a reef $j$ that is released by the same reef $j$.

$$s_j = \frac{C_{jj}}{\sum_i C_{ij}} \tag{2.16}$$

Precisely, the amount of particles $C_{jj}$ released over a reef $j$ and settling over the same reef is divided by the total amount of particles that are settling on this reef $j$. This total amount of particles settling on the reef $j$ is calculated as the sum of all the elements contained in the $j^{th}$ column of the CM. The higher the value of the self recruitment of a specific reef, the more particles it receives from itself compared to what it receives from other reefs. A high value of self recruitment reflects then a high degree of isolation.

### Proportion settled

The proportion settled is the proportion of particles released by a specific reef that settle on an other reef.

$$P_i^{settled} = \frac{\sum_{j \neq i} C_{ij}}{S_i} \tag{2.17}$$

The local retention is excluded from the proportion settled as the latter only considers the particles settling on other reefs. This measure can be interpreted as the ability of the reef to export particles.

### Proportion lost

The proportion lost of a specific reef $i$ is the proportion of particles released by this reef that never settle. The sum of the local retention, the proportion settled and the proportion lost of a specific reef is 1.

$$P_i^{lost} = \frac{S_i - \sum_j C_{ij}}{S_i} = 1 - P_i^{settled} - \lambda_i \tag{2.18}$$

### Weighted connectivity length

The weighted connectivity length of a reef $i$ is the average of the distances between this source reef and all the sink reefs that it seeds, weighted by each connection strength. It actually gives the average distance covered by one larva.

$$WCL_i = \frac{\sum_j (C_{ij} \times L_{ij})}{\sum_j C_{ij}} \tag{2.19}$$

The connection strength, $C_{ij}$, is here defined as the number of larvae released by the source reef $i$ and settling on the sink reef $j$. The connection length, $L_{ij}$, is the radial distance between source and sink reef, that is easily obtained thanks to the coordinates of each reef. The WCL is giving the characteristic length scale of connectivity of a specific reef (Thomas, 2015).

### PageRank

PageRank is an indice introduced here to determine the importance of each reef based on the PageRank algorithm used by Google (Page, 1998). Indeed the PageRank algorithm used by Google is ranking the websites as "important" if they there are many websites pointing to them. Moreover it considers a forward link as more valuable if it is itself pointed at by several websites. In this way it ensures the quality of the forward link and tries and represents the willingness of human to read it. The PageRank of a website $i$, (or Incoming PageRank of a reef $i$) can be expressed as in (2.20)

$$\pi(i) = d \times \sum_{v \in B(i)} \frac{\pi(v)}{N(v)} \tag{2.20}$$

where $d$ is a damping factor, $B(i)$ is the set of websites (or reefs) pointing to $i$, $v$ is a website (or reef) belonging to the set $B(i)$ and $N(v)$ is the set of websites (or reefs) that $v$ is pointing to.

It is used in this study in order to identify both important receiving reefs (Incoming PageRank) and important source reefs (Outgoing PageRank).

The **Incoming PageRank**, written $\pi^{in}$, calculates as the Google's PageRank the importance of a reef based on the quality and the quantity of the incoming connections. It is used in this study in order to identify valuable reefs as reefs that receives larvae from a lot of different reefs and from important reefs themselves. Indeed, the more a reef receives larvae, the higher its resilience is expected to be. Those larvae should also come from different sources to ensure a varied inflow of larvae. So, if one of the source reef gets affected by a disease or weakens, the receiving reef is still receiving larvae from other reefs. Moreover, if the source reefs are themselves receiving larvae from a lot of different reefs, they are themselves less influenced by source reefs diseases and then, more resilient. That makes the final reef even stronger as its providers are reliable.

The **Outcoming PageRank**, written $\pi^{out}$, calculates the importance of a reef based on the quality and quantity of outgoing connections. A reef is valuable if it provides a lot of different reefs in larvae and even more valuable if those receiving reefs are themselves providing a lot of different reefs.

The Incoming and Outgoing PageRank are calculated thanks to the Matlab® function "centrality" with "pagerank" as argument. The incoming links are weighted by the strength of each connection that can be chosen as $C_{ij}$ or $\widetilde{C}_{ij}$. The sum of all the PageRank indices over the chosen network, here the FCRT, is always 1.

#### Betweenness

The Betweenness of a reef $i$ indicates how useful the reef is to establish a connection between any other two reefs. It actually gives a proportion of all the shortest paths connecting any two reefs that are passing through the reef $i$. By "shortest path" is meant a path counting the smallest amount of steps possible to connect two reefs. The betweenness of a reef $i$ can be expressed as in (2.21).

$$B_i = \sum_{r,s \neq i} \frac{n_{r,s}(i)}{N_{r,s}} \tag{2.21}$$

where $N_{r,s}$ is the number of shortest paths connecting the reef $r$ and the reef $s$ and $n_{r,s}(i)$ is the number of shortest paths connecting the reef $r$ and the reef $s$ and passing through the reef $i$.Each $\frac{n_{r,s}(i)}{N_{r,s}}$ is a ratio and hence is lower than 1. However, the sum of those ratios over all the possible couples in the network can give a dimensionless value by far higher than 1. In order to bring the betweenness to values from 0 to 1, it can be normalized by considering that the greatest betweenness of the network should be 1 and the lowest 0. The normalized betweenness is then calculated as in 2.22.

$$\widetilde{B_i} = \frac{B_i - B_{min}}{B_{max} - B_{min}} \tag{2.22}$$

with $B_{min}$, the lowest betweenness found in the network and $B_{max}$, the greatest.

The Betweenness can also be calculated thanks to the Matlab® function "centrality", with "betweenness" as argument. A cost parameter specifiying the degree of attractiveness of a connection can be entered. It is seen as a cost parameter such that the smaller this parameter, the more attractive the connection is. As in this study, a connection with a high number of larvae exchanged is considered as favorable, the cost parameter is set to the inverse of the connection weight ($1/C_{ij}$ or $1/\widetilde{C}_{ij}$).

### 2.3.2 Protection and restoration indices

The indices previously shown allow to assess if a reef is a good importer, a good exporter or if it is isolated. In order to use those indices in coral reef management decision, it is useful to determine which coral reefs need protection and which one need restoration and therefore to define the criteria representing the need for protection or restoration. A reef is considered as needing protection if its exportation is strong but importation weak. Indeed, it means that this reef is useful to the FCRT community but is not resilient itself. A reef is considered as needing restoration if both its exportation and importation are strong. Indeed, it means that this reef is useful for the FCRT community's resilience and for its own resilience too. Both protection and restoration indices can be expressed as functions of the PageRank index.

#### PageRank protection index

The PageRank protection index formulates the need of protection as defined above, by means of the PageRank indices. It is expressed in 2.23 as the difference between the outgoing and the incoming PageRank indices, normalized by their sum.

$$\pi_i^{out-in} = \frac{\pi_i^{out} - \pi_i^{in}}{\pi_i^{out} + \pi_i^{in}} \tag{2.23}$$

Its value ranges between [-1, +1]. The closer it gets to +1, the more the outgoing PageRank is important compared to the incoming PageRank, meaning that the reef needs protection. Inversely, the closer it gets to -1, the more incoming PageRank is important compared to the outgoing PageRank, meaning that the reef is receiving many larvae but not seeding many away. Those reefs do not need protection as there is already good chance that they have a good resilience thanks to those incoming larvae. Moreover, they are not useful for the rest of the network.

#### PageRank restoration index

The PageRank restoration index formulates the need of restoration as defined above, by means of the PageRank indices. It is expressed in 2.24 as the product of the outgoing and of the incoming PageRank.

$$\pi_i^{out\times in} = \pi_i^{out} \times \pi_i^{in} \tag{2.24}$$

This value is directly proportional to both the incoming and the outgoing PageRang indices and therefore, takes the highest value for reefs that are both good source and sink. Such reefs are worth restoring as they are helpful to the resilience of other reefs and once restored, they will be resilient themselves.

### 2.3.3 Communities and reef clusters

As the different connectivity measures have been presented, it is interesting to find out how those connection strengths are actually defining reef clusters. The reefs can be grouped so that the connections between reefs within a specific cluster are stronger than between reefs from different clusters. Clustering gives a better understanding of the general network and can help to read the previous indices. Indeed, by identifying a cluster, it can be expected that the degree of connections of the reefs belonging to it -identified by connectivity indices- is mostly describing connections within the cluster. Moreover, plotting the clusters gives a quick general idea of the connections between reefs and of their scope.

The different methods are described here to define the quality criteria of connections and hence highlight clusters. The first one, Community detection method, detects communities based on the strength of the connections. The second one, strongly connected components (SCC) method, groups the reefs that exchange larvae among themselves in both direction.

#### Community detection

This method is based on the Constant Pott Model (CPM) (Traag et al., 2011, Ronhovde and Nussinov, 2010). The idea is to create communities based on the principle that connections within a community should be strong and between different communities should be weak. The

model is delimiting the communities by optimizing the modularity $H$ (2.25), that means by maximizing the number of connections within a community while minimizing the number of reefs in it.

$$H = -\sum_{c} e_{cc} - \gamma n_c^2 \tag{2.25}$$

The equation (2.25) defines the modularity $H$ across all communities. $e_{cc}$ is the total connection weight within the community $c$, $n_c$ is the number of reefs contained in the community $c$ and $\gamma$ is the resolution parameter. Here, the total connection weight of a community is defined as the sum of the normalized number of larvae released by the community $c$ and settling in this same community.

$$e_{cc} = \sum_{i \in S_c, j \in S_c} \widetilde{C}_{ij} \tag{2.26}$$

The resolution parameter $\gamma$ is balancing the two criteria: maximizing connection weight within a community and minimizing community size. The density of connections, $d_{c,c}$, within a community $c$, respects :

$$d_{c,c} = \frac{e_{cc}}{n_c^2} < \gamma \tag{2.27}$$

as the density of connections $d_{rs}$ between two communities $r$ and $s$ respects :

$$d_{r,s} = \frac{e_{rs}}{n_r n_s} > \gamma \tag{2.28}$$

This resolution parameter is subjective. It is chosen depending on the type of results expected. The higher the value of $\gamma$, the stronger are the internal connections required and this leads to many small communities. The smaller the value of $\gamma$, the weaker are the internal connections tolerated, leading to fewer and larger the communities. A small value of $\gamma$ allows to identify very isolated communities (that are not even weakly connected to the larger communities) and hence, to find the strongest boundaries to the larvae dispersal. A high value of $\gamma$ allows to highlight smaller communities within the larger communities. Hence, to define the weakest boundaries of larvae dispersal.

The evolution of the number of communities as well as the proportion of inter-community connections can be plotted as functions of the resolution parameter. These curves show increasing functions of $\gamma$ with some relatively constant parts. Those constant parts are actually indicating the values of $\gamma$ for which the communities partition is stable. Therefore, the resolution parameter is chosen at the middle of one of those plateaus.

The research for the optimized modularity and hence the optimized community partition is done here thanks to a script written by Thomas (2015), using a modified Louvain Method algortithm (Blondel et al., 2008). It starts by considering each reef as one community. Then it finds which two reefs to put together in order to have a maximized gain of modularity. It puts more and more reefs together in order to maximize the gain of modularity at each step and obtain a final situation with an optimized modularity.

**Strongly connected components**

The method of the strongly connected components groups the reefs that are connected in both direction. That means that every reef belonging to a specific cluster is connected in both direction with every other reefs belonging to this same cluster. It is meant by "connected in both direction" that at least one path that connects the first reef to the second one and at least one path that connects the second reef to the first one exist. Those paths can be completed eventually via multi-step connections (if a reef A gives to a reef B that gives to reef C, there is a connection path from A to C).

### 2.3.4 Interannual variability of the indices

One of the objective of this study is to use those indices as a basis for coral reef management decision. However, they may vary from one year to another. Therefore, the evolution of those indices through different years is studied here. The two main statistical measures, the mean ($\mu_i$) and the standard deviation ($\sigma_i$), can already give an idea of the variability of each index for each reef $i$. They can both be computed from the previous results. The mean is calculated according to (2.29). The standard deviation is giving an indication about the dispersion of the measures over the four years. It has the same units as the index for which it is calculated and is computed according to (2.30).

$$\mu_i = \frac{1}{n} \times \sum_{k=1}^{n} Index_{i,k} \tag{2.29}$$

$$\sigma_i = \left( \frac{1}{n} \times \sum_{k=1}^{n} (Index_{i,k} - \mu_i)^2 \right)^{0.5} \tag{2.30}$$

where $n$ is the number of years on which the variability is computed, and $Index_{i,k}$ is the considered index calculated for the reef $i$ at the year $k$. It can be done for any of the indices presented above.

On one hand, the standard deviation of a large reef, with generally many connections, is expected to be higher than the standard deviation of a small reef that only exchange a few larvae. On the other hand, a measure that has a small standard deviation and a large mean, is less dispersed than a measure that has the same small standard deviation but a smaller mean too. For those reasons, it might be interesting to compute the standard deviation of some indices relatively to their mean. This normalized standard deviation is called the coefficient of variation (CV) and is expressed as in (2.31).

$$\widetilde{\sigma}_i = \frac{\sigma_i}{\mu_i} \tag{2.31}$$

This CV can be calculated only for indices measured on a ratio scale (Brown, 1998). That means that it can not be used for indices that can take a negative value and hence not for the PageRank protection index that ranges from -1 to 1. The CV is dimensionless. It is defined rather as a ratio than a percentage because the standard deviation can be higher than the mean, leading to values greater than 1.

## 2.4 Modeling population evolution

The aim of this last section is to calculate the coral population recovery times, knowing the connectivity patterns between the reefs. We consider that each reef is associated to a different population. As in total 990 reefs are distinguished, there are also 990 different *Acropora Cervicornis* populations. The initial coral cover of all reefs is set to 30% of their maximum level and the time for each reef to recover till 90% of this maximum capacity is calculated. The connectivity patterns are introduced in the model through the connectivity matrices previously generated. The annual variability due to changing hydrodynamics is calculated and in a second time biological uncertainty is assessed. The modelization can be approached in two different ways, by considering the populations' size either as a number of polyps, either as a number of colonies. This study follows the first approach.

### 2.4.1 Model equations and parameters

The following equation (E. Hanert, personal communication) is used to model the population evolution. It is resolved using an explicit Runge-Kutta scheme.

$$\frac{dS_j}{dt} = (1 - c_j(t)) \left( RS_j(t) + r(t) s \sum_i C^*_{ij}(t) \right) \tag{2.32}$$

discretised as :

$$S_{j,n+1} = S_{j,n} \left[ 1 + \Delta t \, R(1 - c_{j,n}) \right] + \Delta t \, r_n \left( \sum_i C^*_{ij,n} \right) s \, (1 - c_{j,n}) \tag{2.33}$$

where $S_{j,n}$ is the size of the coral population on reef $j$ (counted as the number of coral polyps) at time step $n$, $R$ is the net clonal growth rate per polyp, $c_{j,n}$ is the coral cover fraction of reef $j$, $r_n$ is the recruitment factor described below, $s$ is the survival rate of newly settled coral larvae and $C^*_{ij,n}$ is the element of the biological representative connectivity matrix $C^*$ with reef $i$ as source and reef $j$ as sink, so that the term $\sum_i C^*_{ij,n}$ corresponds to total number of incoming larvae at reef $j$ at time step $n$. The biological representative matrix $C^*_{ij}$ represents the actual number of larvae exchanged between the reefs and is created as follow :

$$C^*_{ij,n} = \widetilde{C}_{ij} \, c_{i,n} \, \frac{A_i}{A_{\text{polyp}}} \, e_{\text{polyp}} \tag{2.34}$$

where $\widetilde{C}_{ij}$ is the normalized connectivity matrix which gives the proportion of all the larvae released on reef $i$ that arrive on reef $j$ assuming a coral cover of 100% (cf. section 2.3), $c_{i,n}$ is the coral cover fraction of the source reef $i$, $A_i$ is its surface area, $A_{\text{polyp}}$ is the surface area of a single polyp and $e_{\text{polyp}}$ is the number of eggs produced per polyp.

The equation 2.32 accounts for asexual growth, in other words clonal expansion, through the term $(1 - c_j(t)) \, R \, S_j(t)$ as well as for sexual recruitment through the term $(1 - c_j) \, r(t) \, s \sum_j C^*_{ij}(t)$. This last term is the growth attributed to newly settling larvae and hence depends on the amount of incoming larvae, thus the connectivity matrix. The factor $(1 - c_j)$ reflects that as a population regrows, the free space on the corresponding reef decreases causing the clonal growth to slow down and settlement success to decline. The maximum coral cover capacities are fixed at 40% of each reefs' total area which seems to represent the state of a reasonably healthy reef (Hanert, Personal Communication).

Literature concerning the biological parameters of *Acropora Cervicornis* needed in this model is scarce. Nevertheless, the values chosen are as accurate as possible. The surface area $A_{\text{polyp}}$ is taken to be $1.767 * 10^{-6}\, m^2$, corresponding to the mean surface area of *Acropora Tenuis* as defined by Leuzinger et al. (2003). The net clonal growth rate $R$ is set to 0.07 year$^{-1}$ (Gladfelter et al., 1978). As Szmant (1986) and Soong (1991) respectively observed an egg production of $\pm 35$ eggs and $\pm 8$ eggs, the value for the number of eggs produced per polyp $e_{\text{polyp}}$ chosen in this study is 21, which is the mean of both observations. Also the survival rate $s$, fixed at 12%, corresponds to the mean of two different observations : 11% (Szmant and Miller, 2006) and 13% (Ritson-Williams et al., 2010).

A recruitment factor $r_n$ is implemented in the model to accurately simulate spawning rates that are not constant all year long. In the case of *Acropora Cervicornis* a single spawning event occurs once a year, at the full moon of August (cf. section 1.1.1). This is modeled with a normal probability density function with its mean fixed on mid-August and its standard deviation set to $\sigma = 1/24$, repeated each year. This function is showed in figure 2.6 for three consecutive years.

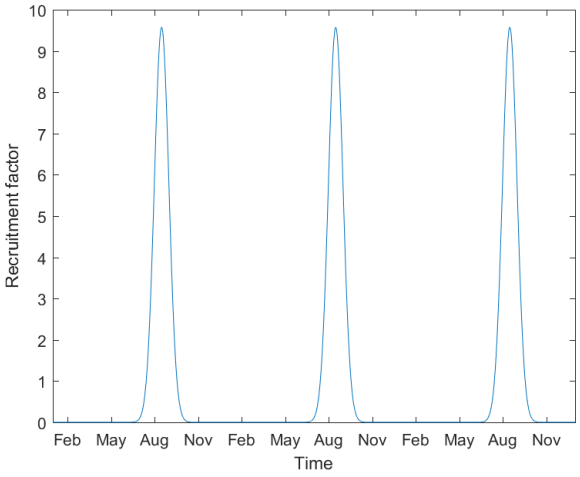


Figure 2.6: Recruitment Factor Function

### 2.4.2 Interannual hydrodynamic variability

Although the coral cover changes are computed over several decades, the connectivity matrix used in the model is not time-dependent. To account for annual hydrodynamic variability the model is run 4 times with in turn the connectivity matrices of 2007, 2008, 2009 and 2010. The model is run a fifth time using a merged connectivity matrix. This matrix is calculated by adding the connectivity matrices of 2007, 2008, 2009 and 2010 (equation 2.35). To obtain the normalized merged connectivity matrix $\widetilde{C}_{merged}$, each element of the previously calculated matrix is divided by the total number of particles seeded on the corresponding source reef over the four years (equation 2.36).

$$C_{merged}\{ij\} = C_{2007}\{ij\} + C_{2008}\{ij\} + C_{2009}\{ij\} + C_{2010}\{ij\} \tag{2.35}$$

$$\widetilde{C}_{merged}\{ij\} = \frac{C_{merged}\{ij\}}{S_{2007}\{i\} + S_{2008}\{i\} + S_{2009}\{i\} + S_{2010}\{i\}} \tag{2.36}$$

### 2.4.3 Biological variability

Considering the great uncertainty about the biological parameters implemented in this model, two additional scenarios are computed, with the purpose to define an incertitude margin. The first scenario supposes low values for the biological parameters resulting in slower coral cover recoveries, whereas the second one supposes high values resulting contrariwise in quick recoveries (table 2.2). The initial values of the biological parameters correspond to the mean of the low and high values.

| **Parameter** | **Low value** | **High value** | **Initial value** |
|---|---|---|---|
| Eggs per polyp $e_{polyp}$ [1] | 8 | 35 | 21 |
| Post-settlement survival $s$ [2] | 11% | 13% | 12% |
| Clonal growth $R$ | 0.035 $year^{-1}$ | 0.105 $year^{-1}$ | 0.07 $year^{-1}$ |
| Polyp suface area $A_{polyp}$ [3] | 1.72 $mm^2$ | 1.814 $mm^2$ | 1.767 $mm^2$ |

Table 2.2: Low, high and initial values of the biological parameters taken for the negative, positive and initial scenarios. [1] Szmant, 1986 and Soong, 1991. [2] Szmant and Miller, 2006 and Ritson-Williams et al., 2010. [3] Porter, 1976.

The values taken for $e_{polyp}$, $s$ and $A_{polyp}$ are the lowest and highest found in literature. The clonal growth rate range is much more difficult to define. The growth rates of an *Acropora Cervicornis* branch range between 40 and 260 mm/year (Huston, 1984), resulting in an annual clonal productivity that can easily exceed 100%. However, this rate is not representative of what is seen on the field. Indeed, over the last decades, *A.Cervicornis* has seen its populations decline of >95% (Drury et al., 2017). This is mainly due to bleaching events, but despite *A. Cervicornis'* remarkable high productivity (i.e. additional growth/initial size), the coral is apparently not capable to recover between two bleaching events. Its extreme sensitivity to environmental conditions and the negative effect of competitors and predators (Schopmeyer et Lirman, 2015), slow down its recovery. We took thus minimum and maximum clonal growth rates that seem to reflect realistically the coral's population dynamics on the field.

# 3 Results and discussion

## 3.1 Simulating the hydrodynamics

The hydrodynamic simulation computed, for each point of the domain, the velocity vector $(u, v)$ as well as the sea surface elevation. The time step used in this model was 15 minutes and the results were extracted for each hour over each simulation period.

The figure 3.1 gives an idea of SLIM's output by showing the instantaneous velocities amplitude around Florida at midnight on August $31^{st}$ 2007. It can be seen that, on that moment, velocities have a greater amplitude along the northern part of the east coast and are in general higher in the deeper part. Though, a light blue area shows relatively high velocities at the entrance of the GoM where the depth is small. Also, the deepest part (up to 2500m deep), in the south-west of the mesh, shows here low velocities compared to the less deep part in the north-east. The picture 3.2 is zooming on the Marquesas Keys and the extremity of Key West, showing this time the instantaneous velocities vectors for the same moment. The Keys are shown by the shapes filled in white. The orientation of each arrow shows locally the direction of the current, their color and size give information about the velocity amplitude. The difference in arrows density is due to the difference in size of mesh elements. The areas closer to the Keys would need a bigger zoom in order to distinguish the different arrows and their orientation. The dark blue color indicates the areas with slow velocities. It actually corresponds to the coral reefs locations, which can be explained, as Frys (2017) outlined, as a result of the ten times higher Manning coefficient taken for reef areas.

The output given by SLIM was compared to other existing data in order to validate the model. First, the velocities' amplitudes and directions were compared for the validation points 1 to 8 (see figure 2.3) with the data given by HYCOM. As HYCOM does not take the tides into account, SLIM's output was also compared to HYCOM data, increased by the tidal currents. Then, the surface elevations were compared to real measurements at the points 9 to 11 (see figure 2.3).

### 3.1.1 Validation of the velocities

Figures 3.3, 3.4 and 3.5 show the comparison of the currents for each year, over the simulation period, respectively for the points 1, 5 and 6. Those three points are located on the outer shelf. The point 6 is situated off the coast in a deep water area. As SLIM model was set to tend towards HYCOM on the boundaries and in deep water, it is expected to observe close values between SLIM and HYCOM results for that point. The points 1 and 5 are relatively near the shore and in shallow water. Bigger differences between the results of the two models are thus expected. To broaden the view on the results both points are shown here. The point 1 is situated at the entrance of the GoM, at the beginning of the Keys, as the point 5 is located to the north along the Florida east coast. The comparison was done for the four years in order to identify any variability or steadiness between the different years.

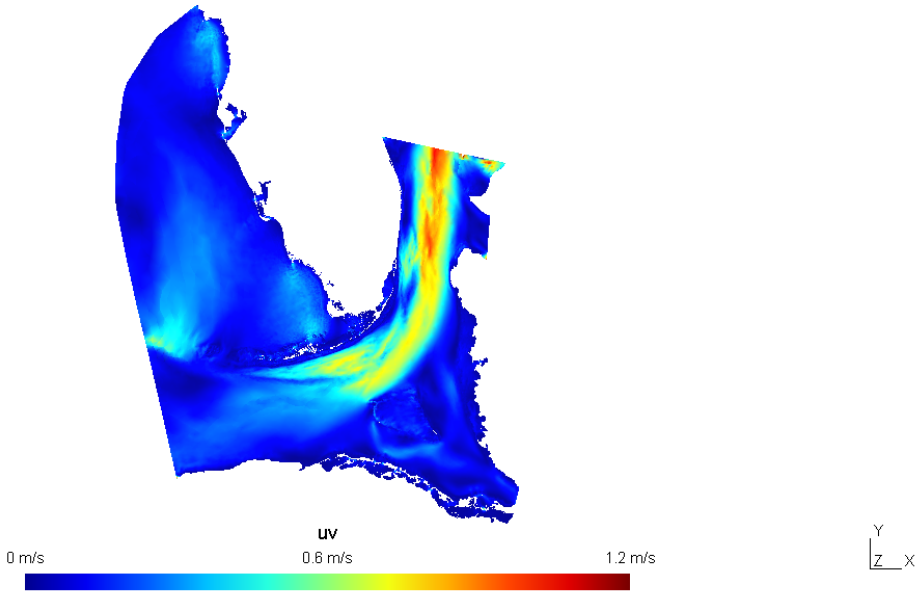


Figure 3.1: SLIM's output: Instantaneous velocities amplitude around Florida at midnight on August $31^{st}$ 2007.

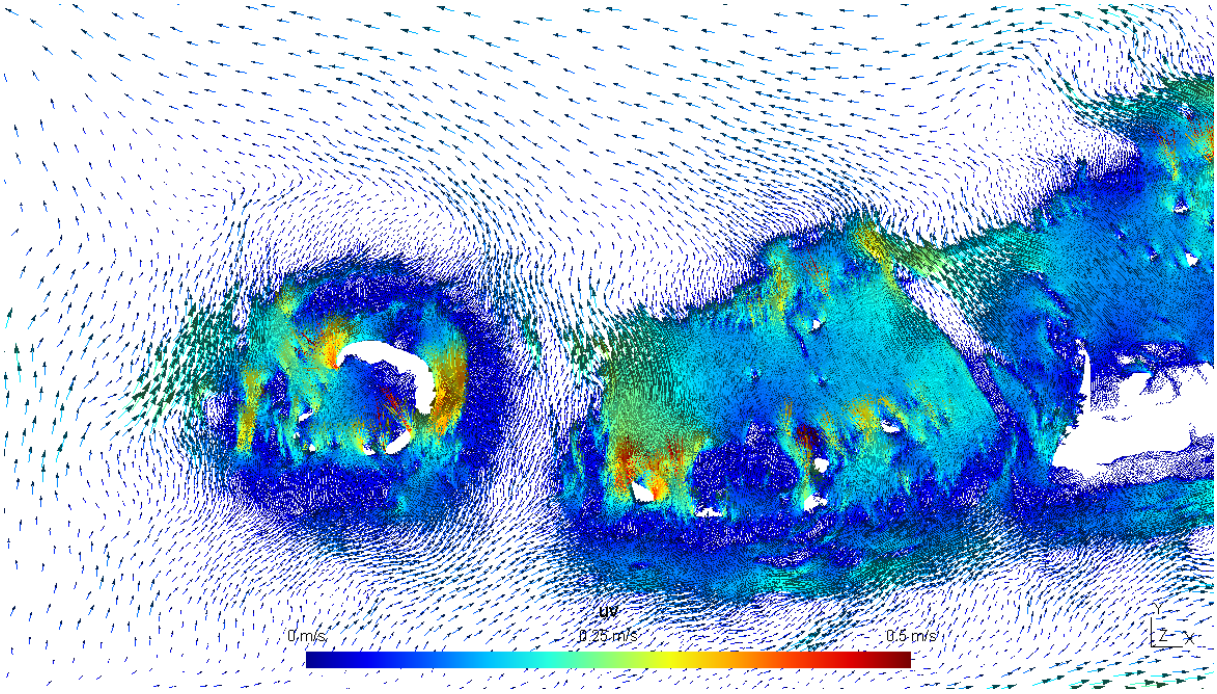


Figure 3.2: SLIM's output: Velocities vectors around the Marquesas Keys and Key West at midnight on August $31^{st}$ 2007.

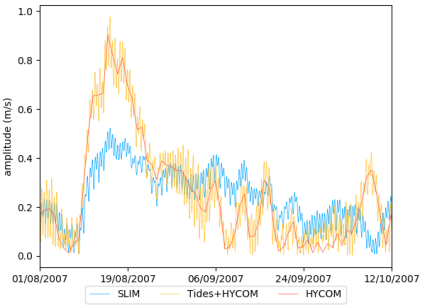


(a) Amplitude 2007

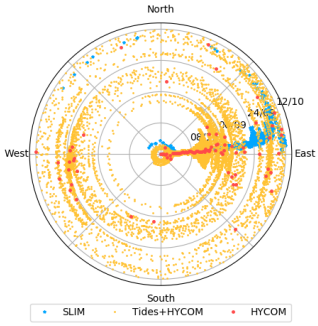


(b) Direction 2007

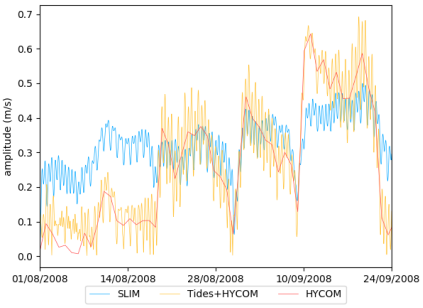


(c) Amplitude 2008

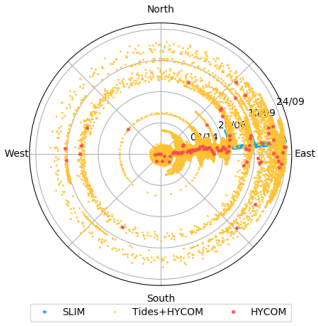


(d) Direction 2008

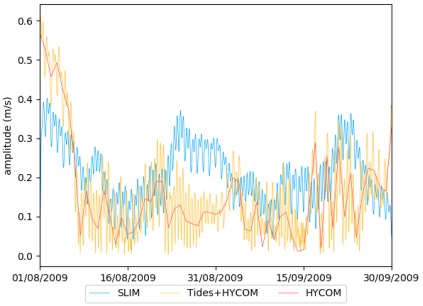


(e) Amplitude 2009

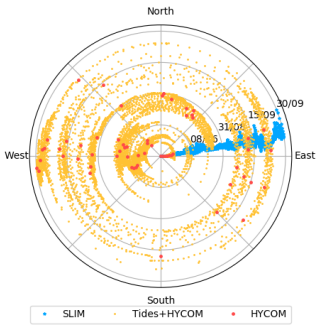


(f) Direction 2009

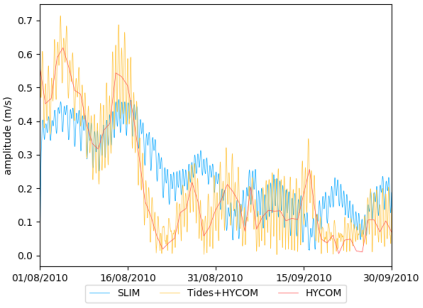


(g) Amplitude 2010

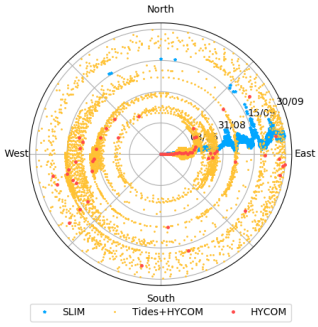


(h) Direction 2010

Figure 3.3: Current amplitudes and directions for the validation point **number 1**, for the years 2007, 2008, 2009 and 2010. On each graph the results from SLIM simulation are given in blue as the results from HYCOM simulation are given in red and orange when tides are added.

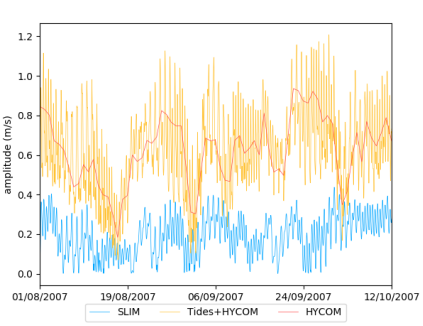


(a) Amplitude 2007

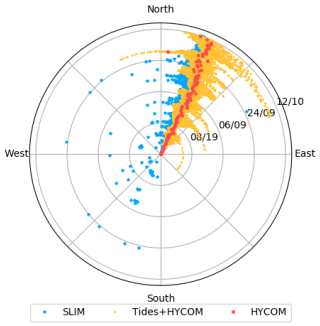


(b) Direction 2007

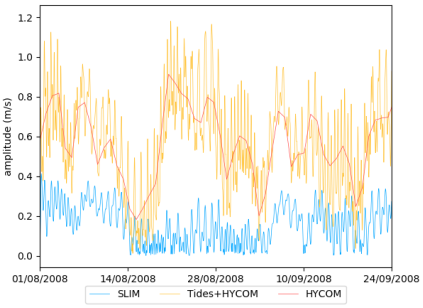


(c) Amplitude 2008

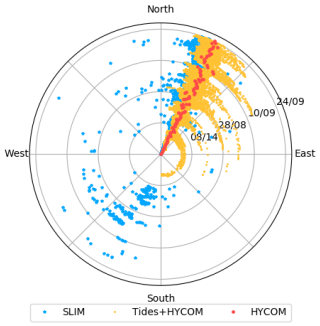


(d) Direction 2008

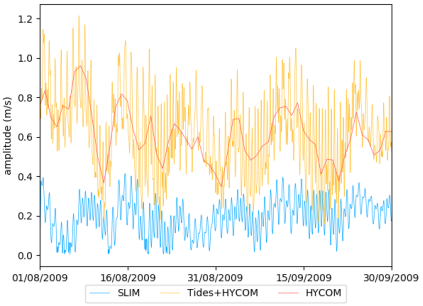


(e) Amplitude 2009

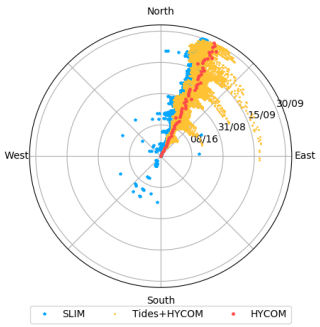


(f) Direction 2009

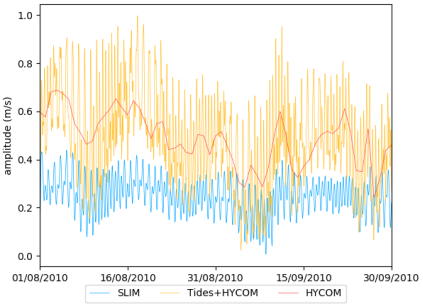


(g) Amplitude 2010

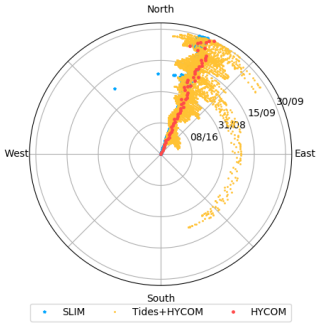


(h) Direction 2010

Figure 3.4: Current amplitudes and directions for the validation point **number 5**, for the years 2007, 2008, 2009 and 2010. On each graph the results from SLIM simulation are given in blue as the results from HYCOM simulation are given in red and orange when tides are added.

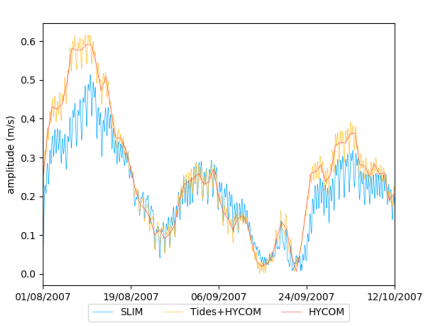


(a) Amplitude 2007

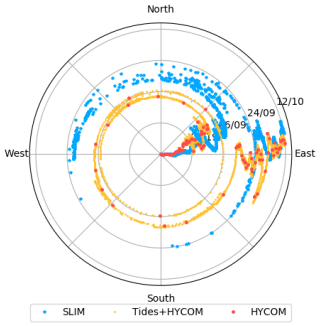


(b) Direction 2007

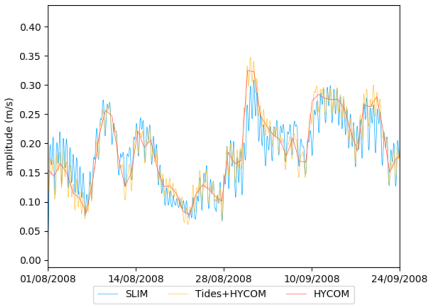


(c) Amplitude 2008

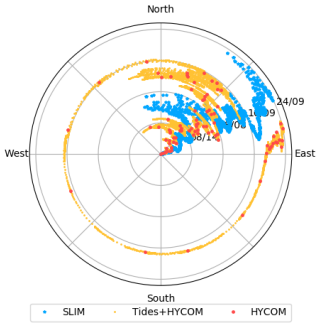


(d) Direction 2008

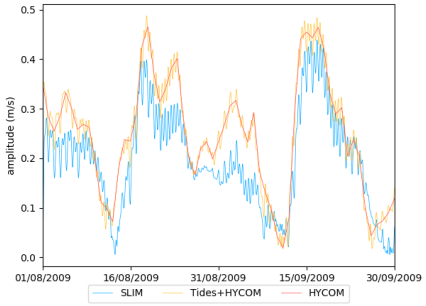


(e) Amplitude 2009

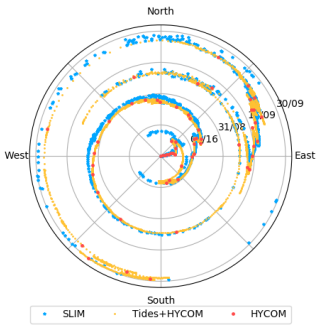


(f) Direction 2009

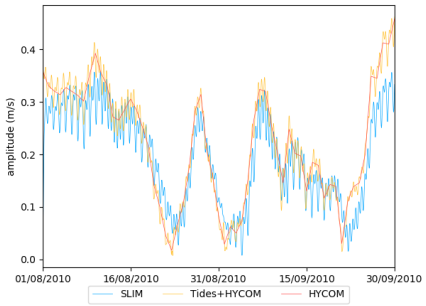


(g) Amplitude 2010

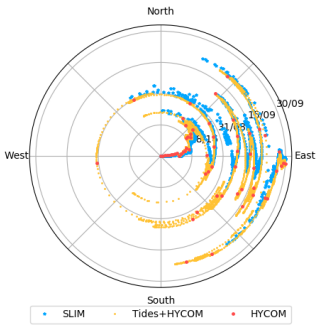


(h) Direction 2010

Figure 3.5: Current amplitudes and directions for the validation point **number 6**, for the years 2007, 2008, 2009 and 2010. On each graph the results from SLIM simulation are given in blue as the results from HYCOM simulation are given in red and orange when tides are added.

For each point the direction of the current calculated by SLIM is generally constant over the simulation period and over the years. At point 1, the direction shown by SLIM is almost constantly east with a slight component towards the north. Only around beginning of August and October 2007 and around mid-September 2010, the current seems to flow more towards the north and the west. On those specific times the amplitudes seem to be at the lowest. However, the directions computed by HYCOM are much more variable, varying from east to west. At point 5, the current is generally flowing towards north-northeast according to both SLIM and HYCOM. However, SLIM's results are slightly more changing especially in 2007 and 2008. At point 6, the directions given by SLIM and HYCOM seem to be roughly the same. However, if the main direction is north-east, there is still a great variability over the simulation period. As this great fluctuation is also depicted by HYCOM without the tides (red points), this shows that is not a tidal effect but might describe eddies modeled by HYCOM. The changes in direction modeled by SLIM are explained by the fact that SLIM is tending to HYCOM in greater depth according to the global circulation forcing.

It seems that for the points near the shore, point 1 and 5, SLIM is giving directions parallel to the coast whereas it gives a variable direction at the point 6 because of the relaxation toward HYCOM. Morevoer, HYCOM is giving variable directions at point 1, which are looking like the ones shown at point 6. It seems that the effect of the coast and of the shallow water is not considered by HYCOM at point 1 as much as it is by SLIM.

The amplitudes are shown on the left part of the figures 3.3 to 3.5. In general, the velocities are smaller than $0.5m/s$ for the selected points, which is equal to a maximum current of 1 knot. In the appendix B.1, a velocity up to $1m/s$ (2 knots) is shown for the validation point 8, which confirms figure 3.1, where a maximum of a $1.2m/s$ is seen in the north-east on August $31^{st}2007$.

The velocity at point 1 is going up to $0.5\,m/s$. Over one simulation period, SLIM seems sometimes to overestimate the velocity amplitude compared to HYCOM and sometimes to underestimate it. However, both models show a similar trend. During the years 2007 and 2010, velocities seem to decrease from end of August on. Apart from that, the velocities seem variable over the different years and over each simulation period. At point 5, SLIM is underestimaiting the velocity compared to HYCOM. Indeed, SLIM's results vary there between $0m/s$ and $0.4m/s$ whereas HYCOM shows velocities up to $1.2m/s$. The tides also seem to have a greater amplitude with HYCOM than wih SLIM. However both models show same trends at the same moment; their maxima are aligned in time. It should be noted that the axes of amplitude are not the same from one figure to another. Therefore, the variation of amplitude at point 5 is of the same order of magnitude as at point 1. At point 6, SLIM's velocities amplitudes are very close to HYCOM's values. The same was observed for the directions. That is explained by the fact that this point is located in deep water and therefore, SLIM's values are tending to HYCOM's.

A strong current is modeled between the west coast of Florida and the Bahamas Banks that corresponds to the Florida Current coming from the Loop Current in the GoM. It is flowing parallel to the coast, off the outer shelf of the Keys towards the north of the studied domain, where it reaches its higher amplitude. The directions and amplitudes computed by SLIM are not absurd. Their tendency coincide with HYCOM's outputs. SLIM results are tending to HYCOM's output in deep water, which is the expected effect of the relaxation towards HYCOM. In shallower water, however, SLIM is producing different results which illustrates the interest of using it in this study. SLIM is showing currents more parallel to the Keys than HYCOM at point 1. It can be imagined that both scenarios would lead to very different larvae dispersion at this point. The validation points are mainly placed off the eastern coast of the Keys and the main land of Florida and hence, do not give any information on the western coast current.

### 3.1.2 Validation of the surface elevation

The surface elevation computed by SLIM was compared at the points 9, 10 and 11 to real measurements, done over each simulation period. The measurement data were found on the European Comission's Institute for Protection and Security of the Citizens website (`http://webcritech.jrc.ec.europa.eu/`). The comparison was not directly made on the raw model output and buoy measurements but on the tidal components constituting each of those two time series. They were computed by TAPPY for each point and for each year, over the simulation period.

In the tables 3.1 and 3.2, are shown the four main harmonic tidal constituents ($M_2$, $K_1$, $S_2$, $O_1$) for each year and for the validation points 9 and 10 respectively. Indeed, for the points 9 and 10, those constituents correspond almost perfectly to the four constituents with the greater amplitude observed. The reason is to keep the table clear and ease the comparison by focusing on the main constituents. The results of the validation point 11 are not shown here but can be found in the appendix B.2.

In each of those tables, the amplitude of the constituent computed by TAPPY is given for SLIM data and measurement data. The relative error of SLIM compared to the measurements is calculated as the absolute difference between the two values divided by the measured value. The phase lag relative to the theoretical equilibrium tide phase is also given for both SLIM and measurement data. The absolute error is the smaller difference on the trigonometrical circle between the two phase lags, given in degrees (the maximum absolute difference is then 180°, when the two phases are opposed on the trigonometrical circle).

At point 9 (table 3.1) the relative error is varying from 1 to 7 % for the constituent S2, which are quite low values. It is around 15 % for the constituents M2 and O1 and reaches up to 29 % for the constituent K1, which is a significant error. However the range of error is similar for each component over the different years. The absolute error between the phase lags ranges from 30° to 60°, which are significant errors. Again, for each constituent, the error on the phase lag is similar over the different years. The tables 3.3 and 3.4 show the variability in time of the error respectively on the amplitude and on the phase lag, for the point 9. The mean ($\mu$) and standard deviation ($\sigma$) over the four years is given for each constituent. The standard deviation is going up to 4.1% for the amplitude and 6°for the phase lag. Despite high absolute errors on the phase lag, their standard deviations are indeed rather small compared to them. It shows that SLIM is at least consistent from one year to another.

At point 10 (table 3.2), the relative error on the amplitude is less than 10% for the years 2008, 2009 and 2010. For 2007, however, it is much larger and especially the amplitude of the constituent S2 that is overestimated by 65% by SLIM. The error on the phase lags is ranging from 50° to 117°. The variability is shown in tables 3.5 and 3.6. The mean of the errors on the amplitude is ranging from 8 to about 21 % with a standard deviation from 1.4 to 6.6 %. However, it can be noticed that if 2007 was removed both the mean and the deviation would become lower. The standard deviation of the errors on the phase lag is also kept under 10° and would be even lower without the year 2007.

Those results show a range of errors on the amplitude that, in general, are kept low for the four main constituents. However, some exceptions are noticed such as the error on the constituent K1 at point 9 or on all constituents for the year 2007 at point 10. On the other hand, the errors on the phase lags are always significant and are varying over a large range of values from one point to another and one constituent to another. Their low variability for a given point and a given constituent over different years shows that SLIM is consistent in its computation of

the surface elevation. Moreover, in shallow water, tidal phase lags are influenced by the level of bottom friction and by the water depth (Speer, 1984). The water depth that was set to a minimum of $5m$ and hence overestimated by SLIM in some shallow water area, could lead to different phase lag than the real measured ones. This could explain the great phase lag errors computed for points located very close to shore.

| | Tidal constituents | Amplitude (cm) | | | Phase lag (°) | | |
|---|---|---|---|---|---|---|---|
| | | SLIM | Measures | Error (%) | SLIM | Measures | Absolute Error |
| 2007 | M2 | 22,94 | 27,47 | 16 % | 185,0 | 144,3 | 40,7 |
| | O1 | 10,76 | 12,59 | 15 % | 62,9 | 3,4 | 59,6 |
| | S2 | 8,33 | 8,63 | 3 % | 200,4 | 168,6 | 31,8 |
| | K1 | 6,95 | 8,95 | 22 % | 45,7 | 11,0 | 34,7 |
| 2008 | M2 | 21,74 | 26,54 | 18 % | 185,2 | 146,4 | 38,8 |
| | O1 | 11,41 | 13,9 | 18 % | 62,3 | 1,4 | 60,9 |
| | S2 | 8,23 | 8,44 | 2 % | 213,6 | 175,2 | 38,4 |
| | K1 | 6,75 | 9,45 | 29 % | 58,7 | 15,2 | 43,5 |
| 2009 | M2 | 22,78 | 27,17 | 16 % | 183,2 | 145,8 | 37,4 |
| | O1 | 11,41 | 13,04 | 13 % | 62,9 | 1,9 | 61,0 |
| | S2 | 8,71 | 8,63 | 1 % | 211,2 | 172,8 | 38,3 |
| | K1 | 7,16 | 8,85 | 19 % | 48,6 | 12,8 | 35,7 |
| 2010 | M2 | 23,68 | 27,12 | 13 % | 180,4 | 146,4 | 34,0 |
| | O1 | 11,12 | 12,88 | 14 % | 60,4 | 3,6 | 56,8 |
| | S2 | 9,31 | 8,72 | 7 % | 206,1 | 170,5 | 35,6 |
| | K1 | 6,1 | 8,21 | 26 % | 46,2 | 17,6 | 28,7 |

Table 3.1: Comparison of the four main harmonic tidal constituents between SLIM computed surface elevations and elevation measurements at **point 9**, for the years 2007, 2008, 2009 and 2010.

| | Amplitude error | | | | | |
|---|---|---|---|---|---|---|
| | 2007 | 2008 | 2009 | 2010 | $\mu$ | $\sigma$ |
| M2 | 28,0 % | 2,2 % | 1,3 % | 0,8 % | 8,1 % | 1,4 % |
| O1 | 24,5 % | 1,7 % | 4,8 % | 4,3 % | 8,8 % | 3,6 % |
| K1 | 17,2 % | 9,4 % | 2,3 % | 7,2 % | 9,0 % | 6,3 % |
| S2 | 65,3 % | 5,2 % | 7,0 % | 7,6 % | 21,3 % | 6,6 % |

Table 3.5: Variability over the years 2007, 2008, 2009 and 2010 of the relative error on the four main constituents amplitude, for the **point 10**.

### 3.1.3 Limitations

While those comparisons with HYCOM as well as with real measurements show the consistency of the model, some of its limitations should be pointed out. Modeling the hydrodynamics in the FCRT is used as a tool to understand the main patterns in larvae connectivity but the real hydrodynamics can not be perfectly reproduced. First, the use of depth integrated model is based on the assumption that water should be vertically well mixed as well as the larvae inside this water column (Thomas, 2015). This 2D model is a cost-effective way to accurately represent complex topography such as coral reefs, with a high horizontal resolution. According

| | Tidal constituents | Amplitude (cm) | | | Phase lag (°) | | |
|---|---|---|---|---|---|---|---|
| | | SLIM | Measures | Error (%) | SLIM | Measures | Absolute Error |
| 2007 | M2 | 22,94 | 17,92 | 28% | 185,0 | 67,5 | 117,5 |
| | O1 | 10,76 | 8,64 | 25% | 62,9 | 353,4 | 69,6 |
| | S2 | 8,33 | 5,04 | 65% | 200,4 | 102,9 | 97,5 |
| | K1 | 6,95 | 5,93 | 17% | 45,7 | 357,6 | 48,1 |
| 2008 | M2 | 17,2 | 17,58 | 2% | 166,4 | 68,0 | 98,4 |
| | O1 | 9,11 | 8,96 | 2% | 63,7 | 350,8 | 73,0 |
| | K1 | 5,19 | 5,73 | 9% | 61,8 | 6,1 | 55,7 |
| | S2 | 4,84 | 4,6 | 5% | 192,7 | 107,5 | 85,2 |
| 2009 | M2 | 18,17 | 17,93 | 1% | 165,5 | 67,5 | 98,0 |
| | O1 | 9,12 | 8,7 | 5% | 63,4 | 351,9 | 71,5 |
| | K1 | 5,69 | 5,56 | 2% | 53,5 | 4,6 | 48,9 |
| | S2 | 5,03 | 4,7 | 7% | 190,8 | 105,1 | 85,7 |
| 2010 | M2 | 17,93 | 17,78 | 1% | 164,0 | 67,8 | 96,2 |
| | O1 | 9,06 | 8,69 | 4% | 65,2 | 352,4 | 72,8 |
| | K1 | 5 | 5,39 | 7% | 59,6 | 4,8 | 54,8 |
| | S2 | 4,97 | 4,62 | 8% | 186,1 | 100,8 | 85,2 |

Table 3.2: Comparison of the four main harmonic tidal constituents between SLIM computed surface elevations and elevation measurements at **point 10**, for the years 2007, 2008, 2009 and 2010.

| | Amplitude error | | | | | |
|---|---|---|---|---|---|---|
| | 2007 | 2008 | 2009 | 2010 | $\mu$ | $\sigma$ |
| M2 | 16,5 % | 18,1 % | 16,2 % | 12,7 % | 15,9 % | 2,3 % |
| O1 | 14,5 % | 17,9 % | 12,5 % | 13,7 % | 14,7 % | 2,3 % |
| S2 | 3,5 % | 2,5 % | 0,9 % | 6,8 % | 3,4 % | 2,5 % |
| K1 | 22,3 % | 28,6 % | 19,1 % | 25,7 % | 23,9 % | 4,1 % |

Table 3.3: Variability over the years 2007, 2008, 2009 and 2010 of the relative error on the four main constituents amplitude, for the **point 9**.

| | Phase lag(°) error | | | | | |
|---|---|---|---|---|---|---|
| | 2007 | 2008 | 2009 | 2010 | $\mu$ | $\sigma$ |
| M2 | 40,7 | 38,8 | 37,4 | 34,0 | 37,7 | 2,8 |
| O1 | 59,6 | 60,9 | 61,0 | 56,8 | 59,6 | 2,0 |
| S2 | 31,8 | 38,4 | 38,3 | 35,6 | 36,0 | 3,1 |
| K1 | 34,7 | 43,5 | 35,7 | 28,7 | 35,6 | 6,1 |

Table 3.4: Variability over the years 2007, 2008, 2009 and 2010 of the absolute error on the four main constituents phase lag, for the **point 9**.

to Burgess (2007), this is required to avoid overestimating larval dispersal. Furthermore, Frys (2017) mentioned the fact that the complex eddies coming from the GoM (see subsection 1.2.1) are occurring in the zone of transition between HYCOM relaxed regions and free of forcing study area. The eddies are therefore not well represented here by SLIM. Lastly, the waves breaking set up are not taken into consideration, even though it induces currents that can "potentially equal if not dominate the tidal current over the reefs" (Thomas, 2015)(Monismith, 2007).

| | Phase lag(°) error | | | | | |
|---|---|---|---|---|---|---|
| | 2007 | 2008 | 2009 | 2010 | $\mu$ | $\sigma$ |
| M2 | 117,5 | 98,4 | 98,0 | 96,2 | 102,5 | 10,0 |
| O1 | 69,6 | 73,0 | 71,5 | 72,8 | 71,7 | 1,6 |
| K1 | 48,1 | 55,7 | 48,9 | 54,8 | 51,9 | 3,9 |
| S2 | 97,5 | 85,2 | 85,7 | 85,2 | 88,4 | 6,1 |

Table 3.6: Variability over the years 2007, 2008, 2009 and 2010 of the absolute error on the four main constituents phase lag, for the **point 10**.

## 3.2 Modeling larval dispersal

A total of $3.55 * 10^6$ particles were released on the reefs during the simulations of 2007 and 2008 and a total of $3.11 * 10^6$ in 2009 and 2010, with an equal density on each reef. Figure 3.6 shows the initial distribution of the particles on the different reefs, the day the *Acropora Cervicornis* corals spawn, i.e. the full moon of August. As this initial distribution only depends on the reefs' locations, it is the same each year.

At each time step the coordinates of the particles' positions can be exported, so to track their paths. Figure 3.7 is a close up view on the Marquesas Keys at three different time steps of 2009's simulation (days 0, 5 and 10 after spawning). On the spawning date the larvae are confined on the reef structures, to progressively spread, mingle and in this case, take a same northeastward direction away from the islands. The level of spreading and mixing as well as the movement directions and speeds vary across the FCRT since they depend on the local hydrodynamics.

The series of snapshots from figure 3.8 show the successive positions of the particles released on nine different reefs throughout the FCRT, on the full moon of 2009 (06 August), five days later (11 August), ten days later (16 August) and fifteen days later (21 August). The larvae can be divided in three groups according to their origin reef. The first group contains the larvae seeded west of the Marquesas Keys, around the **Dry Tortugas** (shown in green), which are quite quickly transported northward. As there are no reefs north of the Dry Tortugas, these larvae won't be able to settle and will be lost. The second group is composed of the larvae seeded in the **inner shelf** of the Keys (pink, brown and orange), which are more stationary so that they will probably settle onto their origin reefs or neighbouring reefs. Though over time they seem to be slowly attracted away from the inner shelf towards the outer shelf. This phenomenon is the most visible for the orange larvae of figure 3.8, however it remains very slight. The larvae seeded in the **outer shelf** area and along the **east coast** of Florida (dark blue and purple; red, light green and yellow) form the last group. They follow a same path that seems to be strongly influenced by the Florida Current, coming from the reefs south of the Lower Keys, plodding on past Key Largo and then moving further northward. This trajectory is consistent with the current directions of the validation points 1, 3, 4 and 5 located within the FC (cf. figures 3.3, 3.4 and appendix B.1). Reefs located near the southeastern Keys are thus able to provide larvae to numerous reefs along the outer shelf region of the Keys and the east coast of Florida. Though in order for the larvae to settle, they must pass right over the destination reefs, so if the FC carries them away in a more seaward direction than the reefs' locations, the larvae would be lost and settlement would decrease. According to the successive positions of the blue and purple larvae on the snapshots of figure 3.8, the risk of this seems to be maximum along the northern Keys and Biscayne National Park, where the radius of curvature of the FCRT is the highest. It should be noted that SLIM does not model the multiple cyclonic eddies present all along the Florida Keys. These eddies could notably influence the particles' paths by slowing down their voyage

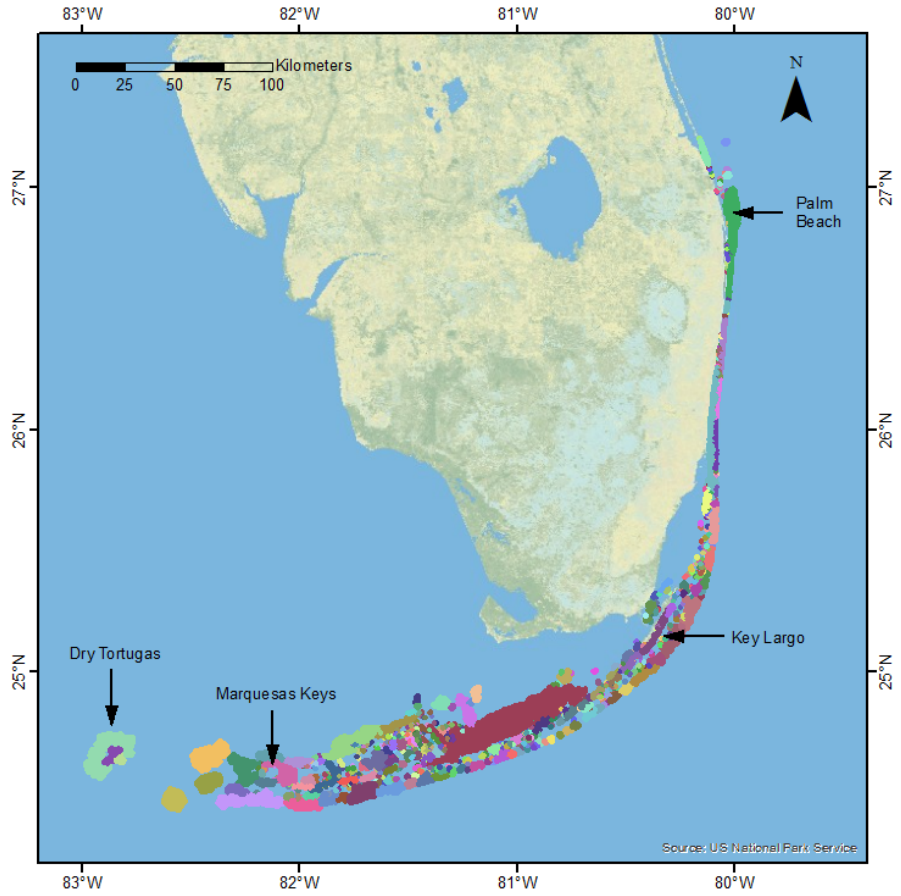


Figure 3.6: Initial distribution of the particles on the full moon of August (= spawning date). Each dot represents a particle. Particles seeded on a same reef are drawn in the same color. The brown/burgundi dots correspond to the particles of the Vaca Reef. This is the largest reef of the FCRT, with a surface of about 860 $km^2$.

and retaining them closer to their mother reefs.

The forcings applied to the hydrodynamics model (the wind stress, the tides and the large scale water circulation) differ each year, resulting in varying currents, and thenceforth in varying particle tracks. Furthermore, the spawning events occur each year on a different day. As the currents have a seasonal component, the positions after a same time lapse are strongly influenced by the spawning date. This interannual variability is illustrated in figure 3.9. This figure shows the larvae's positions ten days after their release for each of the four simulation years. Again, the particles are colored depending on their origin reef.

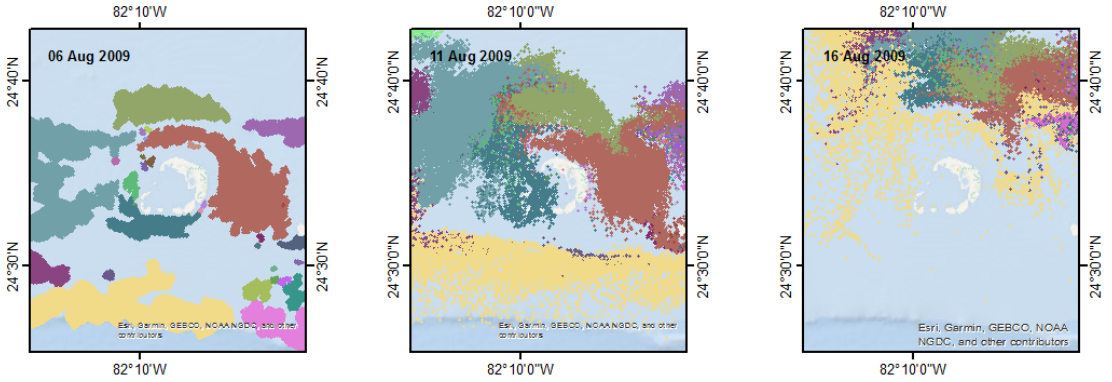


Figure 3.7: Snapshots of the larval dispersal simulation in the region of the Marquesas Keys on the first day of 2009's simulation (August 06), on the fifth day (August 11) and on the tenth day (August 16). The currents seem to transport the particles Northeastward.

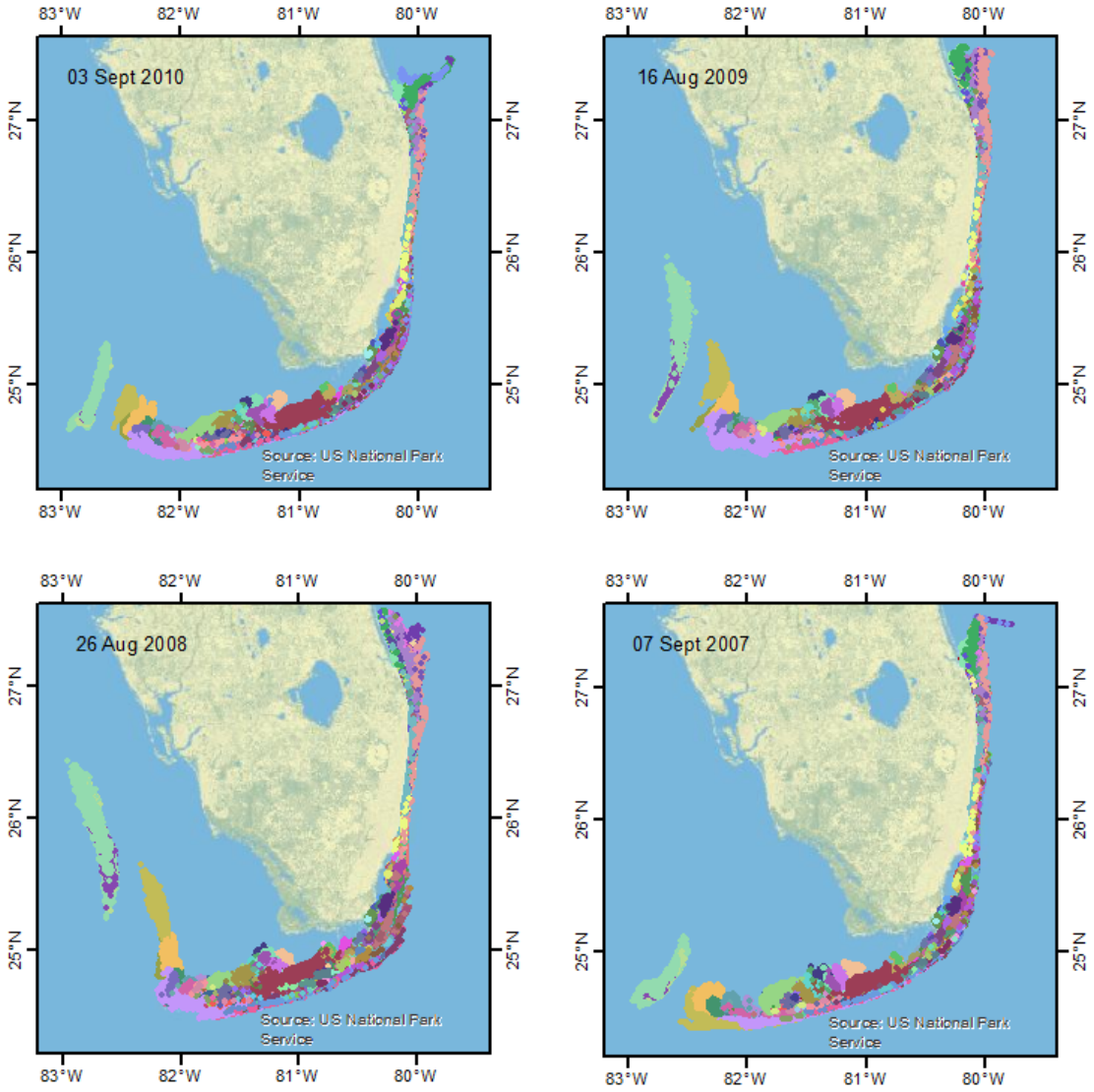


Figure 3.9: Snapshots of the larval dispersal simulation on the 10th day after the full moons of 2010, 2009, 2008 and 2007.

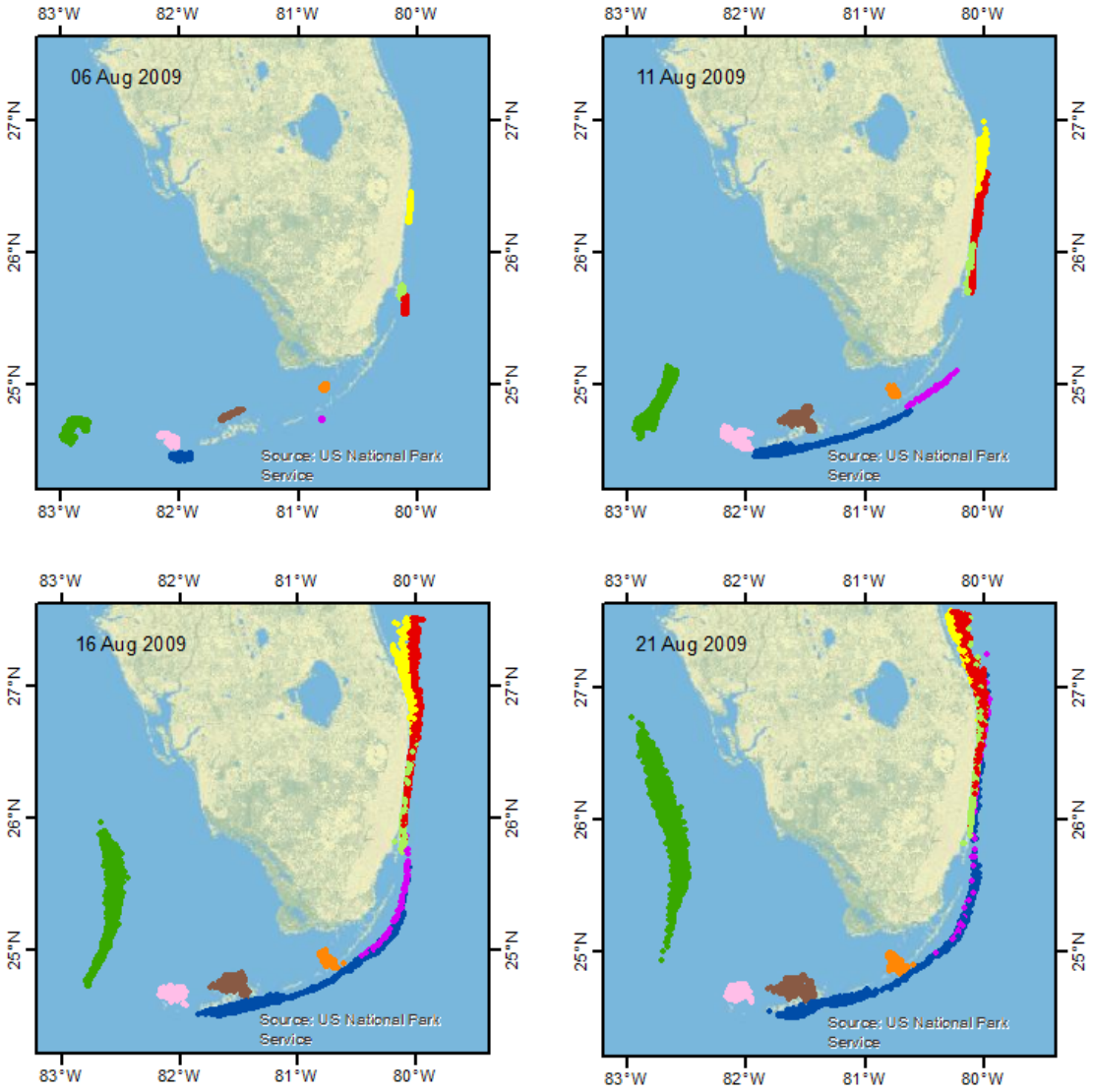


Figure 3.8: Snapshots of the 2009 larval dispersal simulation, on the spawning date, 5 days later, 10 days later and 15 days later. Only the larvae released on nine different reefs are showed.

The earliest spawning date regarding the annual calendar is 6 August 2009, then 16 August 2008, 24 August 2010 and lastly 28 August 2007. From a first look at the four snapshots it is right away apparent that the particles' tracks during 2008 and 2009 are similar, as they are during 2007 and 2010. Indeed, the larvae seeded west of the Marquesas Keys move faster north in 2008 and 2009 than in 2007 and 2010. The current amplitudes of validation point 2, situated on the West Florida Shelf (WFS), corroborate these differences (cf. appendix B.1). Each year the current direction is northwestward, but in 2007 and 2010 the amplitude is about 0.10 $m\,s^{-1}$ during the ten first days of the LPT simulations whereas in 2009 the amplitude approximates 0.20 $m\,s^{-1}$ and in 2008 it even exceeds 0.25 $m\,s^{-1}$, both also during the first ten simulation days. Rather than due to interannual variability, this could also come from **seasonal variability**. Indeed, according to Liu and Weisberg (2012) the winds blowing over the WFS, which are subject to seasonal variability, impose a strong local forcing on the current amplitudes and directions of the WFS, which are thus subject to a similar seasonality. The winds tend to be southerly or southeasterly from June to August and easterly in September. Hence, in mid-August the currents

tend to be more northward directed than at the end of August or the beginning of September, carrying the larvae faster away. The figures 3.10 (a) and 3.10 (b) show the wind directions and speeds at two different time steps of the simulation period, being 16 August 2009 and 01 September 2009 at 00:00. Matching Liu and Weisberg's ascertainments, the winds of the WFS on August 16 are southerly, whereas on September 01 they are easterly to northerly. Moreover, their force ranges between 5 and 9 m/s on August 16 but is less than 3 m/s on September 01. The forcing of strong northward winds on the ocean circulation during mid-August could explain the quick northward transport of the larvae when they are spawned early, as in 2008 and 2009.

Another similitude between 2007 and 2010, differentiating them from 2008 and 2009, is the track of the particles north of Palm Beach. During 2007 and 2010 there seems to be a current that transports the particles eastward, that does not exist in 2008 and 2009. Again this could be a seasonal phenomenon, especially since on the 20th day of 2008's simulation, which is September 5 and falls inbetween the 10th simulation dates of 2007 and 2010, this eastward current is also present (cf. appendix A).

The existence of seasonal currents that influence the particle tracks could make the spawning date an important aspect on marine connectivity in the FCRT. This is subdued by the fact that the seasonality only seems to impact the hydrodynamics on the edges of the FCRT. Nevertheless, more local and smaller seasonal variations can occur between the reefs, not possible to detect on the figure 3.9 and the appendix A). To confirm the effect of seasonal variability and of the spawning date on larval dispersal, and to better assess it, the larval dispersal simulation should be run for additional years. For now the correlation between 2008's and 2009's currents on one hand and 2007's and 2010's currents on the other could be fortuitous.

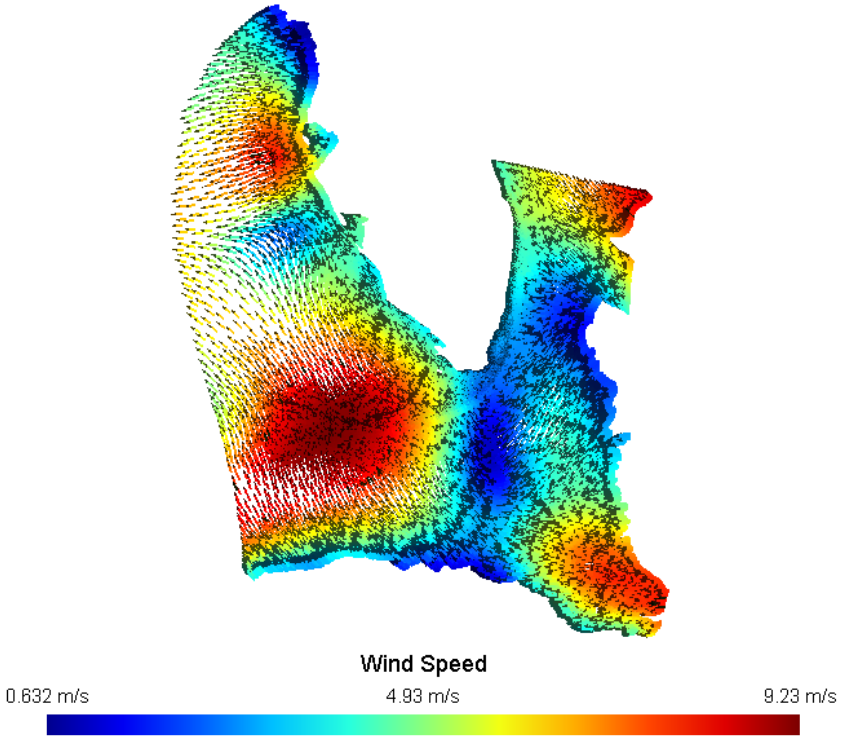


(a) 16 August 2009

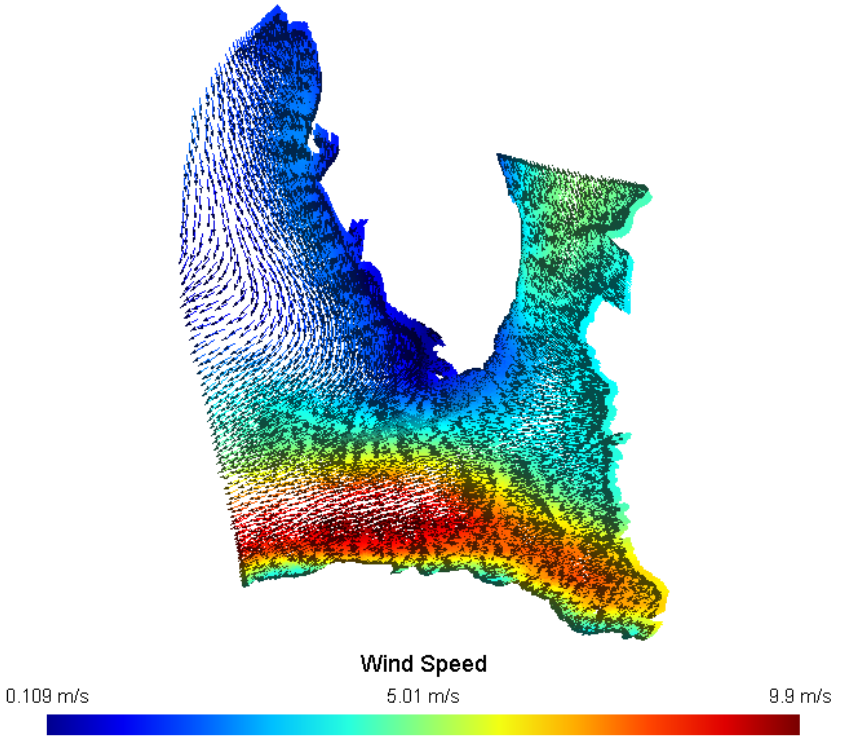


(b) 01 September 2009

Figure 3.10: Wind amplitudes and directions on August 16, 2009 and September 01, 2009. On August 16 the winds blowing over the WFS are strong and southeasterly, whereas on September 01 they are much weaker and more northerly.

## 3.3 Analysing the connectivity matrices

The different indices introduced in section 2.3 were computed for each reef and for each year. Figure 3.11 shows the average over the whole FCRT of the annual self recruitment and PageRank protection indices. The four different values give an idea of the interannual variability of indices over the whole network. For example, it can already be seen on this figure that there is globally more self recruitment during 2010 than during the other years (a) and that the PageRank protection index is globally lower in 2010 than during any other year (b).

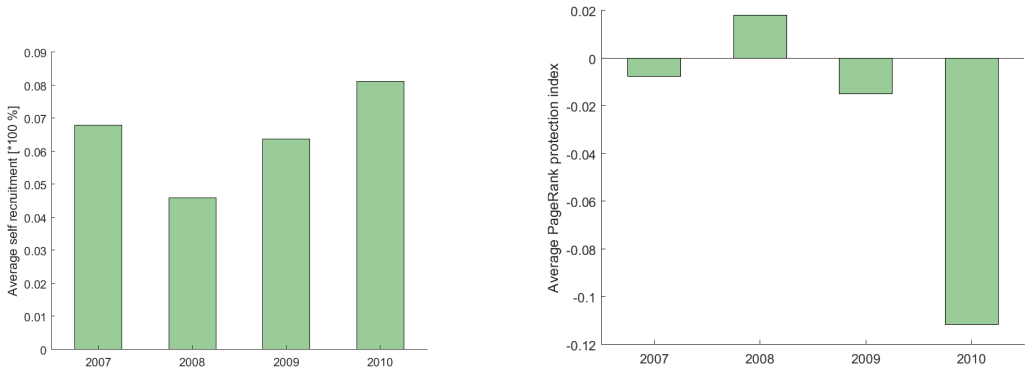


(a) Self recruitment

(b) PageRank protection

Figure 3.11: Average self recruitment and PageRank protection index over the whole FCRT, for each year, giving an idea of the inter-annual variability

In the following subsections, the indices are presented one by one. For each one of them, the mean and the standard deviation over the four years are shown, which allows to represent the local interannual variability. Points shown on the FCRT map give an idea of the value taken locally by each reef thanks to their size and color. Besides, it is relevant for some of them to show the coefficient of variation, which is the relative standard deviation, in order to bring out points with higher relative dispersion. For some indices, the mean and the standard deviation are also compared to the mean and standard deviation obtained using a normalized connectivity matrix. This is interesting in order to determine the influence of the reef size on the index computation.

### 3.3.1 Connectivity indices

#### Local retention

Figure 3.12 shows the mean and the standard deviation of the local retention. The higher values of the mean are found on the **inner shelf**, in the regions of the **Lower** and the **Upper Keys**.

The variability shown by the standard deviations is the greatest north of the **Marquesas Keys** and of the end of Key West but is actually not extreme where the mean is the greatest.

It means that the points marked in red in figure 3.12 (a) indicate indeed reefs that are habitually retaining many of their own larvae compared to what they send away.

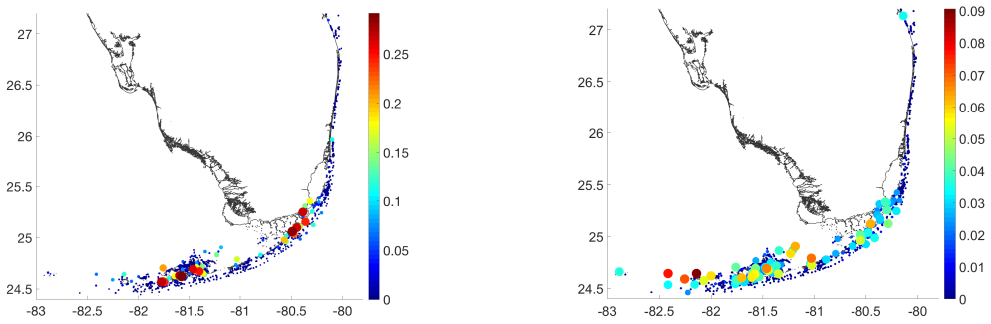


(a) Mean ($\mu$) (b) Standard deviation ($\sigma$)

Figure 3.12: Local retention: mean and standard deviation computed over the 4 years for each reef of the FCRT. High local retention is observed in the inner shelf of the Lower and Upper Keys, while the greatest variability is around the Marquesas Keys.

### Self recruitment

Figure 3.13 shows the self recruitment, which is a measure giving information about the isolation of a reef. As well as for the local retention, the highest values are found in the **inner shelf**, mainly in the **Lower and Upper Keys**. Those large values of local retention and self recruitment in those regions can be explained by the fact that both of them are in the inner shelf, which is not in direct contact with the strong Florida Current. Moreover, they are both characterized by the fact that the reefs are surrounded there by islands which might retain the larvae. For these two reasons, it can be understood that the larvae in those regions have a tendency to remain in the same area and therefore increase the value of local retention and self recruitment.

Some other points near the **Dry Tortugas** or in the **south of Marquesas Keys**, that were not highlighted for the local retention, are however having a high mean value of self recruitment (between 0.5 and 0.8). Although their standard deviations are also very high, the value of the index is almost reaching 1 every year except in 2008, when it is close to 0. The figures representing the indices for each year are shown in appendix C. The year 2008 induces the great variability but the high value of self recruitment still has to be considered for the three other years of those specific points. It represents a high degree of isolation for those points as it represents the amount of larvae that are coming from themselves compared to the amount of larvae they received from other reefs.

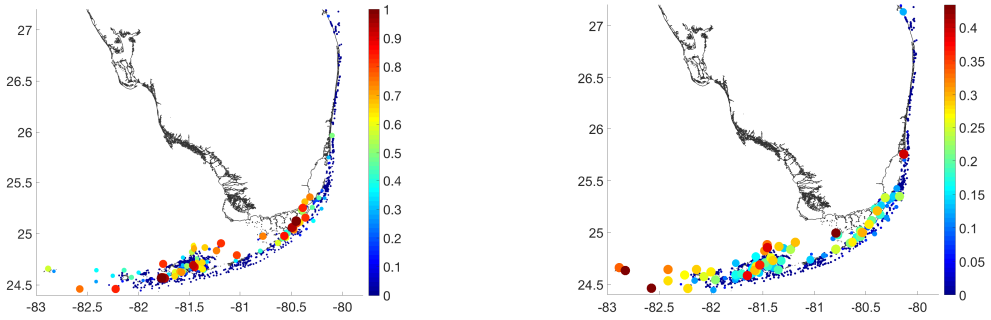


(a) Mean ($\mu$) (b) Standard deviation ($\sigma$)

Figure 3.13: Self recruitment: mean and standard deviation computed over the 4 years for each reef of the FCRT. Like the local recruitment, high local retention is observed in the inner shelf of the Lower and Upper Keys, showing the tendency of the larvae to remain in those regions. High value of self recruitment for the Dry Tortugas reflects their high degree of isolation.

### Proportion settled

Figure 3.14 shows the proportion settled . The average proportion settled over all the reefs is about 25% for each year. It can be seen that most of the inner shelf reefs have a proportion settled greater than 25%.

The **outer shelf** reefs have a lower proportion settled that can be seen via the thin green band along the outer shelf of the lower and Middle Keys. That can be explained by the fact that those reefs are exposed to the strong Florida Current and their larvae might be taken away without having the time to settle.

The reefs along the coast **between Miami and Palm Beach** do not have a large proportion of settling larvae, probably because they are downstream of the FCRT. Their larvae are then brought away to the north and not reaching the reefs considered in this study.

The reefs near the **Dry Tortugas** do not have a large proportion of larvae settling neither. That is mainly due to their isolated location. As it can be observed on figure 3.9, the larvae coming from the Dry Tortugas are directly going northwards and not reaching reefs considered in this study.

The standard deviation is the greatest at the beginning of the Keys, near the **Marquesas Keys**. As those reefs had a low mean, it can be expected that for certain years they only have a few larvae settling and for other years many larvae settling. By looking at the results for each year individually (see appendix C), it can actually be seen that during 2008 and 2009, only a few larvae from those reefs are settling and during 2007 and 2010, many more end up settling. Those spots are subject to variation of currents. Indeed, it confirms what was highlighted in section 3.2 by means of figure 3.9. The currents are much stronger northwestward for 2008 and 2009, bringing the larvae away to the northwest whereas for 2007 and 2008, the current is weaker and the larvae remains longer near the Keys.

An other point with a high standard deviation is found to the north of **Palm Beach**. Again, by looking at the results for each year individually, it can be noticed that the reefs in that region have a higher proportion settled in 2007 and 2010 than in 2008 and 2009. It again points out a difference between 2007-2010 and 2008-2009. However, it is interesting to notice that in section

3.2, an outward current was remarked for years 2007 and 2010 above Palm Beach, that was not noticed for year 2008 and 2009. This current might bring larvae offshore, reducing the proportion settled in this area. But the opposite is observed: high proportion settled when the outward current occurs and inversely. This outward current is actually more north of Palm Beach and does not explain the large proportion settled . However another current phenomenon connected to the outward current might occur in that area and explain the variability in proportion of settling larvae.

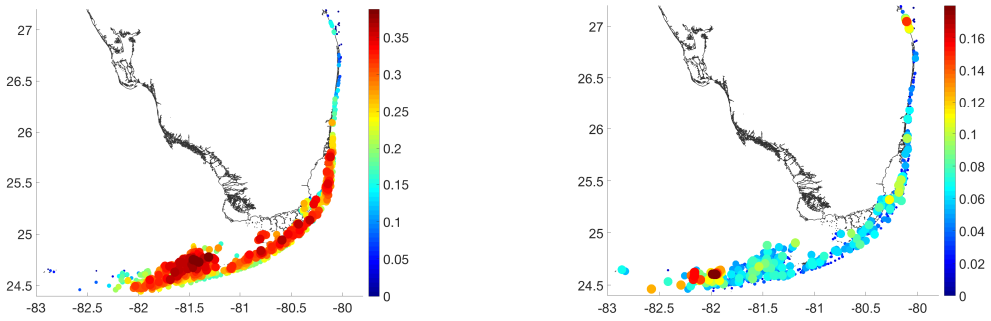


(a) Mean ($\mu$) (b) Standard deviation ($\sigma$)

Figure 3.14: proportion settled: mean and standard deviation computed over the 4 years for each reef of the FCRT. Settlement is higher on the inner shelf, where currents are slower and hindered by lands. High variability is observed near the Marquesas Keys and north of Palm Beach, reflecting interannual current variability.

### Weighted connectivity length

Figure 3.15 shows the weighted connectivity length (WCL), which represents for each reef the average distance covered by one larva that would be seeded by this reef and settle somewhere. The mean WCL is especially large for the **outer shelf** reefs situated on the **Lower and Middle Keys**. It has also an important value for the reefs in front of **Miami**. This is again explained by the fact that the outer shelf reefs are subject to the strong FC that takes the larvae away compared to the inner shelf reefs that are subject to smaller local currents.

The reefs positioned near the **Marquesas Keys** and the **Dry Tortugas** do not have a large mean WCL. This is explained by their isolated position and by the fact that the local current tends to bring the larvae northwestward, where no other reefs can be found.

It can be noticed, however, that the larvae from the reefs located on the **outer shelf in the Upper Keys** do not reach reefs far from their source even though they are on the outer shelf. This can be explained by the observations made in section 3.2 by means of figure 3.8. It can be noticed that the path of the larvae is detaching from the coast from the beginning of the Upper Keys, inducing that the current is not following the coast. Therefore, the larvae seeded from the reefs in that area are not subject to this strong FC and are not taken far away like for the rest of the outer shelf. Pictures of the mean weighted connectivity length and of the larvae path let thus think that the FC flow is detaching from the coast off the Upper Keys, where the coast shows a smaller radius of curvature. Figure 3.1 also confirms this idea as it can be observed that the velocity amplitude is lower in that area.

The standard deviation seems to be the largest where the mean too is the most important.

As explained in the subsection 2.3.4, this might be due to the fact that the absolute value of the standard deviation is affected at each point by the value of the mean. The coefficient of variation is therefore introduced in figure 3.15, to give an idea of the relative standard deviation and hence of the dispersion. The most dispersed points regarding the WCL are found on the **Dry Tortugas** and near the **Marquesas Keys** and at the northern limit of the FCRT. For the isolated reefs, a large dispersion of the WCL could mean that their larvae are sometimes reaching other reefs and sometimes not.

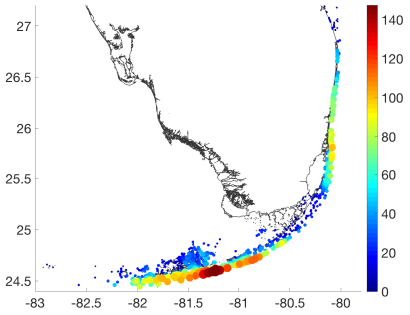


(a) Mean ($\mu$)

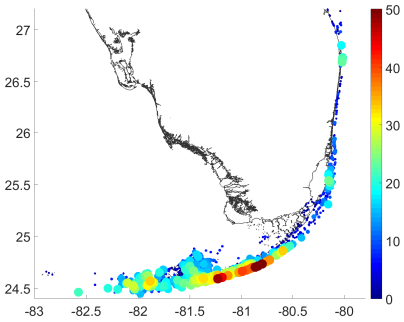


(b) Standard deviation ($\sigma$)

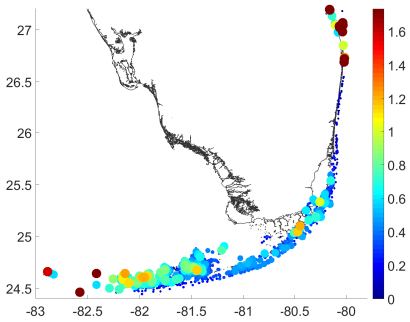


(c) Coefficient of variation $\left(\frac{\sigma}{\mu}\right)$

Figure 3.15: Weighted connectivity length [in km]: mean, standard deviation and CV computed over the 4 years for each reef of the FCRT. Great connectivty length are observed where the settlement was low and inversely. This is explained by the same current phenomena: the FC taking the larvae away along the outer shelf and local circulation of the larvae on the inner shelf. High coefficient of variation is observed around the Dry Tortugas and the Marquesas Keys, as well as north of Palm Beach.

### Outgoing PageRank index

Figure 3.16 shows the outgoing PageRank index. Only a few reefs are brought out with a higher value than the others. They are located mainly in the **inner shelf** of the **Lower Keys**. This would mean that even if their larvae are not transported far from their source, those reefs are seeding to various other reefs that are themselves seeding to other good seeders. Even if they are not directly subject to the FC, one can imagine that their larvae are still attracted by the FC towards the outer shelf. As Frys (2017) pointed it, one can imagine a suction effect towards the FC. It is illustrated for the year 2009 in figure 3.8, where one can observe that the reefs marked in brown and orange are actualy ending up crossing the Keys and reaching the outer shelf. A reef situated to the **south of the Marquesas Keys** is indicated as having the greatest mean outgoing PageRank index. However its standard deviation is relatively high too. By looking at

each year individually, one can notice that its outgoing PageRank index is actually high for the years 2008, 2009 and 2010 and close to 0 only for the year 2007. So despite its great variability this reef shows a relatively constantly high outgoing PageRank index, meaning that it is a good seeder favorable to the downstream reefs. It can be explained by the fact that its location is more to the south than the Marquesas Keys, and hence is subject to the strong FC and not isolated.

In general, the highest standard deviation is found for the reef with the highest mean. The coefficient of variation is therefore introduced here for the outgoing PageRank in order to highlight the reefs with the highest relative dispersion. It can be observed on figure 3.16 (c), that the reefs with the highest relative dispersion are actually the ones at the beginning of the Keys and around **Marquesas Keys**. This is explained, as mentioned before, by the great influence of the currents in that region and the great variability of those currents from one year to another.

Moreover, one can notice the orange point, illustrating a mean value of about 0.04, on the inner shelf in the Middle Keys. This point is indicating the Vaca Reef, north of **Vaca Key**. It is interesting to highlight this reef as it is the largest reef over the FCRT, with an area of more than 850 $km^2$ whereas the median reef area over the FCRT is a bit less than 0.3 $km^2$. It represents on its own an amount of coral individuals much larger than any other reefs. As the amount of larvae was placed on each reef, at the beginning of the simulation, proportionally to the reef area, it is normal that the Vaca Reef is exporting many larvae and has many outgoing connection and hence a high outgoing PageRank index. In order to remove the influence of the reef size, the outgoing PageRank index was also computed from connectivity matrices ($\widetilde{C}_{ij}$), normalized by their seeded vectors. This normalization is similar to normalizing by the reef area as the quantity of larvae seeded is proportional to the reef area. It can be seen on figures 3.16 (d) and (e), that the outgoing PageRank index of the Vaca Reef and its variability are indeed decreased compared to other reefs, when using a normalized CM.

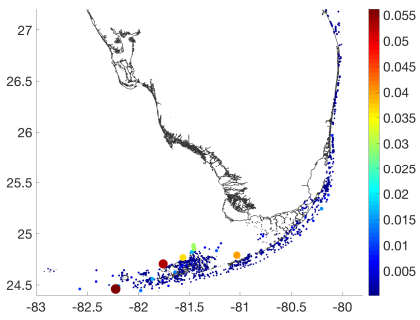


(a) Mean ($\mu$)

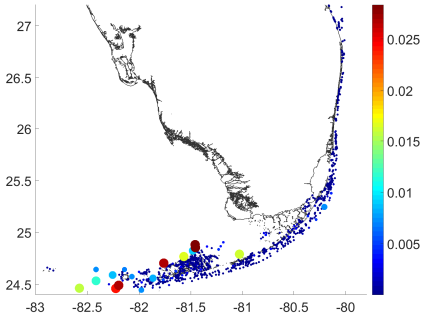


(b) Standard deviation ($\sigma$)

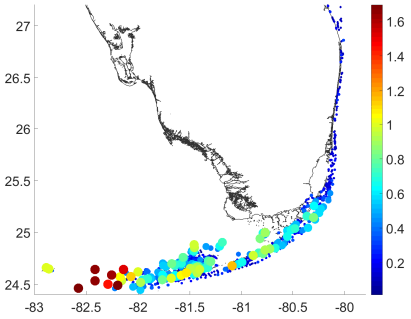


(c) Coefficient of variation $\left(\frac{\sigma}{\mu}\right)$

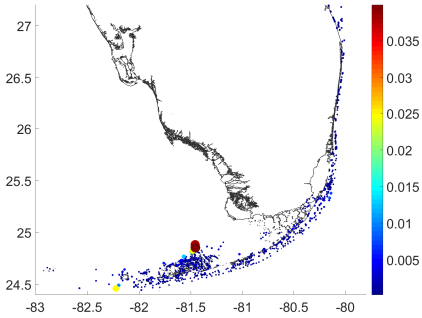


(d) Mean ($\mu$) using normalized CM

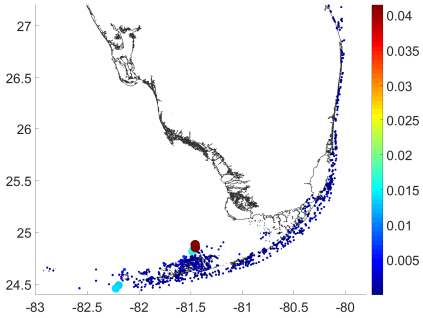


(e) Standard deviation ($\sigma$) using normalized CM

Figure 3.16: Outgoing PageRank index: mean, standard deviation, CV, and normalized parameters computed over the 4 years for each reef of the FCRT. High outgoing PR index is observed south of the Marquesas Keys and in the inner shelf of the Lower Keys. A great relative dispersion, shown by the CV is observed around the Marquesas Keys, reflecting high influence of current variability.

### Incoming PageRank index

Figure 3.17 shows the incoming PageRank index. The highest mean incoming PageRank index is found at northern extremity of the FCRT, in front of **Palm Beach**. That is easily explained as this is the downstream extremity of the FCRT, receiving larvae from all the upstream reefs.

The reefs located on the **outer shelf** of the **Upper Keys** also have a relatively high mean incoming PageRank. This could be contradictory to the fact that the FC is detaching from the

coast in that region and hence should not bring many larvae towards that area. However, this could corroborate the assumption presented by Frys (2017), that there is a suction effect towards the outer shelf. The high degree of incoming connections observed there would originate from the inner shelf reefs that have a great degree of outgoing connections.

The highest standard deviations given on 3.17 (b) are roughly found at the same spots as the highest means. It is then interesting to show the coefficient of variation (c). The points with the highest relative dispersion are located on the **inner shelf**, at the end of the **Lower Keys**, followed by the reefs around **Marquesas Keys**. The northern extremity of the FCRT, near **Palm Beach**, still shows a large dispersion. The variability at this point can be related to the high variability of the proportion of larvae from that area which are settling.

The mean and standard deviation obtained using the normalized connectivity matrices are very similar to the ones using non-normalized CM. Even using a normalized CM, the Vaca Reef shows a high incoming PageRank index compared to other reefs in that area.

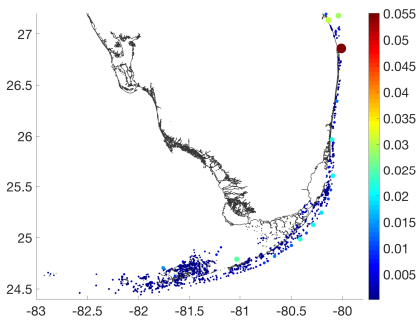


(a) Mean ($\mu$)

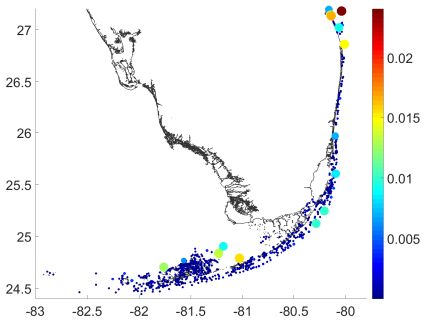


(b) Standard deviation ($\sigma$)

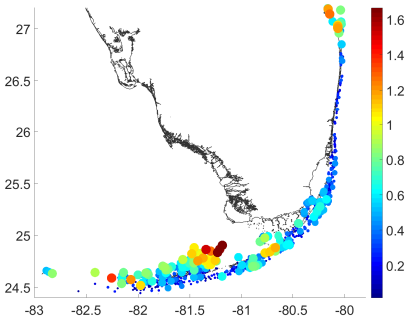


(c) Coefficient of variation $\left(\frac{\sigma}{\mu}\right)$

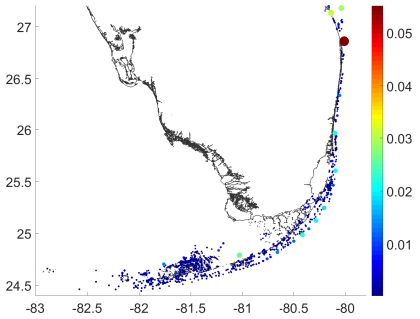


(d) Mean ($\mu$) using normalized CM

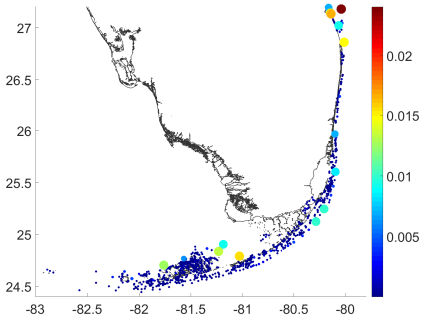


(e) Standard deviation ($\sigma$) using normalized CM

Figure 3.17: Incoming PageRank index: mean, standard deviation, CV, and normalized parameters computed over the 4 years for each reef of the FCRT. Vaca reef shows important incoming connections, even after normalization. CV shows high varibility on the inner shelf of the Lower Keys.

### Betweenness

Figure 3.18 shows the betweenness of each reef. It represents the ability of each reef to establish a connection between any other two reefs. The cost of each connection was set as the inverse of the connection weight, which can be obtained either from the original connectivity matrix or from the normalized one. In figure 3.18, (a) and (b) show respectively the mean and the standard deviation using the original CM. (c) and (d) show respectively the mean and standard deviation using the normalized CM.

In figure 3.18 (a), the **Vaca Reef** has by far the largest mean betweenness, which is about twice as big as the second largest betweenness. High values of betweenness are also found on the **inner shelf of the Lower Keys** and on the **outer shelf of the Upper Keys**. However, the variability (b) in those two regions is the highest whereas the betweenness of the Vaca Reef seem to be steadily the highest.

By looking at the betweenness graphs using the normalized CM, (c) and (d), one can observe that the Vaca Reef is still the most important in terms of betweenness with a standard deviation that only slightly increases. This could mean that the Vaca Reef is really important and strategically positioned in order to allow connections between different reefs, independently from its size. However the normalization is done on the cost parameter, once the connectivity is already computed. The size might, thus, still influence indirectly the importance of the Vaca Reef in terms of betweenness.

It can also be noticed that the importance of the reefs in the inner shelf of the Lower Keys and the ones in the outer shelf of the Upper Keys is increasing when using a normalized matrix. The coefficient of variation is not shown here because many reefs have such a small mean betweenness that using it to divide the standard deviation leads to large coefficients of variation all over the FCRT, making the graph unreadable and the coefficients meaningless.

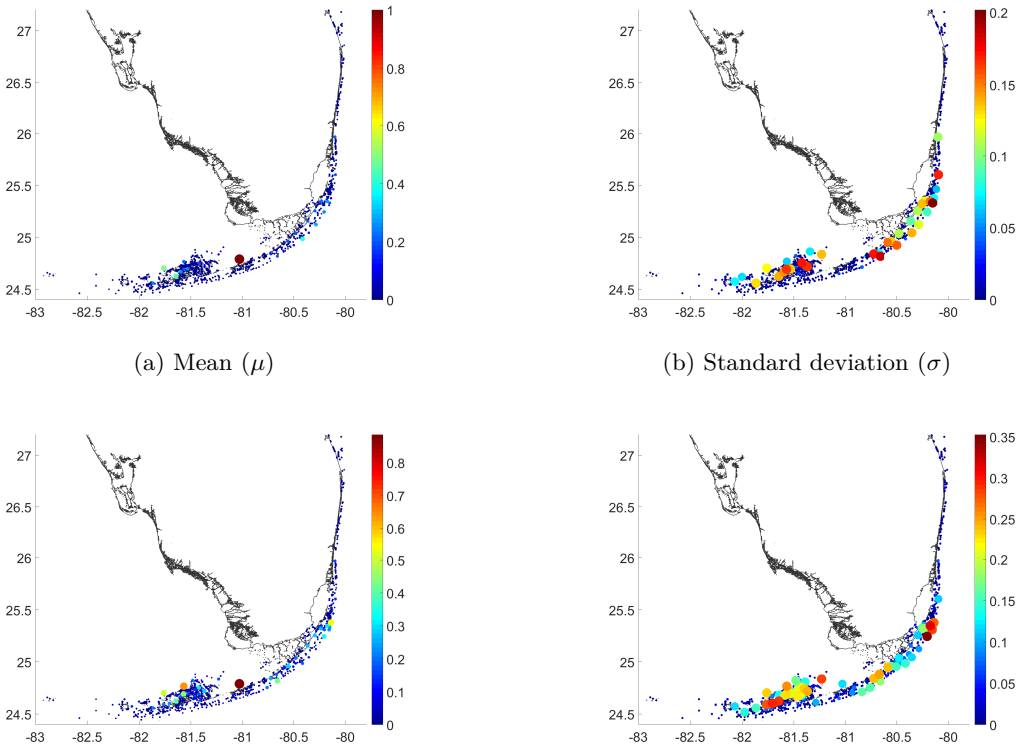


(a) Mean ($\mu$)

(b) Standard deviation ($\sigma$)

(c) Mean ($\mu$) using normalized CM

(d) Standard deviation ($\sigma$) using normalized CM

Figure 3.18: Betwenness: mean and standard deviation computed from the original connectivity matrices and from the normalized ones over the 4 years for each reef of the FCRT. Inner shelf of the Lower Keys as well as the outer shelf of the Upper Keys show relatively high betweenness. Though the highest value is observed for the Vaca reef, appearing as a central reef for the FCRT.

#### Overview of the connectivity indices

It was noticed that the FC has a strong influence on the reef connectivity in the FCRT. It takes the larvae from outer shelf far away from their source sink all along the outer shelf, from south of the Marquesas Keys until Palm Beach. However, this current seems to detach from the coast where the Keys are shaped with a smaller radius of curvature, such that the larvae from the reef located on the outer shelf of the Upper Keys are not moving far away.

The reefs on the inner shelf of the Upper Keys seems to be isolated by the fact they are trapped in the angle between the main coast and the Keys, among little basins and islands. The reefs located on the inner shelf of the Lower Keys are not subject to the strong FC, so that their larvae remain in the same area. However, they are still seeding larvae to other reefs and are good sources for other reefs, even for reefs located on the outer shelf. The Dry Tortugas are also isolated by their position far from all other reefs.

A general great variability is observed for the reefs situated at the beginning of the Keys. They are highly influenced by changes in the currents in that area. As it was shown that those currents were strongly influenced by the amplitude and directions of the wind blowing in that region, the connectivity of those reefs are actually directly influenced by the seasonal winds. The reefs located near Palm Beach are also subject to high variability, which seems to be related to local current phenomenon, yet not precisely described here.

The Vaca Reef was highlighted as a good element to allow transition of larvae (by its betweenness), and that independently from its size. It was also noticed to be a good source and sink (by its outgoing and incoming PageRank) but once normalized by its seeding vector, it appears to be an average seeder with an average outgoing PageRank but still a very good importer.

### 3.3.2 Protection and restoration indices

Now that the main connectivity indices have been presented, it is useful to bring them together in order to try to identify reefs needing protection and the ones worth restoring whilst taking into account their variability. First, the PageRank protection index is presented here. Values computed with both the original CM and the normalized one are shown. Then, the PageRank restoration index is exposed. Again, values obtained with the original and with the normalized matrices are compared.

#### PageRank protection index

Figure 3.19 shows the PageRank protection index over the FCRT. This index brings new reefs to light that were not shown when only considering the incoming or the outgoing PageRank index. It can be seen on (a) that the reef needing the most protection are situated in three main areas: the **outer shelf of the Lower Keys**, to a lesser extent the **inner shelf of the Lower Keys** and, the **inner shelf of the Upper Keys**. It can easily be understood that the two first regions named here need protection as they are situated upstream from the FCRT. They are not likely to receive many larvae but are good providers. Also, the inner shelf of the Upper Keys were not good seeder but they apparently need protection. It means that they proportionally seed more than what they receive.

An other spot needing protection can be noticed on the outer shelf of the Upper Keys, **off Key Largo**. They are actually situated after the strongly curved section of the Florida Keys, where the Florida Current is likely to detach. This should explain why they are not receiving many larvae but well providing other downstream reefs and hence, are worth protecting.

Using a normalized connectivity matrix to plot the PageRank protection index (c) does not change drastically the general appearance of the map but the reefs, situated on the outer shelf of Key Largo seem to need even more protection.

The variability is the greatest for the region on the **inner shelf of the Lower Keys**. Frys (2017) selected this area (north of Torch Key and Big Pine Key) as one of the main spots needing protection. However, now that the comparison was made between different years, reserves can be expressed regarding this area. One can also notice the variability on the **outer shelf on the Upper Keys**. This is especially due to a low need in protection during the year 2010, related to a low outgoing PageRank index. However, the reefs located on the **outer shelf of the Lower Keys** are not subject to a great variability while the mean index is high. Frys (2017) already highlighted this area, especially the southwest of Key West, for important need in protection. Now, that those values are observed to be steady over the years, it can be recognized that the reefs in that area are very good candidates for protection measures.

Lastly, it can be noticed that the **Dry Tortugas** and the **Marquesas Keys** do not need protection. It is explained by the fact that even if they are not receiving many larvae, they are not good providers neither.

The coefficient of variation can not be calculated here as the PageRank protection index is not a rational measure and can take negative value.

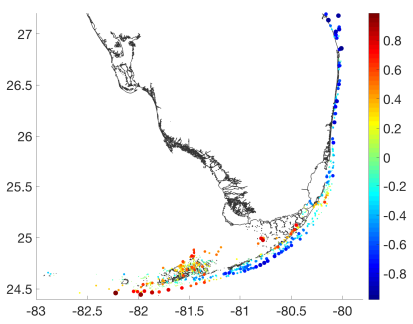


(a) Mean ($\mu$)

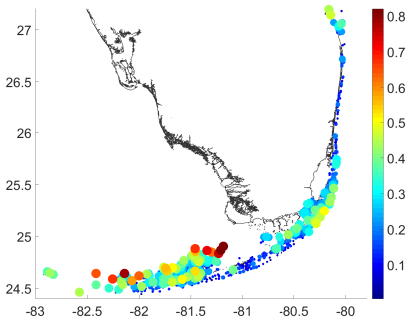


(b) Standard deviation ($\sigma$)

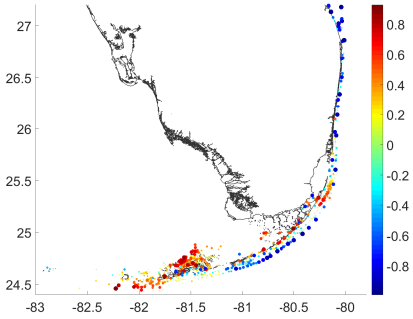


(c) Mean ($\mu$) using normalized CM

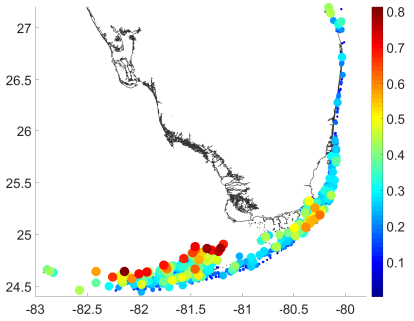


(d) Standard deviation ($\sigma$) using normalized CM

Figure 3.19: PageRank protection indices: mean and standard deviation computed from the original connectivity matrices and from the normalized ones over the 4 years for each reef of the FCRT. High protection is needed for reefs south of the Marquesas Keys and on north of the Big Pine Key. However the latter shows high variability, making the former the strongest candidate for protection measures.

### PageRank restoration index

Figure 3.20 shows the PageRank restoration index over the FCRT. It can be observed that the mean is by far the highest for the **Vaca Reef**, followed by a reef in the **inner shelf of the Lower Keys**. Even though using a normalized matrix does not reduce the importance of the Vaca Reef, it allows to highlight other reefs that would be worth restoring on the inner shelf of the Lower Keys and along the **outer shelf of the Upper Keys**. The Vaca Reef has many incoming connections, which make it resilient. It also is a good provider as shown by its outgoing PageRank index.

The standard deviations seem to be high where the means are high. Therefore, it is interesting to show the coefficient of variation in order to highlight the spot with the higher relative dispersion. The reefs around **Marquesas Keys** are the most subject to variability, together with the reefs belonging to the **inner shelf of the Middle Keys**. The reefs situated downstream from the FCRT are also taking disperse values of restoration index. The two extreme points (Marquesas Keys and Palm Beach) were already noticed to be variable due to their location and the influence there of variable currents.

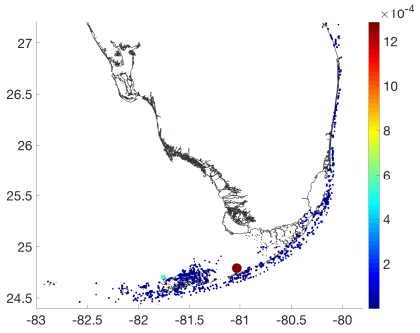


(a) Mean ($\mu$)

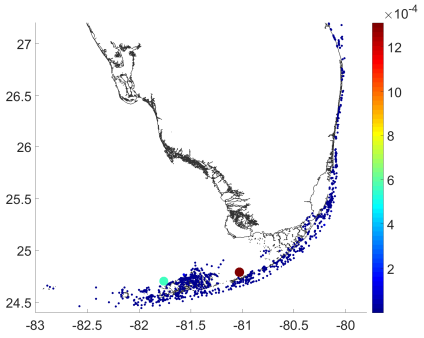


(b) Standard deviation ($\sigma$)

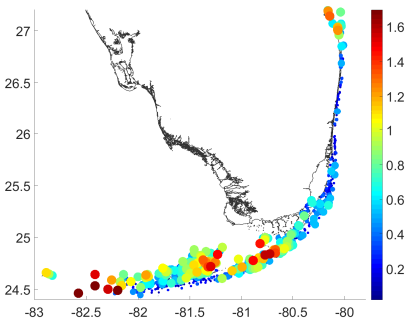


(c) Coefficient of variation $\left(\frac{\sigma}{\mu}\right)$

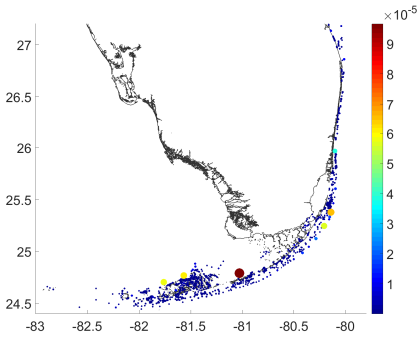


(d) Mean ($\mu$) using normalized CM

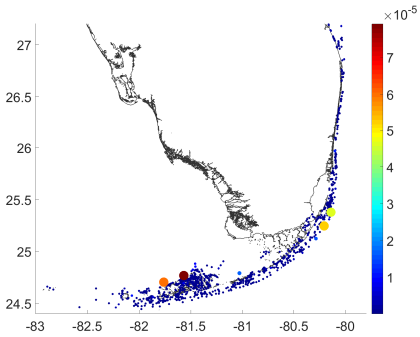


(e) Standard deviation ($\sigma$) using normalized CM

Figure 3.20: PageRank restoration indices: mean and standard deviation computed from the original connectivity matrices and from the normalized ones over the 4 years for each reef of the FCRT, as well as the VC. The Vaca reef is the most important reef in term of incoming connection and hence, is a good candidate for restoration measures. High variability is observed near the Marquesas.

### Vaca Reef

The Vaca Reef is a key point regarding restoration purposes. As its exportation are also above average, it is then a reef useful to the network, while being probably extremely resilient itself. Those observations are still valid even when using a normalized connectivity matrix, suggesting that its good betweenness and connections are indepedent from its size.

However, as Frys (2017) highlighted it, the quantity of reefs located on the Vaca Reef is

largely overestimated and hence the quantity of larvae released and settling on it too.

Moreover, the normalization is done after computing the connections. While the weight of each connection after normalization is such that each reef has a total outgoing weight equal to its proportion settled , the number of connections remains the same as before the normalization. The large number of incoming connections of the Vaca Reef can be explained by its large size because the larger a reef is, the higher the chance is that a particle is transported over it and settles on it. In addition, the incoming connections are not normalized by the size of the sink reef but by the seeder size. For example, in 2010, after normalization, the average total incoming connections weight for one reef is about 0.28 whereas the total weight of the incoming connections of the Vaca Reef is still about 13.8. One should notice that those numbers do not have any unit as they are obtained after normalization. It is then important to remind that the "efficiency" of the Vaca reef should be spread over its whole area, which is extending along the whole inner shelf of the Middle Keys.

In order to have a better idea of the connectivity distribution over the Middle Keys, it would be interesting to partition the Vaca Reef into smaller parts of similar size prior to the LPT computation. To a greater extent, it could be done for every reef.

### 3.3.3 Communities and reef clusters

After computing those indices, main reef clusters were highlighted. Both the community detection method and the strongly connected components method are presented hereafter.

#### Community detection

Figure 3.21 shows, for each year, the clusters defined thanks to the community detection method. The resolution parameter $\gamma$, was chosen for each year so that it provides a stable community partition. Its value is shown in table 3.7 for each year.

| | Resolution parameter $\gamma$ |
|---|---|
| 2007 | $\sim 2 \times 10^{-5}$ |
| 2008 | $\sim 2 \times 10^{-5}$ |
| 2009 | $\sim 2 \times 10^{-5}$ |
| 2010 | $\sim 5 \times 10^{-5}$ |

Table 3.7: Choice of the resolution parameter $\gamma$ for the different years

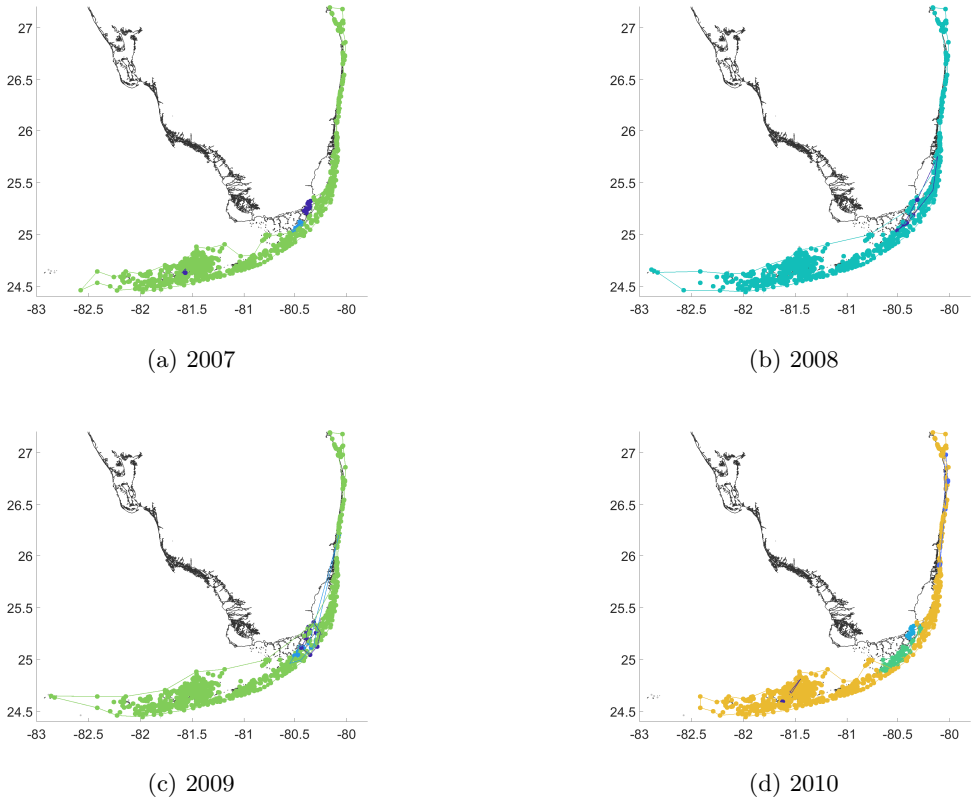


(a) 2007 (b) 2008

(c) 2009 (d) 2010

Figure 3.21: Reef clusters computed with the community detection method from the connectivity matrices of years 2007, 2008, 2009 and 2010. The $\gamma$, was determined for each year in order to have a stable communities partition.

These correspond to low value of $\gamma$ and it is then expected to highlight a few large communities among which connections are weak. It means that between two different clusters, connections are even weaker or maybe non-existent.

Figure 3.21 shows that the clustering for the four years are globally similar. A global community seems to link most of the reefs together, from the beginning of the Keys until Palm Beach, and inner as well as outer regions. This does not give information about the reefs belonging to this cluster.

However, it allows to highlight isolated reefs. As already suggested by the previous indices, the reefs located on the **inner shelf of the Upper Keys** are isolated. Every year, this small community is wedged in the angle between the main coast and the Keys. Some years, this community is even split in two clusters, illustrating the low mixing of water in this area.

The **Marquesas Keys** and their surrounding reefs are every year belonging to the main community, meaning that there is always a minimum amount of connections between this Keys extremity and the rest of the Keys.

Again, years 2007 and 2010 can be distinguished from 2008 and 2009: the **Dry Tortugas** are once connected to the main cluster (2008 and 2009) and once completely isolated (2007 and 2010). It can be noticed however that the opposite would have been expected as the current in 2008 and 2009 brought the larvae from the Dry Tortugas faster northward.

### Strongly connected components

Figure 3.22 shows the clustering obtained thanks to the strongly connected component method. The communities highlighted here are communities inside of which the reefs are all exchanging larvae with one another in both directions, possibly via multistep paths. In order to avoid that only one single larvae would be enough to create a connection, only the normalized connection greater than 1 ‰ are taken into account, representing the demographically significant connections.

Years 2007, 2009 and 2010 are similar to each other while 2008 is different. In general the whole outer shelf is not included in a strongly connected component as the modeled FC is bringing larvae rapidly away along the Keys and the Florida west coast mainly in one direction.

The three similar years are showing two main clusters: one on the **inner shelf of the Lower Keys** and one on the **outer shelf of the Upper Keys**, where the coast has the smallest radius of curvature. As explained previously, those two areas are not strongly influenced by the FC. The inner Lower Keys are not reached by the FC and are subject to local circulation around the reefs, thanks to which larvae are transported locally in all directions creating a strongly connected component. On the outer shelf, near Key Largo, the FC is thought to be detached from the coast, letting local current acting on the reefs and allowing larvae to go in both direction.

Finally, the isolated clusters on the **inner shelf of the Upper Keys** are also represented here. However, it can be noticed that some of them, are connected in both direction with the outer shelf. There is an exchange of larvae through the Keys in that area.

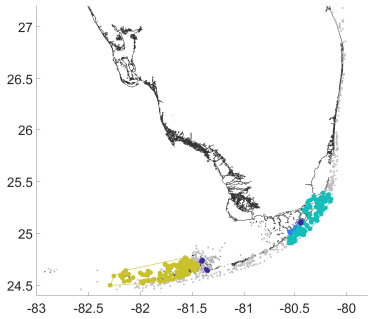


(a) 2007

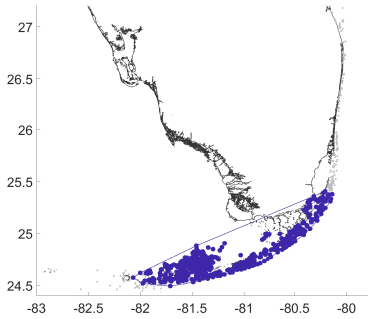


(b) 2008

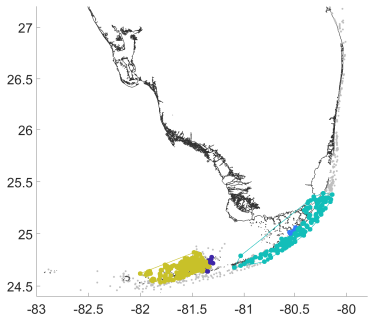


(c) 2009

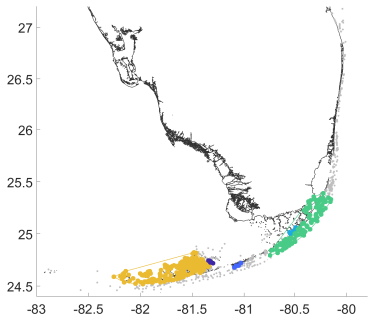


(d) 2010

Figure 3.22: Strongly connected components computed from the connectivity matrices of years 2007, 2008, 2009 and 2010.

A **comparison** can be done with Drury's study that is analyzing the dispersal capacity and genetic relatedness in *Acropora Cervicornis* on the Florida Reef Tract using HYCOM with a 900m horizontal resolution grid (Drury et al., 2018). While the results obtained from his simulation can be compared with the ones presented here, one should keep in mind that those results were obtained with a much coarser grid than the one used here by SLIM on the zones of interest.

First, his model shows a lack of two-directional connections between the region above the Middle Keys and the region of the Lower Keys, which is well in line with the strongly connected components observed here for the years 2007, 2009 and 2010. However, his model created two-directional connections between the Dry Tortugas and the Keys, which is against the hereabove observations, about the isolation of the Dry Tortugas. Also, Drury's model created two-directional connections on the outer shelf of the Lower and Middle Keys. This was only observed here during the year 2008.

The second part of Drury's work was identifying genetic relatedness over the FCRT from samples. The results he obtained are interesting as they show two-directional genetic relations between reefs from all over the FCRT. The hydrodynamics modeled by SLIM and consequent results are not explaining those two-directional flows on the outer shelf.

Drury is suggesting that those genetic mixing can be occurring on a stepwise basis. It can then be imagined that small fluctuations (e.g. tidal back and forth movement) would induce upstream connections reaching the beginning of the Keys in the long term. This considerations are out of the scope of this study, that is mainly focusing on seasonal dispersion to identify sexual reproduction extent. However, it should be reminded that SLIM had difficulties to model the eddies coming from the Golf of Mexico. Taking them into account for modeling larvae dispersion would probably result in more upstream connections along the outer shelf, corresponding to the genetic flow highlighted by Drury.

## 3.4 Modeling population evolution

The time needed for a reef to recover from 30% to 90% of its maximum coral cover capacity (later on referred to as the recovery time or time needed to recover) depends greatly on the reefs' locations. In figure 3.23 each reef is colored according its recovery time, calculated using the merged connectivity matrix, obtained by adding the connectivity matrices of 2007, 2008, 2009 and 2010.

Almost all the reefs of the outer shelf upstream of the lower Keys have a recovery time of less than 4 years, especially along the middle Keys and the east coast of Florida, between Miami and Palm Beach. This is in accordance with the regional hydrodynamics. Indeed the Florida Current transports larvae from reefs on the southern outer shelf to reefs located downstream. Hence recruitment on those reefs is enhanced, which leads to a quicker recovery. The reefs on the outer shelf along the lower Keys together with the reefs west of Key West and those on the inner shelf of the upper Keys have the highest recovery times. Being the most isolated ones (cf. Self Recruitment), this shouldn't come as a surprise. For instance, at each simulated year, the water currents transport the larvae from the reefs west of the Marquesas Keys away in a northwards direction, preventing local retention (cf. figures 3.12). As moreover their location is uttermost upstream of the FC, the water flows inhibit recruitment from reefs located upstream. Consequently these reefs' recoveries are almost only depending on clonal growth. In the inner shelf of the lower Keys, the recovery is more variable, but globally good. The reefs around Biscayne National Park have high recovery times, whereas they are located along the Florida

Current. A similar ascertainment is made concerning the PageRank Protection index (figure 3.19) and the PageRank Incoming connections index (figure 3.17), which bolsters a supposition that these reefs do not have much incoming connections. An explanation would be that the larvae coming from the reefs located upstream pass seawards of these reefs (cf. blue and purple larvae in figure 3.8), hence jeopardizing settlement. The Vaca reef, forming the inner shelf of the Middle Keys, has a recovery time of 5.8 years, which is medium. Yet, as this reef has one of the highest incoming PageRank indexes per surface area (3.17 (d)), it would be expected that it has a very quick recovery capacity.

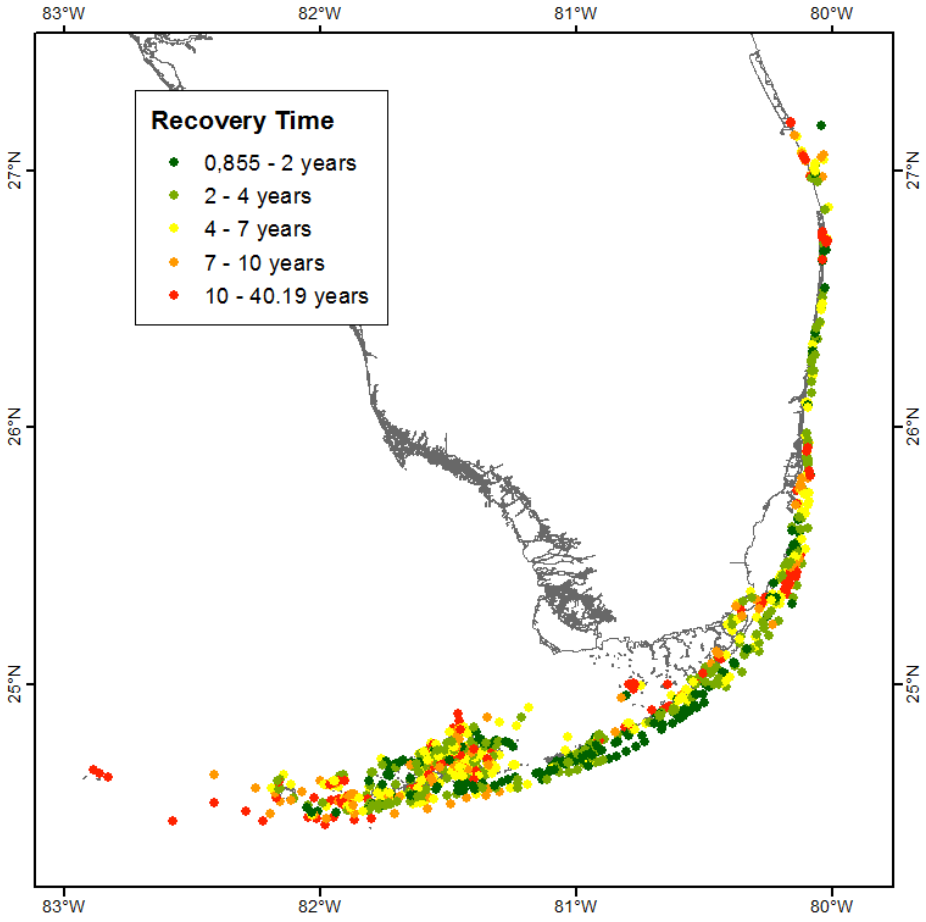


Figure 3.23: Time needed for the 990 reefs to recover from 30% of their maximum coral cover capacity to 90% of this maximum capacity. Reefs on the outer shelf recover quicker than reefs on the inner shelf. The reefs west of Key West recover very slowly.

### 3.4.1 Hydrodynamic variability

The recovery time of each reef was calculated five times : four times using the single-year connectivity matrices produced with the 2007, 2008, 2009 and 2010 hydrodynamics and a fifth time using the merged connectivity matrix. Table 3.8 summarizes for each year the fastest and slowest reefs to recover, as well as the median recovery time, the mean recovery time and the standard deviation of the recovery times of all the reefs. The maximum time is the same each year (43.5 years), and corresponds to the time needed for a reef to recover only by clonal growth. Hence, reefs that need 43.5 years to recover do not have any incoming connections or self recruitment. The minimum recovery times are very similar, all ranging between 10 and 11

months. Considering that the simulation starts in October, a recovery time of 10 months implies that larvae recruitment after the August spawning event is high enough to allow recovery. The median recovery time is each year a lot smaller than the mean recovery time. Indeed, as shown by the histograms in figure 3.24, the recovery times distributions are all right-skewed. Depending on the connectivity matrix used, 40% to 45% reefs recover in less than 4 years, whereas each time fewer than 25% of the reefs recover in more than 10 years. This explains the difference of ±4 years between the median and mean recovery times. Globally, the reefs recover quicker when the 2010 hydrodynamics are considered than when the three other years' hydrodynamics are considered. The standard deviations between the reef recovery times are high since there are great differences between the reefs' recovery times, ranging each year from less than one year to over 40 years. The higher the recovery time mean, the higher the standard deviation, which is rather intuitive.

| Year | Minimum | Maximum | Median | Mean | Standard Deviation |
|---|---|---|---|---|---|
| 2007 | 0.84 | 43.50 | 4.93 | 8.75 | 9.03 |
| 2008 | 0.885 | 43.50 | 4.87 | 8.77 | 9.97 |
| 2009 | 0.86 | 43.50 | 4.91 | 8.14 | 8.33 |
| 2010 | 0.845 | 43.50 | 4.86 | 6.86 | 7.055 |

Table 3.8: For each simulation year, the minimums, maximums, medians, means and variances of the recovery times of the 990 reefs, in *years*.

The following equation allows to calculate the standard deviation of the recovery times of each reef, in order to quantify the dispersion due to interannual hydrodynamic variability :

$$\sigma_{hydro}\{i\} = \sqrt{\frac{\sum_{j=2007}^{2010} (RT_j\{i\} - RT_{mean}\{i\})^2}{4}} \tag{3.1}$$

For a great part of the reefs (over 35%) the standard deviation is less than one year, but for some reefs the interannual variability is very important, leading to standard deviations of over 15 years (figure 3.25). This means that reefs receiving few larvae one year, can receive much more larvae another year.

The hydrodynamic variability can be interannual variability, i.e. differences in water flows from one year to another, but it can also be seasonal variability since each year spawning occurs on a different date, as explained in section 3.2.

Figure 3.26 shows the standard deviations $\sigma$ (left) and the coefficient of variations $\sigma/\mu$ (right) of the reefs by their location. As reefs having high recovery times generally also have high standard deviations, the left map is very similar to figure 3.23. By calculating the CV of the reefs, the hydrodynamic variability of a reef can be determined as a percentage variability relative to its mean. High CV values also often correspond to reefs which recover slowly. This means that even relative to their higher mean recovery time, slowly recovering reefs have a higher variability than quickly recovering reefs. For the reefs around the Marquesas Keys a high CV is also observed for most connectivity indexes, such as proportion settled, incoming and outgoing connections and PageRank restoration. Indeed, as visible on figure 3.9, in 2008 and 2009 the currents transport the larvae seeded around the Marquesas Keys away northward, whereas in 2007 and 2010 these larvae are much more stagnant. Hence, this most probably leads to a great variability in connectivity patterns, and thus in recruitment and recovery. The reefs located on the inner shelf of the Lower Keys and of the beginning of the Upper Keys also have a high CV. Even though obvious differences in larval dispersal aren't noticeable on figure 3.9, the high coefficients of variation of most connectivity indexes suggest a high local small-scale variability in connectivity patterns and hence recruitment. Such local small-scale variability, not noticeable

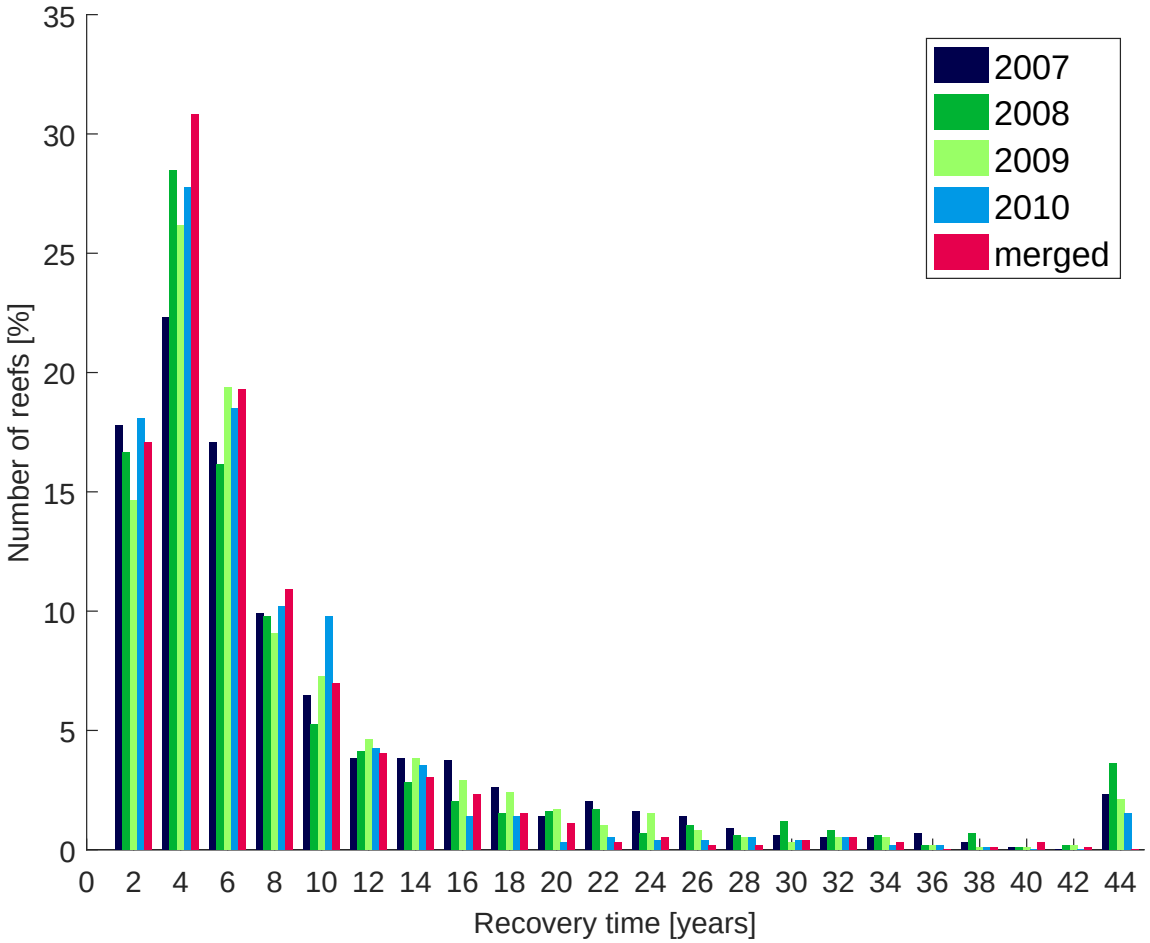


Figure 3.24: Histogram of the recovery times of the 990 reefs using the connectivity matrices of 2007, 2008, 2009 and 2010 and the merged connectivity matrix. Each time the histogram distribution is right-skewed.

on figure 3.9, is also probably present around the reefs north of Palm Beach, especially since figure 3.9 indicates highly variable water flows north of these reefs. Lastly high CV values are observed for the reefs on the outer shelf along Biscayne National Park. This is plausibly due to the variability of the larvae transport by the Florida Current, which is more or less seaward of these reefs according to the year considered (figure 3.9), impacting the possibility of settlement of the larvae on them. Globally the reefs on the Keys' outer shelf and along Florida's east coast from Miami to Palm Beach have low coefficients of variation.

The maximum, minimum, median, mean and standard deviation of the recovery times calculated for the 990 reefs using the merged connectivity matrix are shown in table 3.9. All values are smaller than for each of the connectivity matrices separately, since the matrix includes all the connections existing throughout the simulated four years. Hence this merged connectivity matrix contains more connections than what is possible during one single year, and will thus consider too optimistic connectivity patterns. But, contrary to single-year connectivity matrices, this merged connectivity matrix adequately represents the reefs that are connected over time lapses of several years. The maximum time is 40.19 years, which is about three years less than 43.50, the time needed to recover only by clonal growth, thus without any recruitment. Yet, for each year separately the maximum recovery time is always 43.50 years, as there is at least one reef that has zero incoming connections. This implies that the reefs having no incoming

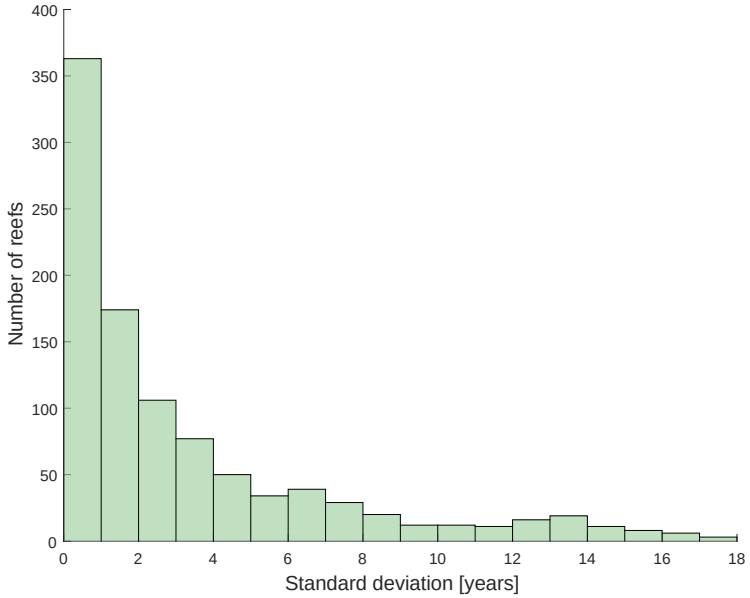


Figure 3.25: Histogram of the standard deviations of each of the 990 reefs. Most of the reefs recover in a similar time laps each year, but for a few reefs the standard deviation is over 15 years.

connections change from year to year so that none of the reefs has no incoming connections at all over the four years. The fact that the median recovery time decreases less than the mean recovery time suggests that also reefs with few recruitment capacity aren't all the same each year. That way there are less reefs with high recovery times when using the merged connectivity matrix than when using each year's connectivity matrix separately. Indeed the tail of the histogram distribution of the merged connectivity matrix (figure 3.24) is smaller than that of the four other histogram distributions.

| | **Minimum** | **Maximum** | **Median** | **Mean** | **Standard Deviation** |
|---|---|---|---|---|---|
| **Merged** | 0.855 | 40.19 | 4.83 | 6.30 | 5.62 |

Table 3.9: Minimum, maximum, median, mean and standard deviation (in *years*) of the recovery times of the 990 reefs, for the merged connectivity matrix.

### 3.4.2 Biological variability

Considering the uncertainty on the biological parameters (cf. 2.4.3), the absolute recovery times calculated are gross estimates. But when the purpose is to compare the differences in recovery behaviors between the 990 reefs or to analyze interannual hydrodynamic variability, as in the previous section, the exact absolute recovery times are not essential. This section exposes the results obtained by varying the values of the biological parameters, so to assess the sensitivity of the model to these biological parameters and so to estimate a range of possible recovery times. A positive and a negative scenario are calculated in addition to the initial scenario. The input values of the parameters are those of table 2.2 and all three scenarios are run using the merged connectivity matrix.

Figure 3.27 shows the histograms of the three scenarios and table 3.10 presents their minimum, maximum, median and mean recovery times, as well as the standard deviations. The maximum recovery times correspond to reefs with very few recruitment. Therefore they are close to the

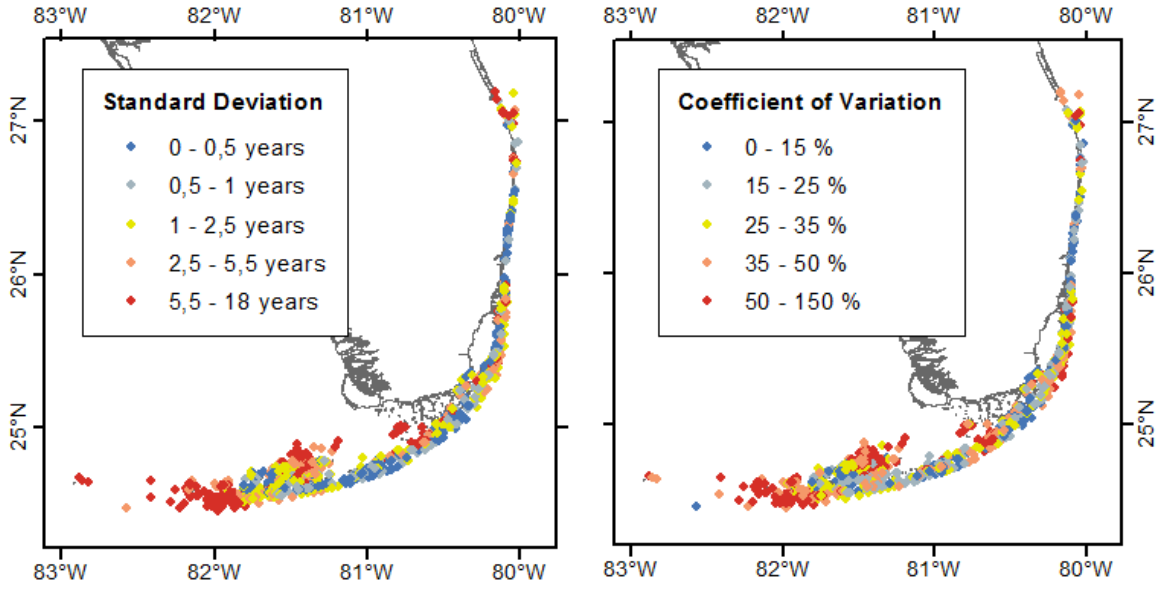


Figure 3.26: Standard deviation of each reef considering the hydrodynamics of 2007, 2008, 2009 and 2010.

recovery times obtained if they would only rely on clonal growth, which are 29 years for the positive scenario, 43.50 years for the initial scenario and 87 years for the negative scenario (figure 3.28). The values of the clonal growth rate were respectively 0.105, 0.07 and 0.035 $year^{-1}$, so there is a perfect negative linear relationship between the clonal growth rate and the recovery times, if recruitment is omitted. Indeed, the clonal growth rate being multiplied by 3 between the negative and the positive scenario, reefs recover three times faster. As 19% of the reefs recover in less than 6 years considering the negative scenario (figure 3.27), the same amount of reefs should recover in less than 2 years when considering the positive scenario. Yet, 41.6% of the reefs recover in less than 2 years. The 22.6% additional reefs come from a more efficient recruitment, mainly due to the higher amount of eggs produced per polyp and to a lesser extent to the decrease in post-settlement mortality and the increase in the mean size of a polyp. Hence, differences in maximum recovery time are almost proportional to clonal growth rate variation, since recruitment is extremely low, whereas reefs which receive incoming connections will see their recovery time change by more then the proportional shift in clonal growth rate. This is amplified the more incoming connections a reef receives. Recruitment not only accelerates recovery, but also enhances genotypic diversity. This is important for the sexual reproduction of *Acropora Cervicornis* as this coral needs two gametes of different genotypes for fertilization to occur. Hence egg production per polyp is dependent on the genotypic diversity of the coral population.

| | **Minimum** | **Maximum** | **Median** | **Mean** | **Standard Deviation** |
|---|---|---|---|---|---|
| **Initial scenario** | 0.855 | 40.19 | 4.83 | 6.30 | 5.62 |
| **Negative scenario** | 0.92 | 82.25 | 11.87 | 15.78 | 12.87 |
| **Positive scenario** | 0.835 | 26.41 | 2.86 | 3.80 | 3.47 |

Table 3.10: The minimums, maximums, medians, means and variances of the recovery times of the 990 reefs, in *years*, considering the most and the less optimal biological parameters.

The minimum recovery times are quite similar : 11 months for the negative scenario and 10 months for the positive scenario. Indeed even in the negative scenario the recruitment of some (exactly two) reefs is high enough to recover during the first spawning event.

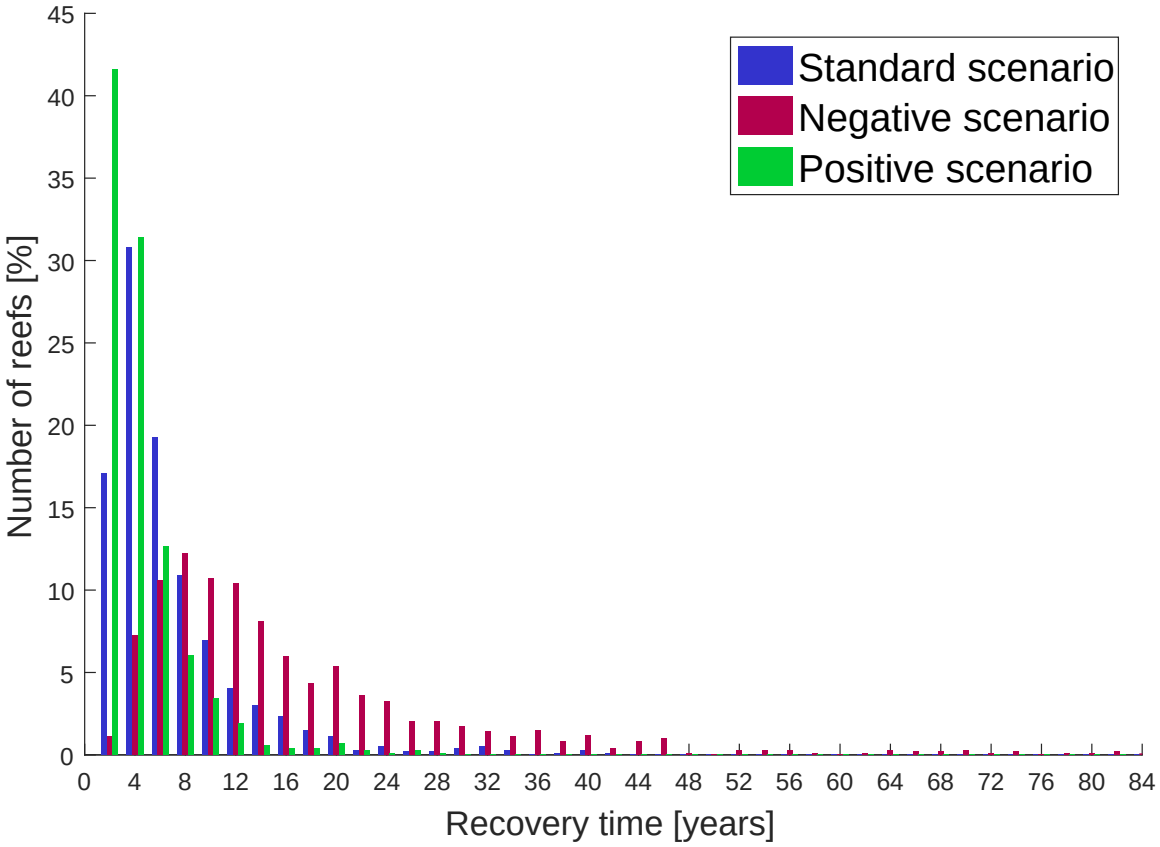


Figure 3.27: Histograms of the three different scenarios, considering consecutively the low, high and initial values of the biological parameters.

The biological variability can be compared to the hydrodynamic variability, in order to estimate which impacts most coral cover recovery : changes in biological behavior, for instance due to modified environmental conditions, or changes in connectivity patterns, due to interannual hydrodynamic variability. To quantify this, the biological variability is taken to be the standard deviation calculated using the following equation :

$$\sigma_{bio}\{i\} = \sqrt{\frac{(RT_{pos}\{i\} - RT_{mean}\{i\})^2 + (RT_{neg}\{i\} - RT_{mean}\{i\})^2}{2}} \tag{3.2}$$

The hydrodynamic variability is also defined as the standard deviation, calculated according to equation 3.1. The relative importance of biological variability $P_{bio}$ is calculated as :

$$P_{bio}\{i\} = \frac{\sigma_{bio}\{i\} - \sigma_{hydro}\{i\}}{\sigma_{bio}\{i\} + \sigma_{hydro}\{i\}} \tag{3.3}$$

For reefs with a $P_{bio}$ value close to 1 the hydrodynamic variability is low and the biological variability is high. This is inverted for $P_{bio}$ values close to -1. For values around 0 biological and hydrodynamic variability are equally important. Clearly biological variability has generally more impact than hydrodynamic variability. This is coherent with the fact that the hydrodynamic variability is lower than 2 years for over 50% of the reefs and has a maximum value of 18 years (cf. 3.25) whereas the biological variability can go up to 28 years. But it is very important to be cautious when interpreting this, because the hydrodynamic variability and the biological

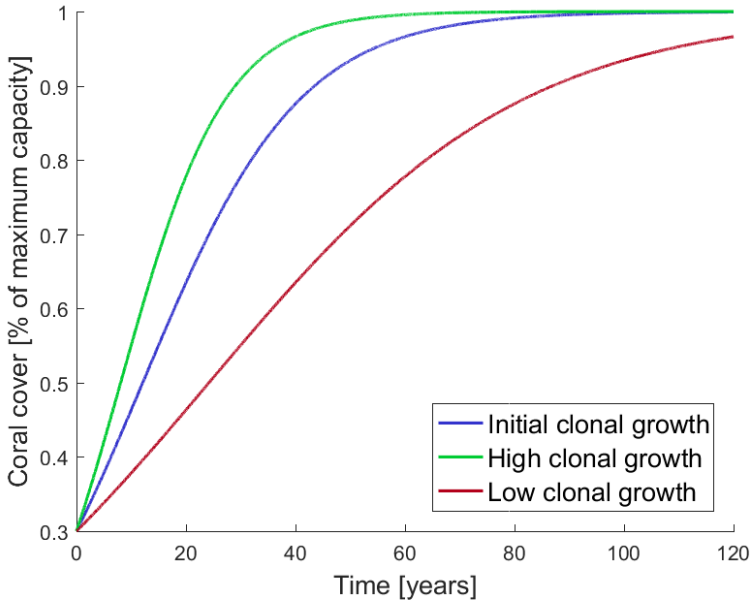


Figure 3.28: Clonal growth recovery considering $R_{low} = 0.035$ (negative scenario), $R_{initial} = 2 * R_{low} = 0.07$ (initial scenario) and $R_{high} = 3 * R_{low} = 0.105$ (positive scenario). Increasing the clonal growth rate results in a proportional increase in coral cover recovery rate.

variability aren't determined the same way. The hydrodynamic variability is assessed using the outputs of the hydrodynamic simulations of 2007, 2008, 2009 and 2010. Hence its value is the result of an entirely objective calculation. The only way to improve its determination would be by considering the hydrodynamics of additional years, which would most probably increase its value. The biological variability entirely depends on the values chosen for the biological parameters of the positive and negative scenarios. By decreasing the uncertainty range and thus reducing the difference between both scenarios, the biological variability would be reduced. Accordingly, the importance of biological variability compared to hydrodynamic variability entirely depends on the data used. More exhaustive and more accurate knowledge of the hydrodynamics and the biology of *Acropora Cervicornis* would most probably increase the relative importance of hydrodynamic variability.

Nevertheless the biological variability could also be higher than what is estimated in this study, if the uncertainty ranges of the biological parameters are extended. *Acropora Cervicornis* is extremely sensitive to its environment, hence the values of its biological parameters are highly depending on the conditions in which it grows. These conditions can temporary be modified by disturbances such as hurricanes, and will certainly be modified due to climate change and coastal urban development. Hurricanes cause high physical damage to *A. Cervicornis* colonies, leaving loads of small fragments behind. The growth rate of fragments decreases with the size of these fragments (Lirman et al., 2014). Hence, as the passage of a hurricane causes an increase in the number of small fragments, the clonal growth rate will increase. But a hurricane also leads to an increase in water turbidity and heavy sedimentation, which slows down growth and recovery by reducing light availability. Climate change causes an increase in water temperature and acidity, which will impact the biology of *A. Cervicornis* in a way that is at this day still hard to assess. Urban development increases the concentrations of pollutant and nutrients in coastal waters, mainly by run-off. As the FCRT is located along a highly urbanized region, the water quality there is even more likely to decay. An enrichment of nitrate and phosphate concentrations from $\pm 0.4$ µ$M$ to $\pm 5$ µ$M$ and from $\pm 0.05$ µ$M$ to $\pm 2$ µ$M$ respectively leads to clonal growth rates of *A. Cervicornis* fragments that are three times slower (Renegar and Riegl, 2005). Already

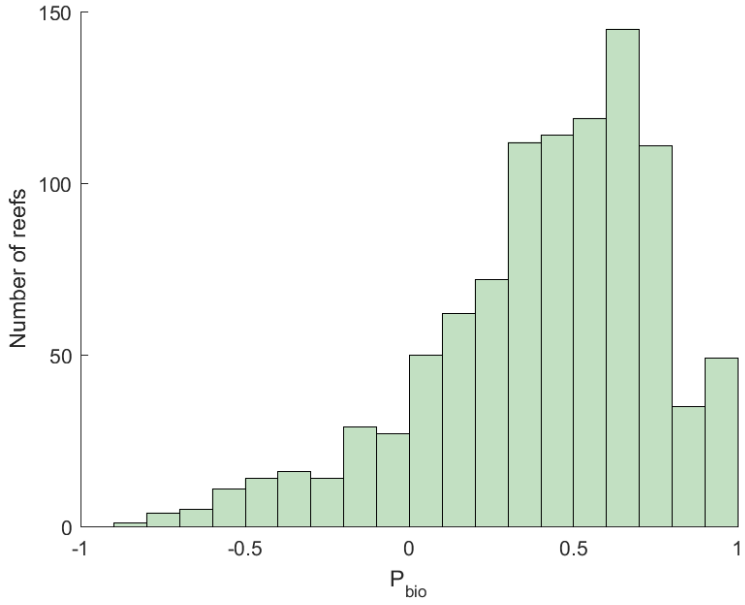


Figure 3.29: Histogram of $P_{bio}$. This index represents the relative importance of biological and hydrodynamic variability. Values close to 1 correspond to high biological variability whereas values close to -1 correspond to high hydrodynamic variability.

before 1995 the nitrate concentrations in the FCRT ranged between 0 and 2 µ$M$ and phosphate concentrations ranged between 0 and 1.2 µ$M$ (Szmant and Forrester, 1995).

During bleaching events or disease breakouts, the corals are stressed and hence are less productive, resulting in much lower clonal growth rate, less eggs production, smaller colony sizes and higher mortality. Such extreme biological variability is not taken into account in the previous variability assessment, even though bleaching events and disease breakouts become more an more prevailing. For instance nowadays the median return time between successive severe bleaching events is only 6 years, a trend that will continue according to climate model projections (Hughes et al., 2018).

Over the last decades coral nurseries and outplants have known a great upsurge. In such artificial environments the conditions are different from natural conditions. For instance the mean annual productivity of *A. Cervicornis* coral fragments in nurseries and outplants is respectively 4.3 and 4.6 (Schopmeyer et al., 2017). A colony's or fragment's productivity corresponds to the length of additional tissue produced divided by the initial TLE (= total linear extension, the total length of the colony's or fragment's branches). Productivity is thus a dimensionless number.

The effects of the environmental condition modifications listed above on the biology of *Acropora Cervicornis* are very diverse and almost impossible to define. This suggests that the uncertainty range of the biological parameters could be a lot larger than that taken in this study, consequently increasing the biological variability of the recovery times. To further improve the metapopulation model, varying biological parameters should be used, according to the environmental conditions of the reefs.

### 3.4.3 Recovery after a major disturbance : the Irma case

The hydrodynamic model, the larval dispersal simulation and finally the population model can be used to estimate coral recovery after major disturbances. Such a disturbance could be localized on one reef, caused for instance by a local disease outbreak. This would be simulated by reducing the coral cover only on the affected reef and keeping the other reefs' coral cover at their current state. Disturbances affecting multiple reefs would be simulated in the same way, thus reducing the coral cover of all concerned reefs. Of course when only one reef is affected it will recover quicker than when also its neighbouring reefs are affected since healthy reefs produce more larvae than disturbed reefs.

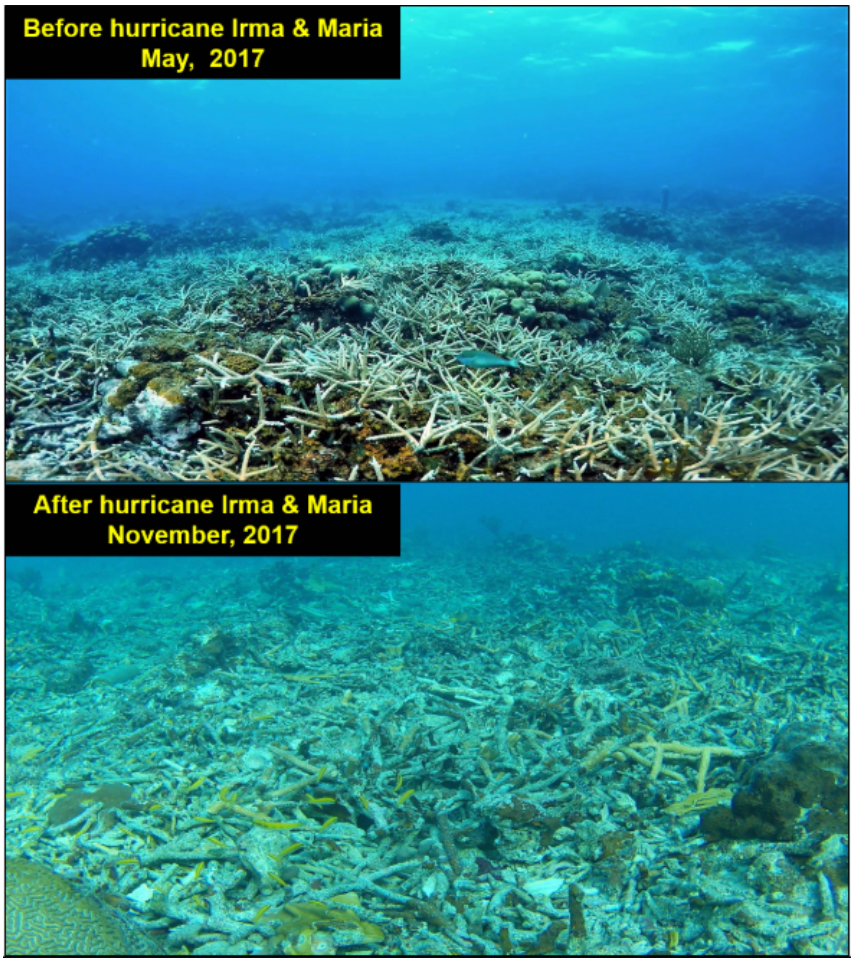


Figure 3.30: State of an *Acropora Cervicornis* thicket in Flat Cay, St. Thomas, U.S. Virgin Islands, attesting of the huge physical damage occasioned by the passage of hurricanes Irma and Maria. Photo Credit : Colin Howe & Hanae Spathias.

In this study we tried to simulate at which rate the reefs affected by hurricane Irma will recover over the next years. On September 10, 2017 this hurricane crossed the Florida Coral Reef Tract right through the Lower Keys, generating extensive damage. Century-old corals collapsed into reef trenches, water turbidity caused increased sedimentation (figure 1.2), nutrients were re-suspended enhancing macroalgal and phytoplankton growth and both death and high physical damage altered numerous coral colonies, among which *Acropora Cervicornis* (figure 3.30) (NOAA, n.d.). All these processes impacted severely coral cover extension on multiple reefs. According to an assessment made by the National Oceanic & Atmospheric Administration (NOAA, 2018), the damages were high on the reefs within 16 kilometers distance of the hurricane track. They were medium between 16 and 24 km distance on the west side of the track as they were between 16

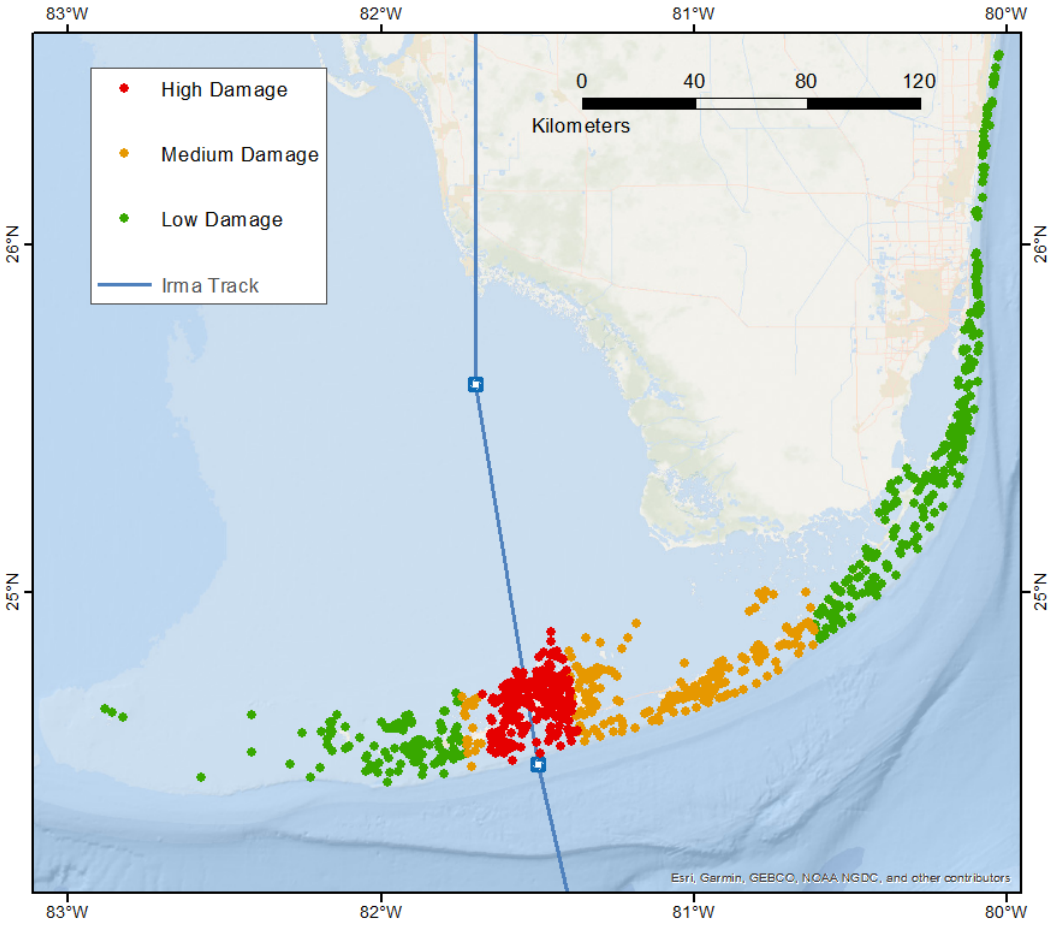


Figure 3.31: According to their distance to the Irma track, reefs suffered gradually less. At less than 16 km on both sides of the track damage was high, till 24 km west and 105 km east of the track damage was medium. On the remaining reefs damage was low.

and 105 km on the east side. The remaining reefs suffered much fewer damage. This is illustrated on figure 3.31.

In order to simulate the recovery rate, we assume that the coral cover on highly damaged reefs was reduced to 10% of their maximal capacity, and to 50% on medium damaged reefs. Reefs on which damage was low are considered healthy and are not taken into account in the model. Instead of assessing each reef's recovery separately, the mean total coral cover was calculated at each time step, following equation 3.4. This way the global coral cover recovery can be simulated.

$$CC_{mean}(t) = \frac{\sum_i^{N_{high}+N_{medium}} CC_i(t)}{N_{high} + N_{medium}} \tag{3.4}$$

with $CC_{mean}(t)$ the mean coral cover at time step $t$, $CC(t)$ a vector containing the coral covers of all damaged reefs at time step $t$, $N_{high}$ the number of highly impacted reefs, thus on which $CC = 0.1$ at $t = 0$ and $N_{medium}$ the number of reefs with medium impact, thus on which $CC = 0.5$ at $t = 0$.

The recovery is calculated using the negative, positive and initial scenarios from section 3.4.2, in order to estimate an uncertainty margin relative to the incertitude as well as the variability of the biological parameters. Each time, the merged connectivity matrix is used. The plots of the three scenarios are shown in figure 3.32. The times needed to recover at 90% are 3.89 years for

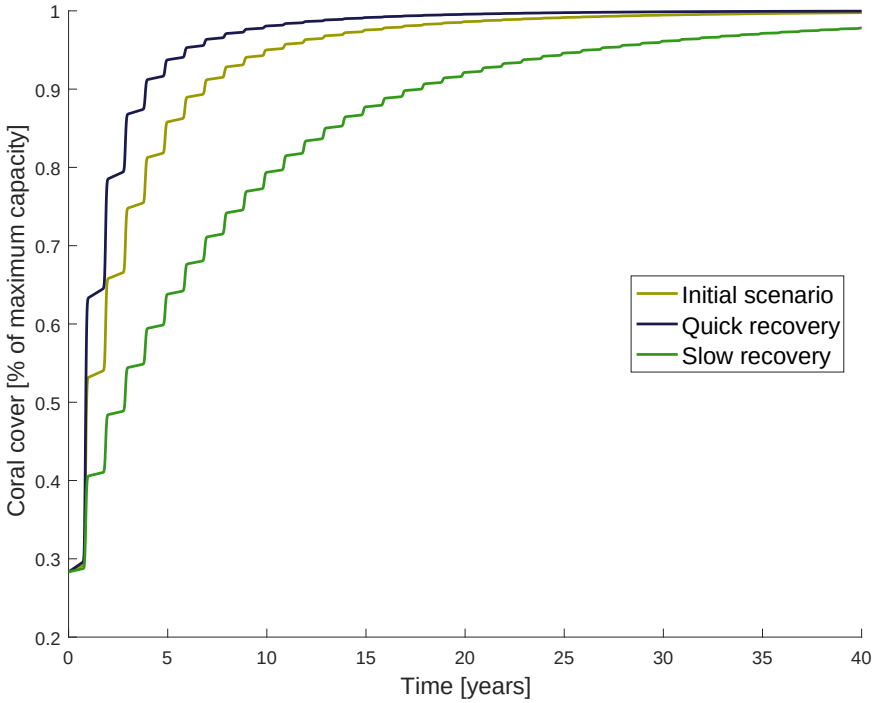


Figure 3.32: Evolution of the mean coral cover of all the reefs impacted by hurricane Irma, considering positive, negative and intermediate values for the biological parameters.

the positive scenario, 6.86 years for the middle scenario and 17.78 years for the negative scenario. As explained previously, even tough an uncertainty margin including biological variability is given, there still exist a high incertitude on these results, especially because of the difficulties to define the biological parameters. Moreover, since the merged connectivity matrix is used, annual connectivity is over-estimated (cf. page 62). The most accurate solution would be to define each year's connectivity patterns by randomly picking one of the single-year connectivity matrices. That way all the possible connections over several years would be taken into account and annual connectivity wouldn't be overestimated. Moreover considering the actual decline in *Acropora Cervicornis* populations, it is huge overestimation to suppose that all the undamaged reefs have a coral cover of 100% of their maximum capacity. Estimating the real actual coral cover would thus highly enhance the accuracy of the model. To date precise data of coral cover percentages is scarce.

# 4 Conclusion

By assessing *Acropora Cervicornis* connectivity patterns in the Florida Coral Reef Tract, this study intends to offer guidance on the selection of adequate locations for coral outplants as well as for reef restoration and protection. The connectivity patterns were determined by simulating larval dispersal thanks to a Lagrangian particle tracker that uses a high-resolution ocean model as input and that considers the competency acquisition and loss rates as well as the mortality rate of *Acropora Cervicornis*. The ocean model is computed by SLIM, a multiple-scale model allowing the use of an unstructured mesh and hence increasing resolution in areas of interest. The connectivity patterns are derived from a connectivity matrix, containing the weighted connections between all reef pairs. This matrix was produced four times, using the external forcings (i.e. tides, wind forcing and external water circulation) of 2007, 2008, 2009, 2010 as inputs of the ocean model. Henceforth interannual variability could be evaluated. Useful information was extracted from the connectivity matrices, on one hand through the calculation of indexes and reef clusters and on the other through the computation of a metapopulation model, which calculates the recovery rates of the reefs. The main conclusions are summarized below.

With a view to supporting reef management decisions, two possible actions are distinguished: protection and restoration. Reefs are marked as in need of protection if considered helpful for the network resilience but if they are poorly supplied themselves. The need for protection is thus correlated to long recovery time. Results, aligned with Frys' conclusions (2017), highlight two main spots meeting these criteria: south of Marquesas Keys and north of Big Pine Key, on the southern inner shelf. It appears however from variability study that, while the latter shows variability over the four years, it is not the case of the former, making it a strong candidate for protection measures. Results also suggest a need for protection downstream of this point, along the southern outer shelf. Reefs from that area have outgoing connections going to the rest of the Florida Tract via the Florida Current but are themselves not well supplied. However, modeling eddies would allow recirculating the larvae dispersal and might lead to more incoming connections towards these reefs, reducing their need for protection. The constant isolation of the Dry Tortugas reefs prevents them to share their larvae with the rest of the network. Useless for the FCRT resilience, they are not meeting the need for protection criteria. However, their capacity of recovery depends almost only on the clonal growth making them a very vulnerable spot. Results imply that if no measures are taken to protect them they would end up disappearing and hence one can wonder how they actually still exist.

Secondly, reefs are marked as worth restoring if considered as helpful to the network resilience and as resilient themselves, implying short recovery time. Results points three main areas worth considering for restoration measures: the outer shelf of the Middle Keys, the inner shelf of the Lower Keys and the Vaca Reef. Besides, reefs show short recovery time from Miami to Palm Beach but as they are situated downstream the FCRT, they do not supply enough reefs to be worth restoring. The Vaca reef is a strong link between inner and outer shelf reefs, allowing multiple incoming and outgoing connections. One should however keep in mind that its coral cover is largely overestimated in this model, inducing an overstatement of its connections. Moreover, its normalization is done after the computation of the Lagrangian particle tracker and only on the outgoing connections, impacting only slightly its large incoming connections weight, consequent to its size. In addition, its recovery time seems to be average rather than low, just as its need for protection is low. Indeed, the recovery time seems surprisingly more correlated to

the protection index than to the PageRank incoming index.

Interannual variability of connectivity patterns is partly due to the fact that the regional and local water circulations, which define larval dispersal, differ each year. This arises from two distinct aspects. The first one is the "random" annual variability, resulting each year in unique water flows. Yet these water flows follow each year the same seasonal fluctuations, which brings about the second aspect of interannual hydrodynamic variability. Indeed, as each year the spawning time of *Acropora Cervicornis* changes according to August's full moon date, the water flows affecting larval dispersal vary. Thenceforth this results in a connectivity pattern variability induced by the seasonal variability of water circulation in the FCRT. This study confirmed the importance of seasonal variability as larval dispersal after end-August spawning events (24/08/2010 and 28/08/2007) on one hand and begin/mid-August spawning events (06/08/2009 and 16/08/2008) on the other hand showed the most similarities. The full moon of August 2018 falling on the 26th, we expect that this year's larval dispersal will be closer to those of 2007 and 2010 than to those of 2008 and 2009.

Variability in reef resilience and recovery can also be caused by biological variability. Indeed, *Acropora Cervicornis* is extremely sensible to the environmental conditions. This is taken into account in this study by defining a range of possible values for the biological parameters used in the population model. For the biological parameters of the Lagrangian particle tracker no variability range is defined as this would have massively increased the use of computational resources. For most reefs the variability due to the environmental conditions, i.e. biological variability, is much greater than the interannual hydrodynamic variability. But this result has to be put in perspective as hydrodynamic variability could increase when considering the water circulation patterns of additional years and biological variability could either decrease by better assessing the environmental conditions on the reefs or increase by taking into account major disturbances as hurricane damage or disease breakouts. Moreover both water circulation and environmental conditions will most certainly be modified over the upcoming years due to climate change and coastal urban development.

As the impact of future climate change on coral ecosystems is undoubtable, assessing how the coral connectivity patterns determined in this study will evolve is a major key to efficiently target reef protection and restoration. Furthermore, to enhance the reliability and accuracy of the results, the limitations of the hydrodynamic model, of the Lagrangian particle tracker and of the population model should be as few as possible and the precision of the input parameters should be as high as possible. An important limitation is the failure of the hydrodynamic model to adequately simulate the eddies along the Florida Current, entailing an overestimation of the downstream connections and an underestimation of the upstream connections. Hence computing an eddy-resolving simulation would give a new insight in the connectivity patterns. Also, in order to use initial conditions corresponding to the actual state of the FCRT, the current percentage of coral cover on the reefs should be determined. As for now this data is lacking, we assumed in the LPT that the larvae were released equally over the total area of each reef. Such data could also be used as input for the population model. Assessing coral cover percentage would expected to be of especially great importance for the Vaca reef, as this reef of over 800 $km^2$ is only partly covered by reefs. Moreover, as mentioned in the previous paragraph, the estimation of variability could be improved : hydrodynamic variability by computing the hydrodynamics of additional years and biological variability by increasing knowledge about the biology of the coral species studied, in this case *Acropora Cervicornis*.

This study was realized in the context of global willingness to protect coral reefs all over the world. Hopefully, all combined efforts will allow to safeguard on a long-term perspective this endangered ecosystem, vital to coastal and maritime environments.

# Bibliography


Andutta F. P., Ridd P. V. and E. Wolanski (2011). "Dynamics of hypersaline coastal waters in the Great Barrier Reef." In: *Estuarine, Coastal and Shelf Science* 94, pp. 299–305.

Aronson R., Bruckner A. Moore J. Precht B. & E. Weil (2008). *Acropora cervicornis. The IUCN Red List of Threatened Species.*

Blondel, Vincent D. et al. (2008). "Fast unfolding of communities in large networks". In: *Journal of Statistical Mechanics: Theory and Experiment*, p. 10008.

Brin, Sergey and Lawrence Page (1998). "The anatomy of a large-scale hypertextual Web search engine". In: *Computer Networks and ISDN Systems* 30.1-7, pp. 107–117.

Brown, Charles E. (1998). *Coefficient of Variation.*

Brye B., de Brauwere A. Gourgue O. Karna T. Lambrechts-J. Comblen R. de and E. Deleersnijder (2010). "A finite-element, multi-scale model of the Scheldt tributaries, river, estuary and ROFI." In: *Coastal Engineering* 57.9, pp. 850–863.

Burgess, Sc, Mj Kingsford, and Kp Black (2007). "Influence of tidal eddies and wind on the distribution of presettlement fishes around One Tree Island, Great Barrier Reef". In: *Marine Ecology Progress Series* 341, pp. 233–242.

Cera, T. (1991). *Tappy. Free Software Foundation, Inc., 675 Mass Ave, Cambridge, MA 02139, USA.*

Cinner, Joshua Eli et al. (2016). "A framework for understanding climate change impacts on coral reef social–ecological systems". In: *Regional Environmental Change* 16.4, pp. 1133–1146.

Connolly, S. R. and A. H. Baird (2010). "Estimating dispersal potential for marine larvae: dynamic models applied to scleractinian corals". In: *Ecology* 91.12, pp. 3572–3583.

Cushman-Roisin, B. and J.-. M. Beckers (2011). *Introduction to Geophysical Fluid Dynamics.* Elsevier.

Drury, Crawford, Derek Manzello, and Diego Lirman (2017). "Genotype and local environment dynamically influence growth, disturbance response and survivorship in the threatened coral, Acropora cervicornis". In: *PLOS ONE* 12.3.

Egbert, G. D. and S. Y. Erofeeva (2002). "Efficient Inverse Modeling of Barotropic Ocean Tides." In: *Journal of Atmospheric and Oceanic Technology* 19.2, pp. 183–204.

Ferrario, Filippo et al. (2014). "The effectiveness of coral reefs for coastal hazard risk reduction and adaptation". In: *Nature Communications* 5.1.

Figueiredo J., A. H. Baird and S. R. Connolly (2013). "Synthesizing larval competence dynamics and reef-scale retention reveals a high potential for self-recruitment in corals". In: *Ecology* 94.3, pp. 650–659.

Figueiredo J., A. H. Baird S. Harii and S. R. Connolly (2014). "Increased local retention of reef coral larvae as a result of ocean warming". In: *Nature Climate Change* 4.6, pp. 498–502.

Frys, C. (2017). "Modeling marine connectivity in the Florida Coral Reef Tract." MA thesis. Université Catholique de Louvain.

Gladfelter, Elizabeth H, Rosemary K Monahan, and William B Gladfelter (1978). "Growth Rates of Five Reef-Building Corals in the Northeastern Caribbean". In: *Bulletin of Marine Science* 28, p. 7.

Hoegh-Guldberg, Ove (1999). "Climate change, coral bleaching and the future of the world's coral reefs". In: *Marine and Freshwater Research* 50.8, p. 839.

Hunter J. R., Craig P. D. and Phillips H. E. (1993). "On the use of random waml models with spatially variable diffusivity." In: *Journal of Computational Physics* 106.

Kourafalou, V. H. and H. Kang (2012). "Florida Current meandering and evolution of cyclonic eddies along the Florida Keys Reef Tract: Are they interconnected?" In: *Journal of geophysical research* 117.

Lambrechts, J. (2011). "Finite element methods for coastal flows: application to the Great Barrier Reef." PhD thesis. Université catholique de Louvain.

Lee, T. N. and D. A. Mayer (1977). "Low-frequency current variability and spin-off Southeast Florida." In: *J. Mar. Res.* 35, pp. 193–220.

Lee, T. N. and E. Williams (1999). "Mean distribution and seasonal variability of coastal currents and temperature in the Florida Keys with implications for larval recruitment." In: *Bulletin of Marine Science* 64.1, pp. 35–56.

Leuzinger, Sebastian, Kenneth R. N. Anthony, and Bette L. Willis (2003). "Reproductive Energy Investment in Corals: Scaling with Module Size". In: *Oecologia* 136.4, pp. 524–531.

Lirman, D. et al. (2010). "Propagation of the threatened staghorn coral Acropora cervicornis: methods to minimize the impacts of fragment collection and maximize production". In: *Coral Reefs* 29.3, pp. 729–735.

Lirman, Diego et al. (2014). "Growth Dynamics of the Threat ed Caribbean Staghorn Coral Acropora cervicornis: Influence of Host Genotype, Symbiont Identity, Colony Size, and Environmental Setting". In: *PLoS ONE* 9.9.

Liu, Yonggang and Robert H. Weisberg (2012). "Seasonal variability on the West Florida Shelf". In: *Progress in Oceanography* 104, pp. 80–98.

Miller, M W, A S Bourque, and J A Bohnsack. "An analysis of the loss of acroporid corals at Looe Key, Florida, USA: 1983–2000". In:

Monismith, Stephen G. (2007). "Hydrodynamics of Coral Reefs". In: *Annual Review of Fluid Mechanics* 39.1, pp. 37–55.

NOAA (2017). *Florida Keys National Marine Sanctuary Ecosystems: Coral Reefs.*

— (2018). *NOAA and partners assess reef, aid recovery following Hurricane Irma.*

— (n.d.). *Story Map Journal.*

Okubo, A. (1971). "Oceanic diffusion diagrams." In: *Deep Sea Research* 18, pp. 789–802.

Pham Van, C. (2014). "Development of a finite element model simulating flow and sediment dynamics: Application to the Mahakam land-sea continuum (Indonesia)." PhD thesis. Université Catholique de Louvain.

Porter, James W. (1976). "Autotrophy, Heterotrophy, and Resource Partitioning in Caribbean Reef-Building Corals". In: *The American Naturalist* 110.975, pp. 731–742.

Rakestraw, Charlotte. *Status and Lessons Learned from a Large-Scale Coral Disease Outbreak.*

Renegar, Da and Bm Riegl (2005). "Effect of nutrient enrichment and elevated CO2 partial pressure on growth rate of Atlantic scleractinian coral Acropora cervicornis". In: *Marine Ecology Progress Series* 293, pp. 69–76.

Rinkevich, Baruch (2005). "Conservation of Coral Reefs through Active Restoration Measures: Recent Approaches and Last Decade Progress". In: *Environmental Science & Technology* 39.12, pp. 4333–4342.

Ritson-Williams, R. et al. (2010). "Larval settlement preferences and post-settlement survival of the threatened Caribbean corals Acropora palmata and A. cervicornis". In: *Coral Reefs* 29.1, pp. 71–81.

Schopmeyer, Stephanie A. and Diego Lirman (2015). "Occupation Dynamics and Impacts of Damselfish Territoriality on Recovering Populations of the Threatened Staghorn Coral, Acropora cervicornis". In: *PLOS ONE* 10.11.

Schopmeyer, Stephanie A. et al. (2017). "Regional restoration benchmarks for Acropora cervicornis". In: *Coral Reefs* 36.4, pp. 1047–1057.

Smagorinsky, J. (1963). "General circulation experiments with the primitive equations." In: *Monthly Weather Review* 91.3, pp. 99–164.

Smith, S. D. and E. G. Banke (1975). "Variation of the sea surface drag coefficient with wind speed." In: *Quarterly Journal of the Royal Meteorological Society* 101, pp. 665–673.

Soong, Keryea (1991). "Sexual Reproductive Patterns of Shallow-water Reef Corals in Panama". In: *BULLETIN OF MARINE SCIENCE* 49, p. 15.

Spagnol S., Wolanski E. Deleersnijder E. Brinkman R. McAllister F. Cushman-Roisin B. and E. Hanert (2002). "An error frequently made in the evaluation of discretizedadvective transport in two-dimensional Lagrangian models of advection-diffusion in coral reef waters." In: *Marine Ecology Progress Series* 235, pp. 299–302.

Speer, Paul E. "Tidal Distortion in Shallow Estuaries". In:

Stanley, G. D. (2006). "Photosymbiosis and the evolution of modern coral reefs." In: *Science* 312, pp. 857–858.

Szmant, A M and A Forrester. "Water column and sediment nitrogen and phosphorus distribution patterns in the Florida Keys, USA". In:

Szmant, Alina M. (1986). "Reproductive ecology of Caribbean reef corals". In: *Coral Reefs* 5.1, pp. 43–53.

Szmant A., Miller M. (2006). *Settlement preferences and post-settlement mortality of laboratory cultured and settled larvae of the Caribbean hermatypic corals Montastraea faveolata and Acropora palmata in the Florida Keys, USA.* Proceedings of 10th International Coral Reef Symposium.

Talley, Lynne D. et al. (2011). "Gravity Waves, Tides, and Coastal Oceanography". In: *Descriptive Physical Oceanography.* Elsevier, pp. 223–244.

Thomas, C. (2015). "Modelling marine connectivity in the Great Barrier Reef and exploring its ecological implications." PhD thesis. Université Catholique de Louvain.

Thomas C., Lambrechts J. Wolanski E. Traag V. Blondel V. Deleersnijder-E. and E. Hanert (2014). "Numerical modelling and graph theory tools to study ecological connectivity in the Great Barrier Reef." In: *Ecological Modelling* 272, pp. 160–174.

Traag, V. A., P. Van Dooren, and Y. Nesterov (2011). "Narrow scope for resolution-limit-free community detection". In: *Physical Review E.* 84.1.

Tunnicliffe, V. (1981). "Breakage and propagation of the stony coral Acropora cervicornis". In: *Proceedings of the National Academy of Sciences* 78.4, pp. 2427–2431.

# APPENDICES

# A Snapshots of the larval dispersal simulation on the 20th day after the full moons of 2010, 2009, 2008 and 2007.

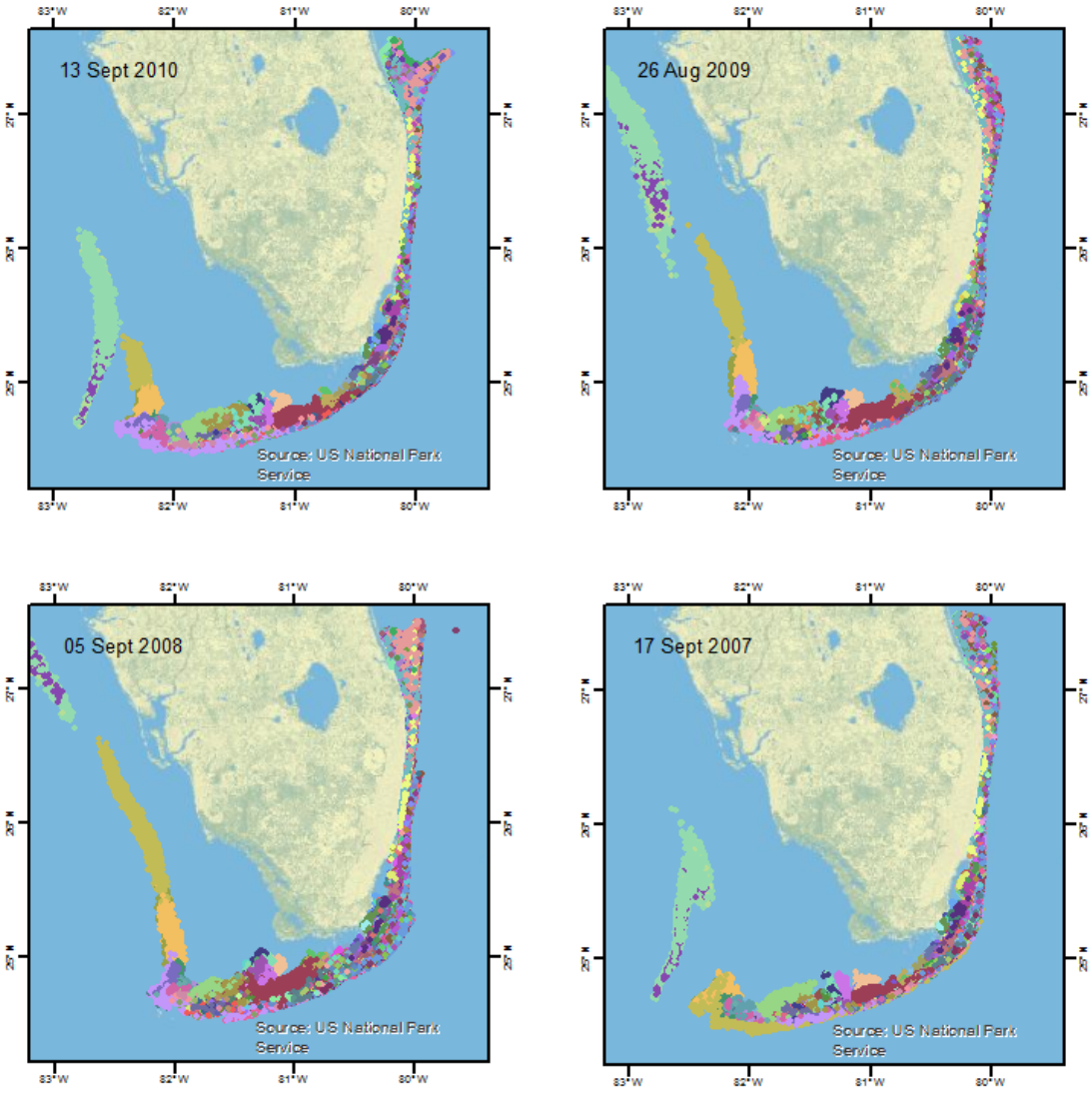


Figure A.1: Snapshots of the larval dispersal simulation on the 20th day after the full moons of 2010, 2009, 2008 and 2007.

# B Validation of the hydrodynamic model

## B.1 Validation of the velocities

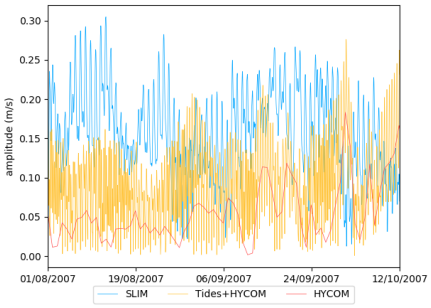


(a) Amplitude 2007

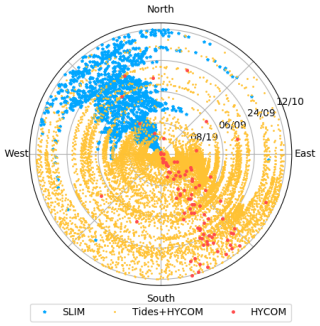


(b) Direction 2007

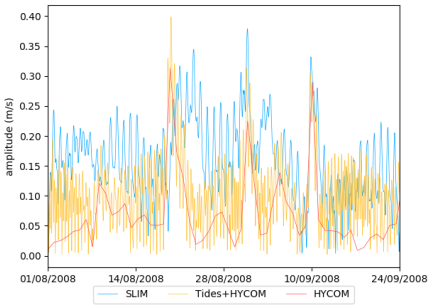


(c) Amplitude 2008

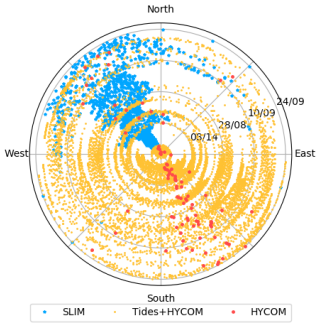


(d) Direction 2008

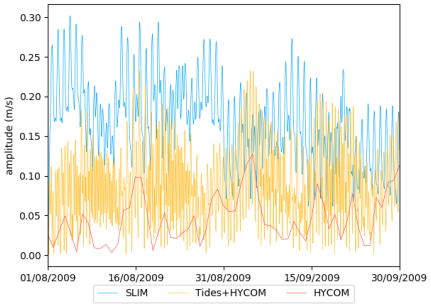


(e) Amplitude 2009

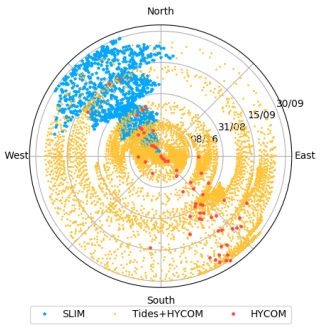


(f) Direction 2009

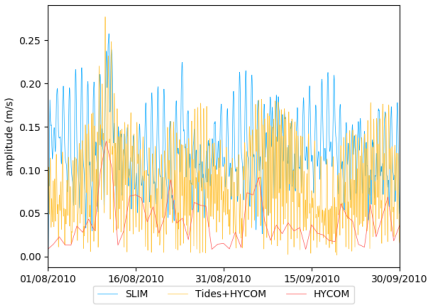


(g) Amplitude 2010

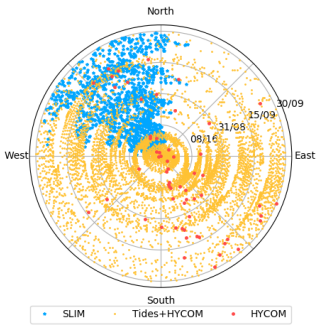


(h) Direction 2010

Figure B.1: Current amplitudes and directions for the validation point **number 2**, for the years 2007, 2008, 2009 and 2010. One can see that the currents computed by SLIM (blue) and by HYCOM (orange) are flowing in opposite directions. According to Liu and Weisberg (2012) the winds blowing over the WFS, which are subject to seasonal variability, impose a strong local forcing on the current amplitudes and directions of the WFS, which are thus subject to a similar seasonality. The winds tend to be southerly or southeasterly from June to August and easterly in September. As this validation point is situated in the shallow water of the GoM, this tends to confirm SLIM's results.

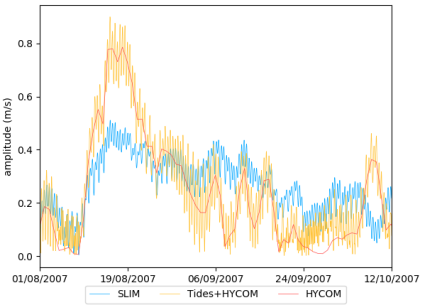


(a) Amplitude 2007

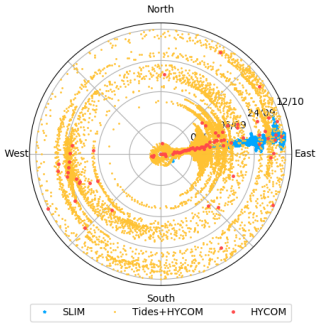


(b) Direction 2007

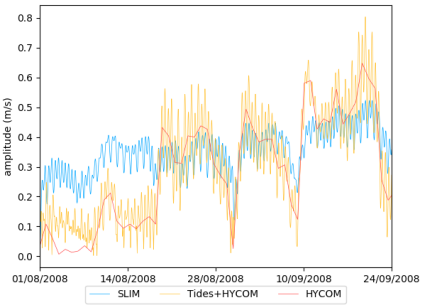


(c) Amplitude 2008

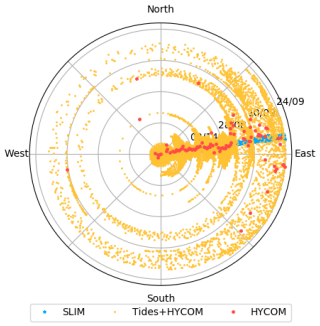


(d) Direction 2008

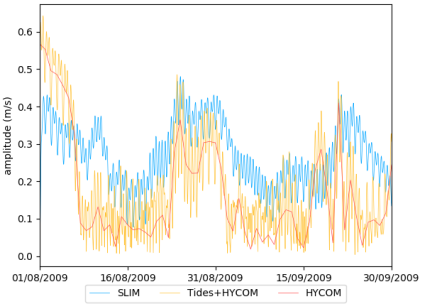


(e) Amplitude 2009

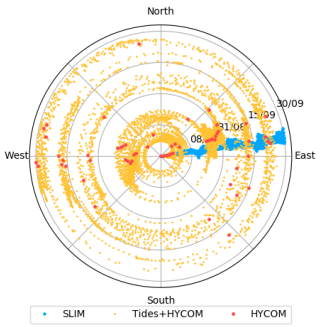


(f) Direction 2009

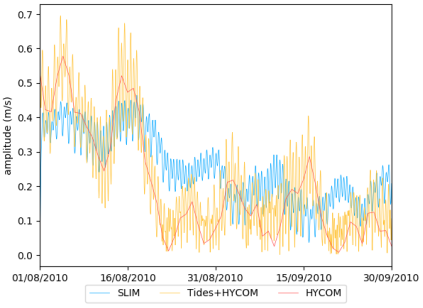


(g) Amplitude 2010

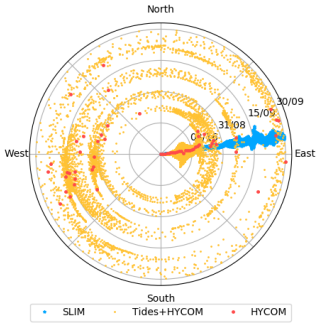


(h) Direction 2010

Figure B.2: Current amplitudes and directions for the validation point **number 3**, for the years 2007, 2008, 2009 and 2010. On each graph the results from SLIM simulation are given in blue as the results from HYCOM simulation are given in red and orange when tides are added.

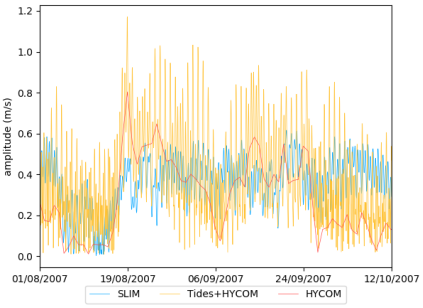


(a) Amplitude 2007

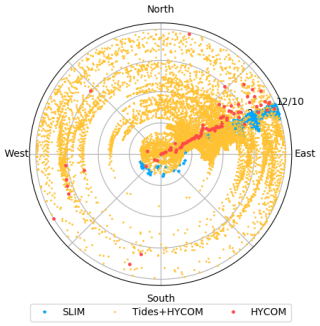


(b) Direction 2007

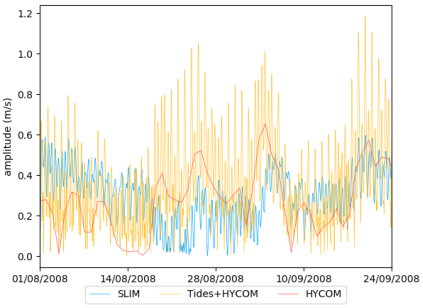


(c) Amplitude 2008

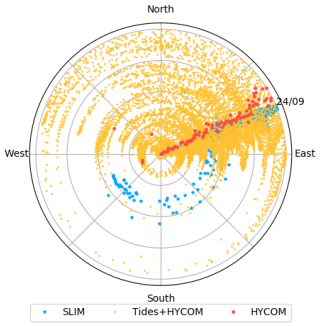


(d) Direction 2008

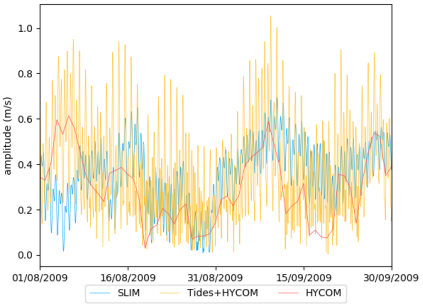


(e) Amplitude 2009

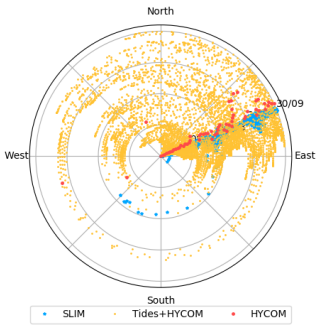


(f) Direction 2009

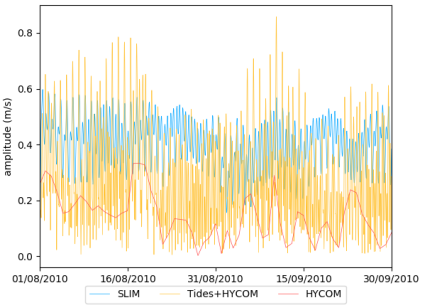


(g) Amplitude 2010

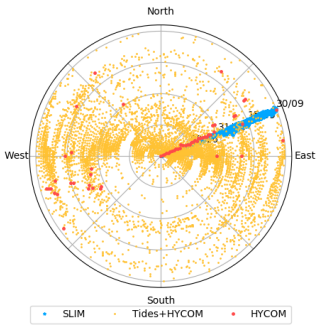


(h) Direction 2010

Figure B.3: Current amplitudes and directions for the validation point **number 4**, for the years 2007, 2008, 2009 and 2010. On each graph the results from SLIM simulation are given in blue as the results from HYCOM simulation are given in red and orange when tides are added.

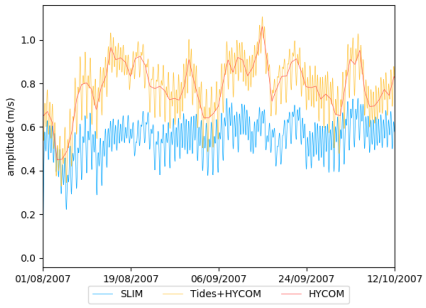


(a) Amplitude 2007

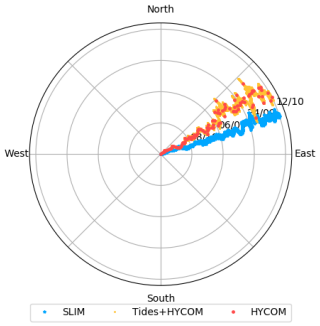


(b) Direction 2007

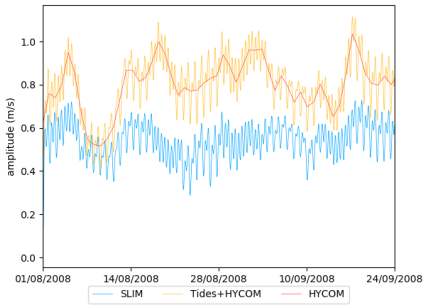


(c) Amplitude 2008

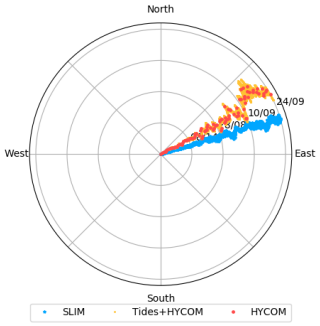


(d) Direction 2008

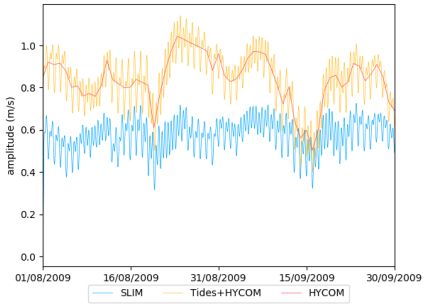


(e) Amplitude 2009

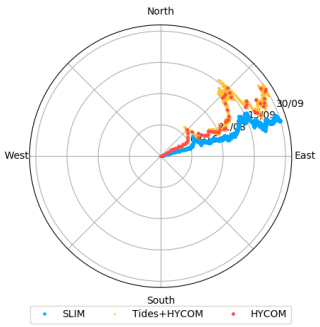


(f) Direction 2009

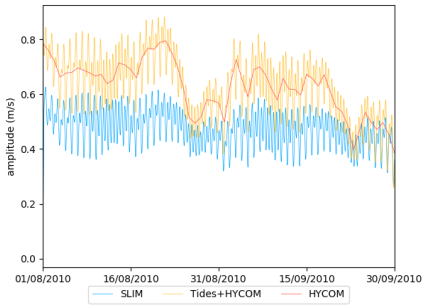


(g) Amplitude 2010

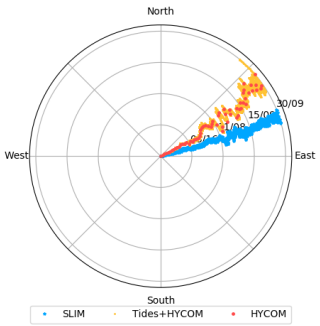


(h) Direction 2010

Figure B.4: Current amplitudes and directions for the validation point **number 7**, for the years 2007, 2008, 2009 and 2010. On each graph the results from SLIM simulation are given in blue as the results from HYCOM simulation are given in red and orange when tides are added.

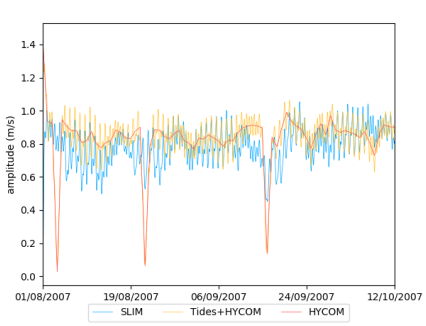


(a) Amplitude 2007

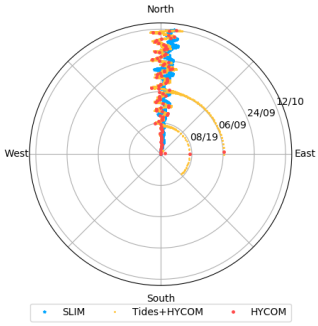


(b) Direction 2007

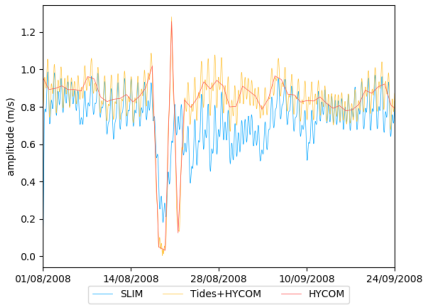


(c) Amplitude 2008

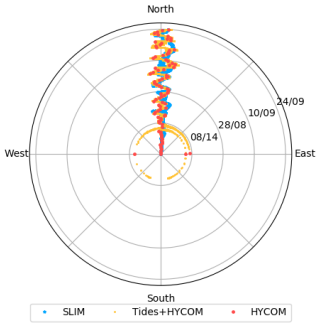


(d) Direction 2008

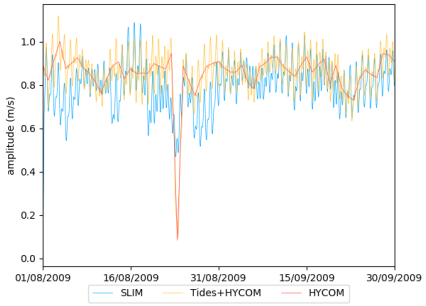


(e) Amplitude 2009

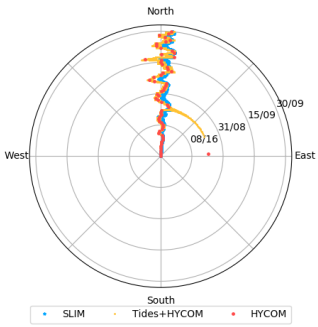


(f) Direction 2009

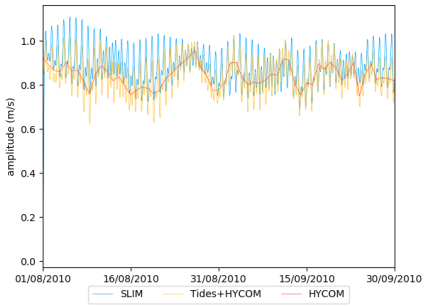


(g) Amplitude 2010

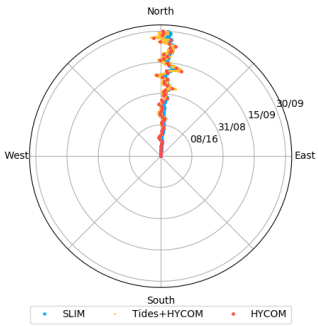


(h) Direction 2010

Figure B.5: Current amplitudes and directions for the validation point **number 8**, for the years 2007, 2008, 2009 and 2010. Unexplained extreme peaks can be seen on HYCOM's amplitude (red). SLIM (blue) seems to follow those extremes tendency, which is due to the fact that the point 8 is situated in the middle of deep water area, where the relaxation towards HYCOM is high.

## B.2 Validation of the surface elevation

| | Tidal constituents | Amplitude (cm) | | | Phase lag (°) | | |
|---|---|---|---|---|---|---|---|
| | | SLIM | Measures | Error (%) | SLIM | Measures | Absolute Error |
| 2007 | M2 | 24,53 | 29,82 | 18 % | 113,2 | 40,0 | 73,2 |
| | S2 | 4,69 | 5,01 | 6 % | 146,3 | 84,3 | 61,9 |
| | O1 | 2,24 | 2,73 | 18 % | 123,6 | 294,7 | 171,1 |
| | K1 | 1,55 | 2,17 | 29 % | 182,7 | 263,7 | 81,0 |
| 2008 | M2 | 24,5 | 29,46 | 17 % | 111,3 | 39,7 | 71,6 |
| | S2 | 4,41 | 4,66 | 5 % | 149,9 | 85,0 | 64,9 |
| | O1 | 3,06 | 2,85 | 7 % | 125,4 | 290,3 | 164,9 |
| | K1 | 1,77 | 1,9 | 7 % | 185,6 | 272,2 | 86,6 |
| 2009 | M2 | 25,26 | 29,86 | 15 % | 112,4 | 38,8 | 73,6 |
| | S2 | 4,9 | 4,73 | 4 % | 142,7 | 83,8 | 59,0 |
| | O1 | 2,76 | 2,52 | 10 % | 133,5 | 285,6 | 152,1 |
| | K1 | 1,66 | 2,15 | 23 % | 189,1 | 263,8 | 74,7 |
| 2010 | M2 | 23,5 | 29,26 | 20 % | 113,1 | 40,5 | 72,6 |
| | S2 | 4,47 | 4,6 | 3 % | 142,4 | 81,5 | 60,9 |
| | O1 | 2,35 | 2,76 | 15 % | 131,6 | 284,5 | 152,9 |
| | K1 | 1,61 | 2,28 | 29 % | 187,9 | 261,0 | 73,1 |

Table B.1: Comparison of the four main harmonic tidal constituents between SLIM computed surface elevations and elevation measurements at **point 11**, for the years 2007, 2008, 2009 and 2010. Only the four main constituents are shown although other constituents as Msf, N2 and Mm are among the most important constituents in term of amplitude.

| | Amplitude error | | | | | |
|---|---|---|---|---|---|---|
| | 2007 | 2008 | 2009 | 2010 | $\mu$ | $\sigma$ |
| M2 | 17,7 % | 16,8 % | 15,4 % | 19,7 % | 17,4 % | 1,8 % |
| S2 | 6,4 % | 5,4 % | 3,6 % | 2,8 % | 4,5 % | 1,6 % |
| O1 | 17,9 % | 7,4 % | 9,5 % | 14,9 % | 12,4 % | 4,8 % |
| K1 | 28,6 % | 6,8 % | 22,8 % | 29,4 % | 21,9 % | 10,5 % |

Table B.2: Variability over the years 2007, 2008, 2009 and 2010 of the relative error on the four main constituents amplitude, for the **point 11**.

| | Phase lag(°) error | | | | | |
|---|---|---|---|---|---|---|
| | 2007 | 2008 | 2009 | 2010 | $\mu$ | $\sigma$ |
| M2 | 73,2 | 71,6 | 73,6 | 72,6 | 72,8 | 0,9 |
| S2 | 61,9 | 64,9 | 59,0 | 60,9 | 61,7 | 2,5 |
| O1 | 171,1 | 164,9 | 152,1 | 152,9 | 160,3 | 9,3 |
| K1 | 81,0 | 86,6 | 74,7 | 73,1 | 78,8 | 6,2 |

Table B.3: Variability over the years 2007, 2008, 2009 and 2010 of the absolute error on the four main constituents phase lag, for the **point 11**.

# C Connectivity measures

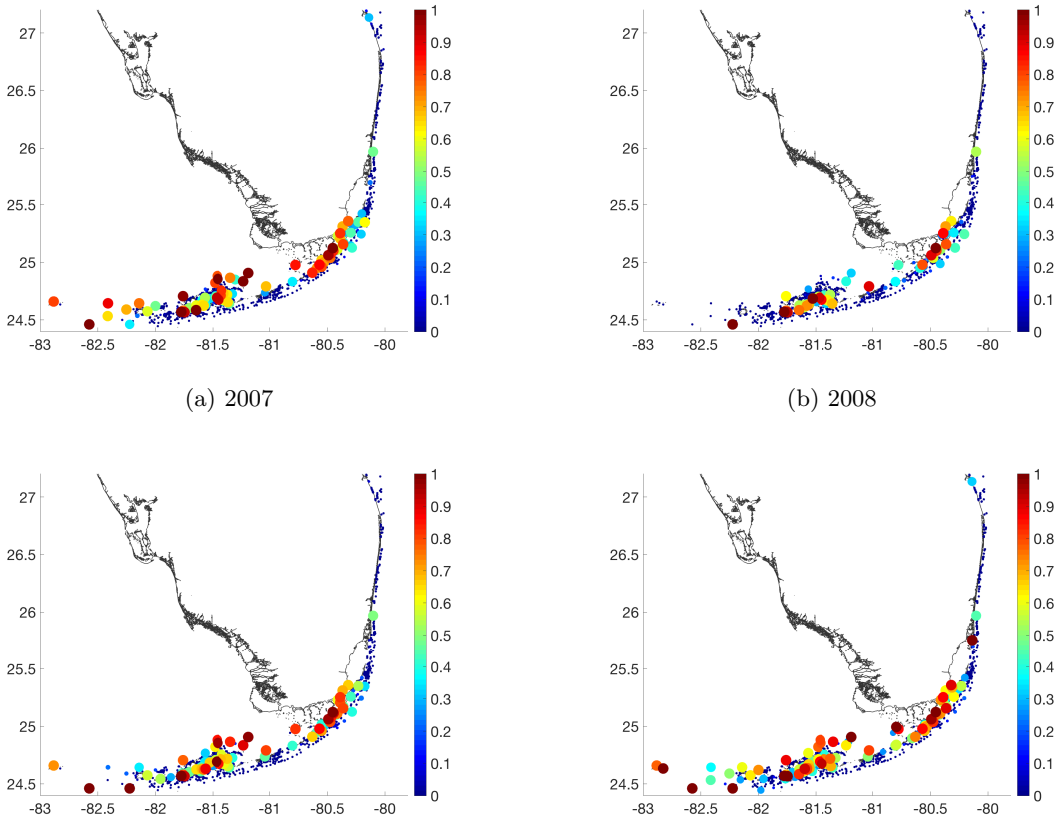


(a) 2007

(b) 2008

(c) 2009

(d) 2010

Figure C.1: Self recruitment computed from the connectivity matrices of years 2007, 2008, 2009 and 2010: Although the Dry Tortugas and the reefs to the south of the Marquesas Keys have high standard deviation over the 4 years, it can be seen that their self recruitment index is high for each year except for 2008.

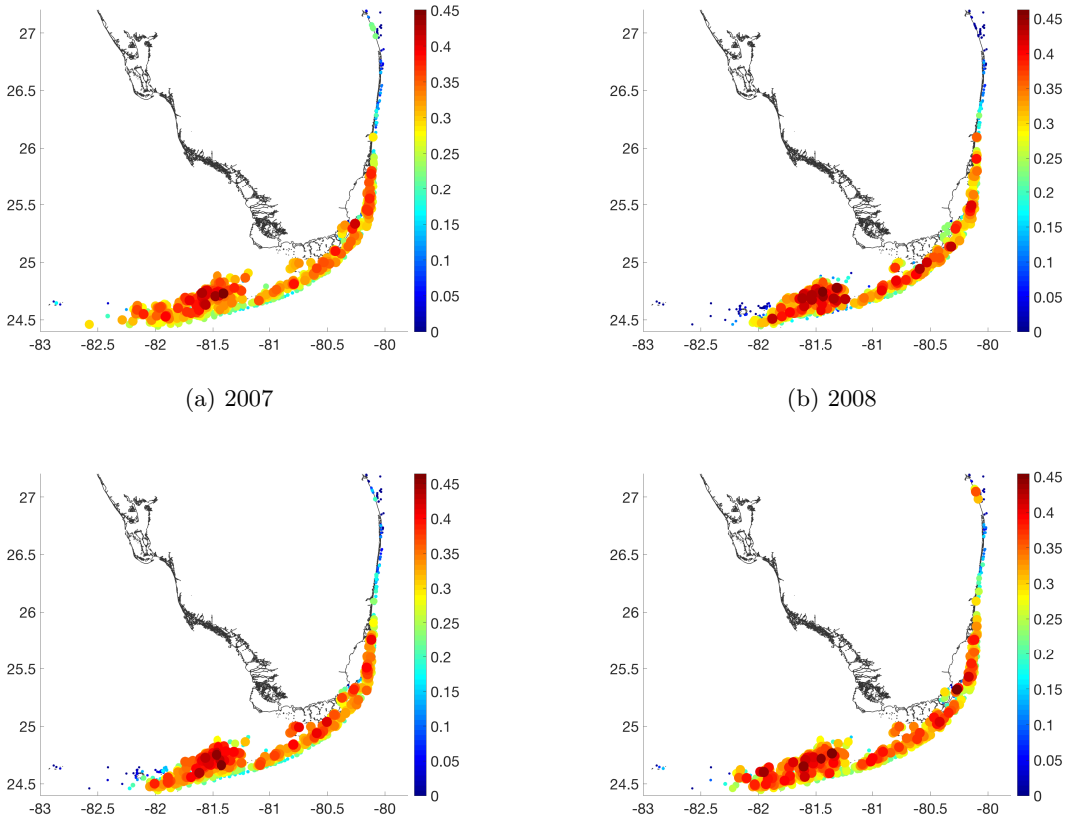


(a) 2007

(b) 2008

(c) 2009

(d) 2010

Figure C.2: Proportion settle computed from the connectivity matrices of years 2007, 2008, 2009 and 2010: it can be seen that during 2008 and 2009, the reefs near the Marquesas Keys have a low proportion settle during and higher in 2007 and 2010. Those spots are subject to variation of currents.

Rue Archimède, 1 bte L6.11.01, 1348 Louvain-la-Neuve **www.uclouvain.be/epl**